

International Max Planck Research School for Molecular Biology

**The identification and characterization of Mio10
and MINOS1 as novel regulators of
mitochondrial inner membrane organization**

Ph.D. Thesis

in partial fulfilment of the requirements
for the degree “Doctor of Philosophy (Ph.D.)”
in the Molecular Biology graduate program
at the Georg August University Göttingen,
Faculty of Biology

Submitted by
Alwaleed Alkhaja

born in
Manama, Bahrain

2012

Thesis Committee Members:

Prof. Dr. Peter Rehling

Department of Biochemistry II
University of Göttingen
Göttingen

Prof. Dr. Reinhard Jahn

Department of Neurobiology
Max-Planck-Institute for Biophysical Chemistry
Göttingen

Prof. Dr Markus Zweckstetter

Department for NMR-Based Structural Biology
Max-Planck-Institute for Biophysical Chemistry
Göttingen

Date of thesis submission: 31/03/2012

Date of oral examination: 02/05/2012

Part of this thesis has been previously published:

Alkhaja, A. K., Jans, D. C, Nikolov, M., Vukotic, M., Lytovchenko, O., Ludewig, F., Schliebs, W., Riedel, D., Urlaub, H., Jakobs, S., and Deckers M. (2012). MINOS1 is a conserved component of mitofilin complexes and required for mitochondrial function and cristae organization. *Mol. Biol. Cell.* 23, 247–57.

I hereby declare that this PhD thesis entitled “*The identification and characterization of Mio10 and MINOS1 as novel regulators of mitochondrial inner membrane organization*” has been written independently with no other aids or sources than quoted.

Alwaleed Alkhaja

Göttingen, 30.03.12

to my parents

TABLE OF CONTENTS

TABLE OF CONTENTS	I
LIST OF FIGURES	IV
LIST OF TABLES	VI
ABBREVIATIONS AND SYMBOLS	VII
1. ABSTRACT	1
2. INTRODUCTION	2
2.1 DUAL GENOMIC MITOCHONDRIAL PROTEOME	3
2.2 PROTEIN IMPORT AND BIOGENESIS	4
2.3 OXIDATIVE PHOSPHORYLATION	7
2.4 RESPIRATORY SUPERCOMPLEX FORMATION	7
2.5 F ₁ F ₀ ATPASE: FROM STRUCTURE TO FUNCTION	9
2.6 HIGH ORDERED ORGANIZATION OF THE F ₁ F ₀ ATPASE: FROM DIMERS TO OLIGOMERS	10
2.7 FUNCTIONAL ROLES OF THE F ₁ F ₀ ATPASE DIMERS	11
2.8 F ₁ F ₀ ATPASE DIMERIZATION FACTORS	12
2.9 F ₁ F ₀ ATPASE DIMERIZATION AND MAINTENANCE OF CRISTAE MORPHOLOGY	14
2.10 THE INNER MEMBRANE AND CRISTAE MEMBRANE ARCHITECTURE	15
2.11 MODELS OF CRISTAE BIOGENESIS	19
2.12 AIMS OF THIS STUDY	23
3. MATERIALS AND METHODS	24
3.1 MATERIALS	24
3.1.1 <i>Chemicals</i>	24
3.1.2 <i>General buffers and solutions</i>	25
3.1.3 <i>Instruments</i>	26
3.1.4 <i>Kits</i>	28
3.1.5 <i>Enzymes</i>	29
3.1.6 <i>Antibodies</i>	29
3.1.7 <i>Yeast strains</i>	30
3.1.8 <i>Yeast growth medium</i>	31
3.1.9 <i>Bacterial medium</i>	31
3.1.10 <i>Bacterial strains</i>	31
3.1.11 <i>Miscellaneous products</i>	31
3.2 GROWTH OF BIOLOGICAL SYSTEMS	32
3.2.1 <i>Cultivation of bacteria</i>	32
3.2.2 <i>Cultivation of yeast</i>	32
3.2.3 <i>Yeast cryo stock</i>	32
3.2.4 <i>Growth analysis of yeast</i>	32
3.2.5 <i>Cultivation of HEK293T cells</i>	33
3.3 MOLECULAR BIOLOGY TECHNIQUES	33
3.3.1 <i>PCR amplification</i>	33
3.3.2 <i>Determination of nucleic acid concentrations</i>	33
3.3.3 <i>DNA electrophoresis</i>	33
3.3.4 <i>Sequencing DNA</i>	34
3.3.5 <i>Transformation of E.coli</i>	34
3.3.6 <i>Transformation of yeast</i>	34
3.3.7 <i>Yeast genomic DNA preparation</i>	35
3.4 PROTEIN BIOCHEMISTRY	35
3.4.1 <i>TCA precipitation</i>	35
3.4.2 <i>Whole cell extracts</i>	35
3.4.3 <i>SDS-PAGE analysis</i>	36

3.4.4 BN-PAGE Analysis.....	36
3.4.4.1 First Dimension BN-PAGE	36
3.4.4.2 Second Dimension BN-PAGE	37
3.4.5 Coomassie staining.....	38
3.4.6 Western blotting and immunodetection.....	38
3.4.7 Size exclusion chromatography.....	38
3.4.8 Digital autoradiography.....	39
3.4.9 Isolation of mitochondria from yeast.....	39
3.4.10 Isolation of mitochondria from HEK 293T cells	40
3.4.11 Labeling of precursor proteins with [³⁵ S] methionine	40
3.4.12 Import and assembly of radiolabeled precursor protein.....	41
3.4.12.1 Import into yeast isolated mitochondria.....	41
3.4.12.2 Import into HEK293T isolated mitochondria	41
3.4.13 Protein localization analysis.....	42
3.4.14 Membrane association analysis.....	42
3.4.15 In-gel activity assays.....	42
3.4.16 Protein complex isolation by immunoprecipitation	43
3.4.17 Crosslinking antibodies for co-immunoprecipitations.....	44
3.4.18 Co-immunoprecipitation from isolated yeast mitochondria	44
3.4.19 Co-immunoprecipitation from HEK293T cells.....	45
3.5 ANALYTICAL TOOLS.....	45
3.5.1 In silico analysis and multiple sequence alignments.....	45
3.5.2 Mass spectrometry and data analysis.....	45
3.5.3 Fluorescence microscopy.....	46
3.5.4 Electron microscopy	47
3.5.4.1 High-pressure-freezing.....	47
3.5.4.2 Chemical fixation	48
4. RESULTS	49
4.1 IDENTIFICATION OF A PUTATIVE F ₁ F ₀ ATPASE DIMERIZATION FACTOR IN HIGHER EUKARYOTES (<i>H. SAPIENS</i>).....	49
4.1.1 in silico analysis: identification of Mio10 and MINOS1.....	49
4.1.2 Mio10 and MINOS1 sequence analysis and alignments.....	51
4.2 TOPOLOGICAL ANALYSIS OF MIO10 AND MINOS1	54
4.2.1 Antibody generation and specificity.....	54
4.2.2 Topological analysis of Mio10.....	55
4.2.3 Subcellular localization of MINOS1 by immunofluorescence.....	56
4.2.4 Topological analysis of MINOS1.....	57
4.3 ANALYSIS OF MIO10 AND MINOS1 ASSOCIATION WITH THE F ₁ F ₀ ATPASE.....	59
4.3.1 in vitro import of Mio10 and analysis by SDS-PAGE	59
4.3.2 Mio10 and MINOS1 assembly analysis by BN-PAGE	60
4.3.3 Comparison of Mio10 complexes assembly with the F ₁ F ₀ ATPase.....	61
4.3.4 Analysis of Mio10 assembly in the absence of F ₁ F ₀ ATPase dimers	63
4.3.5 Second dimension analysis of Mio10 complexes in atp20Δ mitochondria	65
4.3.6 Biochemical isolation of F ₁ F ₀ ATPase components.....	66
4.4 MIO10 DELETION MUTANT ANALYSIS.....	67
4.4.1 Growth analysis of MIO10 deletion mutant mitochondria.....	67
4.4.2 Analysis of respiratory chain complexes in mio10Δ.....	68
4.4.3 Assessment of F ₁ F ₀ ATPase activity and oligomerization in mio10Δ mutants	69
4.5 IDENTIFICATION OF MIO10 AND MINOS1 INTERACTION PARTNERS.....	71
4.5.1 Identification of Mio10 interaction partners.....	71
4.5.2 Identification of MINOS1 interaction partners.....	74
4.6 CHARACTERIZATION OF MIO10 AND MINOS1 INTERACTION WITH FCJ1 AND MITOFILIN	76
4.7 INVESTIGATION OF THE ROLE OF MIO10 IN MITOCHONDRIAL MORPHOLOGY	78
4.7.1 Growth test: SG /SD medium at 18°C.....	78
4.7.2 Protein steady state analysis of mitochondria grown at 18°C.....	79
4.7.3 Live-cell fluorescence microscopy analysis of mio10Δ mitochondria.....	80

4.7.4 Analysis of <i>mio10Δ</i> mitochondria by electron microscopy.....	82
5. DISCUSSION	86
5.1 MIO10 AND MINOS1 ARE NOT F ₁ F ₀ ATPASE DIMERIZATION FACTORS.....	86
5.1.1 Identification of the inner membrane proteins: <i>Mio10</i> and <i>MINOS1</i>	86
5.1.2 <i>Mio10</i> and <i>MINOS1</i> complexes comigrate but not physically associate with the F ₁ F ₀ ATPase	88
5.1.3 <i>Mio10</i> and <i>MINOS1</i> are not stably associated with the F ₁ F ₀ ATPase.....	89
5.1.4 <i>Mio10</i> does not affect F ₁ F ₀ ATPase activity or oligomerization.....	90
5.1.5 F ₁ F ₀ ATPase dimerization in higher eukaryotes	91
5.2 THE MINOS COMPLEX: MITOCHONDRIAL INNER MEMBRANE ORGANIZING SYSTEM COMPLEX.....	92
5.2.1 Identification of the yeast <i>MINOS</i> complex.....	92
5.2.2 Identification of the human <i>MINOS</i> complex.....	94
5.2.3 <i>Mio10</i> and <i>MINOS1</i> form a large complex (the <i>MINOS</i> complex)	95
5.2.4 The identification of additional <i>MINOS</i> components.....	97
5.3 CONCLUSIONS AND OUTLOOK.....	99
6. REFERENCES	105
ACKNOWLEDGMENTS	116
CURRICULUM VITAE	117

LIST OF FIGURES

- Figure 1 Overview of various mitochondrial import pathways
- Figure 2 Overview of mitochondrial respiratory chain and oxidative phosphorylation.
- Figure 3 Structural organization of respiratory chain supercomplexes in yeast
- Figure 4 Nomenclature and organization of F₁F₀ATPase subunits in yeast and *H.sapiens*.
- Figure 5 Stepwise assembly of the F₁F₀ATPase dimer
- Figure 6 Aberrant mitochondrial morphology in *ATP20* and *ATP21* deletion mutants
- Figure 7 Overview of factors involved in cristae biogenesis and maintenance
- Figure 8 Hypothetical models of cristae biogenesis
- Figure 9 Identification of Mio10 and MINOS1 by *in silico* analysis
- Figure 10 Molecular organization of selected proteins
- Figure 11 Alignment of Mio10 yeast homologs
- Figure 12 Alignment of MINOS1 homologs
- Figure 13 Antibody specificity test
- Figure 14 Mio10 is a mitochondrial IMS protein
- Figure 15 MINOS1 is a mitochondrial localized protein
- Figure 16 MINOS1 is a mitochondrial IMS protein
- Figure 17 Topology of Mio10 and MINOS1
- Figure 18 Import of Mio10 into mitochondria is membrane potential independent
- Figure 19 Mio10 and MINOS1 assemble into high molecular sized mitochondrial complexes
- Figure 20 Mio10 comigrates with F₁F₀ATPase complexes
- Figure 21 Mio10 assembly requires the presence of Atp20
- Figure 22 Mio10-containing complexes in *atp20Δ* mutants

- Figure 23 Mio10 and MINOS1 are not stably associated with the F₁F₀ATPase
- Figure 24 Mio10 is not required for mitochondrial respiration or supercomplex assembly
- Figure 25 F₁F₀ATPase activity and oligomerization are not affected in *mio10Δ* mutants
- Figure 26 Mio10 interacts with Fcj1
- Figure 27 Schematic of SILAC approach and mass spectrometric analysis
- Figure 28 MINOS1 interacts with Mitofilin
- Figure 29 Mio10/Fcj1 and MINOS1/Mitofilin form large mitochondrial complexes
- Figure 30 *MIO10* and *FCJ1* deletion mutants' growth defect at low temperatures
- Figure 31 Protein steady-state levels are unaffected in *mio10Δ* mutants
- Figure 32 Mitochondrial morphology is altered in *mio10Δ*
- Figure 33 Aberrant cristae morphology in *mio10Δ* mitochondria
- Figure 34 Absence of apparent cristae and cristae tips in *mio10Δ* mitochondria
- Figure 35 MINOS complex is critical for cristae biogenesis
- Figure 36 MINOS is a multifunctional protein
- Figure 37 Overview of MINOS roles in cristae biogenesis

LIST OF TABLES

Table 1	Details of various antibodies used in this study
Table 2	Details of yeast strains used in this study including genotype and source
Table 3	SDS-PAGE pipetting scheme
Table 4	BN-PAGE pipetting scheme
Table 5	Composition of in-gel activity assay buffers
Table 6	Experimental conditions for various immunoprecipitation assays
Table 7	Identified proteins of the Mio10 ^{SF} StrepTactin-chromotography
Table 8	The MINOS components as identified by various studies

ABBREVIATIONS AND SYMBOLS

°C	Degrees centigrade	IMS	Intermembrane space
%	Percent	KCl	Potassium Chloride
≤	Less than or equal to	kDa	Kilo Dalton
ADP	Adenosine diphosphate	KPi	Potassium Phosphate
AIM	Altered inheritance of mitochondria	L	Liter
ATP	Adenosine triphosphate	LB	Luria Bertani
ATPase	ATP synthase	LC/MS/MS	liquid chromatography tandem mass spectrometry
APS	Ammoniumpersulfate	M	Molar
AVO	Antimycin, Valinomycin, Oligomycin	mA	Milliampere
BN	Blue Native	MgCl ₂	Magnesium Chloride
BSA	Bovine serum albumin	Min(s)	Minute(s)
C-terminus	Carboxyl terminus	MINOS	Mitochondrial inner membrane organizing system
CK	Creatine Kinase	μl	Microliter
CP	Creatine Phosphate	mg	Milligram
COX	Cytochrome c oxidase	MDa	Mega Dalton
Complex I	NADH dehydrogenase	mL	Milliliter
Complex III	Cytochrome bc ₁ complex	mM	Millimolar
CN	Clear native	MOPS	3-(N-morpholino)propanesulfonic acid
CSM	Complete Supplement Mixture	MPP	mitochondrial presequence protease
dH ₂ O	Distilled water	mRNA	Messenger ribonucleic acid
DAB	3,3' Diaminobenzidine	mtDNA	Mitochondrial DNA
DMP	Dimethyl pimelidate dihydrochloride	mV	Milli volt
DMSO	Dimethylsulfoxide	N-terminus	Amino terminus
DMEM	Dulbecco's Modified Eagle Medium	NADH	Nicotinamide adenine dinucleotide
DNA	Deoxyribonucleic acid	NBT	4-Nitrotetrazoliumchloride blue
DNase	Deoxyribonuclease	ng	Nanogram
DTT	Dithioreitol	nm	Nanometer
E-value	Expect value	OD ₆₀₀	Optical Density at 600 nm
<i>E.coli</i>	<i>Escherichia coli</i>	ORF	Open reading frame
ECL	Enhanced chemiluminescence	PAGE	Polyacrylamide gel electrophoresis
EDTA	Ethylene diamine tetraacetic acid	PAS	Protein A Sepharose
FADH ₂	Flavin adenine dinucleotide	PBS	Phosphate buffered saline
Fcj1	Formation of cristae junction 1	PEG-4000	Polyethylene glycol 4000
H ⁺	Hydrogen ions	PCR	Polymerase chain reaction
<i>H.sapiens</i>	<i>Homo Sapiens</i>	PFA	Paraformaldehyde
H/L	High over low	pH	Cologarithm of activity of free H ⁺
HCl	Hydchloric acid	PMSF	Phenylmethylsulphonylfluoride
HPF	High pressure freezing	PK	Proteinase K
Hrs	Hours	PVDF	Polyvinylidene Fluoride
IBM	Innerboundary membrane		
IgG	Immunoglobulin G		
IMMT	Mitofilin		

rpm	Revolutions per minute
RNA	Ribonucleic acid
RNAi	RNA interference
RT	Room temperature
SD	Synthetic glucose
SDS	Sodium dodecyle sulfate
SGD	<i>Saccharomyces</i> Genome Database
SG	Synthetic glycerol
SEM	Sucrose EDTA MOPS
SILAC	Stable isotope labeling of amino acids in cell culture
<i>S.cerevisiae</i>	<i>Saccharomyces cerevisiae</i>
SF	Streptavidin FLAG
<i>Taq</i>	<i>Thermus aquaticus</i>
TAE	Tris-acetate-EDTA
TBS	Tris buffered saline
TBST	Tris buffered saline tween
TCA	Trifluoroacetic acid
TEMED	N,N,N',N'-Tetramethylethylene diamine
TIM	Translocase of inner membrane
TM	Transmembrane
TOM	Translocase of outer membrane
TX-100	Triton X-100
Tris	Tris(hydroxymethyl)-aminomethane
URA	Uracil
V	Volt
v/v	Volume per volume
Vero	African green monkey epithelial cells
w/v	Weight per volume
YPD	Yeast extract, peptone, dextrose
YPG	Yeast extract, peptone, glycerol
YPS	Yeast extract, peptone, sucrose
ZZ	Protein-A

1. ABSTRACT

Various mitochondrial inner membrane proteins contribute to the structure of cristae membranes and to the overall dynamic morphology of the inner membrane. These proteins include the F₁F₀ATPase dimers, which contribute to the curvature and angular shape of cristae. Also, Fcj1/Mitofilin are involved in cristae junction formation and act in an antagonistic manner in inner membrane curvature with respect to F₁F₀ATPase dimers. Whereas several small proteins mediate F₁F₀ATPase dimerization in yeast by binding sequentially at monomer interfaces, the exact nature of what promotes F₁F₀ATPase dimerization in higher eukaryotes is yet to be determined. To this end, the initial aim of this study was to identify novel F₁F₀ATPase dimerization factors in higher eukaryotes that parallel the action of small dimerization factors in yeast. An *in silico* approach to identify novel F₁F₀ATPase dimerization factors resulted in the identification of the human mitochondrial protein MINOS1 as a potential candidate. MINOS1, along with its human homolog, Mio10, were investigated. These proteins however were found not to be stably associated with the F₁F₀ATPase. Moreover, Mio10 did not affect F₁F₀ATPase dimerization, oligomerization, or enzymatic activity. Thus a role of Mio10 and MINOS in dimerization was excluded. Instead by using an affinity purification based mass spectrometric analysis, Mio10/MINOS1 were identified as novel interaction partners of Fcj1/Mitofilin. Topological analysis of Mio10 and MINOS together with results of size exclusion chromatography indicated that the two proteins form large mitochondrial inner membrane complexes. Furthermore, analysis of a *MIO10* deletion strain by fluorescence and electron microscopy provided evidence for the critical role that Mio10 plays in inner membrane organization. Mitochondria from *mio10Δ* and *fcj1Δ* strains exhibited leaflet-like stacked cristae membranes and appeared to have lost defined cristae tips. The complex that contains Mio10/Fcj1 in yeast and MINOS1/Mitofilin in human mitochondria was hence termed as the MINOS complex (Mitochondrial Inner membrane Organizing System). The presented findings highlight the functional and evolutionary significance of the MINOS complex as a player in mitochondrial inner membrane architecture as well as a multifunctional component in eukaryotic mitochondria and potentially in other cellular organelles.

2. INTRODUCTION

Ancient. Versatile. Dynamic. Mitochondria are eukaryotic organelles of α -proteobacterial origins, possessing their own genome as well as having a protein translational machinery (Gray *et al.*, 1999; Fontanesi *et al.*, 2006; Mick *et al.*, 2011). The mitochondrial proteome is of dual genomic origin: a mosaic of mitochondrial and nuclear encoded proteins. Besides their accustomed role in ATP synthesis by oxidative phosphorylation, mitochondria are also involved in cellular metabolism of amino acids, lipids and iron-sulfur clusters as well as playing a role in aging and disease exemplified by their central roles in apoptosis and production of reactive oxygen species (Scorrano *et al.*, 2002; Pan, 2011).

Mitochondria are highly compartmentalized, due to their enclosure by two specialized membranes: the outer and inner membrane. The inner membrane, which surrounds the mitochondrial matrix, can be characterized by two distinguishable regions: the inner boundary membrane (IBM), consisting of membrane stretches adjacent to the outer membrane, and cristae membranes, which are tubular structured invaginations of the inner membrane that extend into the mitochondrial matrix (Zick *et al.*, 2009). Cristae membranes increase the inner membrane surface-to-volume ratio (Frey and Mannella, 2000). They also promote the formation of a diffusion barrier between the intermembrane space (IMS) and the intracristal space, leading to various bioenergetic consequences, such as the regulation of oxidative phosphorylation by limiting diffusion of metabolites like protons and ADP (Mannella *et al.*, 2001). Furthermore, it appears that inner membrane complexes localize differentially: with the respiratory chain and mitochondrial translational machinery residing in the cristae membranes, and the protein import machinery primarily localized at the IBM (Vogel *et al.*, 2006). In addition, electron micrographs also revealed that cristae membranes are attached to the IBM by narrow openings termed cristae junctions, which appear to be constant in size and shape in various organisms (Frey and Mannella, 2000).

Mitochondrial morphology is dynamic and characterized by variable shapes and sizes of often interconnected networks; these networks can vary from simple tubular networks to more branched elaborate networks (Visser *et al.*, 1995; Egner *et*

al., 2002; Okamoto and Shaw, 2005). The nature of the mitochondrial network is dependent on opposing processes of mitochondrial fusion and fission (Okamoto and Shaw, 2005; Hoppins *et al.*, 2007). Moreover, some outer membrane proteins, such as Mmm1, Mdm10, and Mdm12 influence mitochondrial morphology (Okamoto and Shaw, 2005). However it appears that inner membrane proteins, such as the F₁F₀ ATP synthase (F₁F₀ATPase), OPA1, and Mitofilin play a more critical role in determining inner membrane architecture and the biogenesis of cristae membranes. The following section reviews the determinants of mitochondrial morphology from its dual-genomic respiratory chain complexes to inner membrane proteins that regulate cristae biogenesis and architecture.

2.1 Dual genomic mitochondrial proteome

Phylogenetic analysis and reconstructions based on mitochondrial-encoded proteins such as subunits of the cytochrome *c* oxidase, have illustrated that contemporary mitochondria have originated from an ancestral endosymbiot of α -proteobacterial origin (Sicheritz-Ponten *et al.*, 1998; Gray *et al.*, 1999; Gray, 2011). Acquisition of the bacterium by early eukaryotic cells is hypothesized to have occurred approximately two billion years ago, a time point in which an environmental global event led to a dramatic increase in atmospheric oxygen levels (Holland, 1994). The symbiotic relationship between the eukaryote and the bacterium, which has potential for aerobic respiration signified by the presence of various respiratory chain subunits, provided the metabolic advantage leading to mitochondrial selection and subsequent evolution (Anderson *et al.*, 2002; Dolezal *et al.*, 2006; Szklarczyk and Huynen, 2010). Evolution of mitochondria itself is not only incremental, having occurred over millions of years, but also dependent on differential symbiotic relationships and environmental conditions, as illustrated by a wide array of mitochondrial genome sizes of different organisms (Gray *et al.*, 1999; Gray, 2011). Moreover, the modern mitochondrial proteome is a result of a series of processes. These processes consist of the loss of ancestral mitochondrial genes, the transfer and integration of mitochondrial genes to the nucleus, and also the evolution of nuclear encoded sequences, which are then imported to the mitochondria and contribute to the majority of its proteome (Anderson *et al.*, 2002). About 99% of the mitochondrial proteome consists of nuclear encoded proteins; with the remaining 1% being products of the mitochondrial genome

(Chacinska *et al.*, 2009). The yeast mitochondrial genome encodes mainly large multi-transmembrane hydrophobic subunits of the respiratory chain such as Cox1 of the cytochrome *c* oxidase (Fontanesi *et al.*, 2006).

Nuclear encoded proteins, which are synthesized on cytosolic ribosomes, are imported by the mitochondrial import machinery, consisting of the necessary complexes, TOM, SAM, TIM23, TIM22, and MIA (Neupert and Herrmann, 2007; Chacinska *et al.*, 2009; van der Laan *et al.*, 2010). Translocases of the outer and inner membranes, TOM and TIM respectively, have no bacterial orthologs, having evolved from the host nuclear genes during endosymbiosis (Karlberg *et al.*, 2000; Dolezal *et al.*, 2006). Most of the components of the transport machinery formed *de novo* from nuclear encoded genes with some minor exceptions (Anderson *et al.*, 2002; Dolezal *et al.*, 2006). The outer membrane protein Sam50 is related to the bacterial outer membrane protein BamA (Omp85), whereas homologs of TIM proteins (Tim23 and Tim44) can be found in α -proteobacteria (Karlberg *et al.*, 2000; Paschen *et al.*, 2003). Furthermore, Tom7, Tom22, and Tom40 of the TOM complex are suggested to have an endosymbiotic origin (Maćasev *et al.*, 2004).

2.2 Protein import and biogenesis

Protein import into mitochondria is dependent on a mitochondrial targeting signal and the mitochondrial import machinery, which ensures the correct localization of the protein within the highly compartmentalized mitochondria. Proteins can be targeted to the mitochondria by containing either an N-terminal cleavable presequence, or alternatively by internal signals which span various segments of the protein sequence (Pfanner and Geissler, 2001; Neupert and Herrmann, 2007). Import into various mitochondrial compartments is dependent on the intrinsic characteristics of the protein: being either a precursor with presequence, a multi-spanning membrane hydrophobic precursor, or a β -barrel precursor (Neupert and Herrmann, 2007; van der Laan *et al.*, 2010). Import contains mainly two components: a sorting/insertion mechanism and a receptor, the TOM complex, which is a common component in all import pathways (Figure 1). The protein translocating channel of the TOM complex, a β -barrel translocase, is composed of Tom40 (Ahting *et al.*, 2001; Becker *et al.*, 2005). Tom22 acts as the receptor for presequence containing precursors whereas Tom70 acts as a

receptor for hydrophobic precursors (Muto *et al.*, 2001; Wu and Sha, 2006). However, various proteins have been shown to be dependent on both Tom22 and Tom70 (van der Laan *et al.*, 2010). In most cases, precursor proteins interact with Tom20 and Tom5 after binding to the receptor: this allows the interaction with Tom40 and the consequent translocation to the inner membrane (Chacinska *et al.*, 2009). In the case of β -barrel precursor proteins, after binding to the TOM complex, the proteins are passed to the SAM complex, which then mediates the proper insertion into the mitochondrial outer membrane (Wiedemann *et al.*, 2003). Similarly, hydrophobic precursors are passed to the TIM22 complex in the mitochondrial inner membrane, which then allows the proper insertion and maturation of the protein (Rehling *et al.*, 2003; Peixoto *et al.*, 2007). In both cases, SAM and TIM22 mediated import; precursors interact with small TIM chaperones, composed of Tim9 and Tim10 (Curran *et al.*, 2002).

Alternatively, precursors with presequences interact with the TIM23 complex in the mitochondrial inner membrane. The TIM23 complex exists in two distinct forms in equilibrium, the TIM23^{CORE} and the TIM23^{SORT}: The TIM23^{CORE} complex mediates the translocation of precursor proteins to the matrix whereas the TIM23^{SORT} mediates lateral sorting of inner membrane targeted precursor proteins that contain a stop-transfer signal adjacent to their N-terminal presequence (van der Laan *et al.*, 2010). The TIM23^{CORE} works in concert with the PAM complex, which is composed of various J-proteins (PAMs) and the mtHsp70 ATPase; the PAM complex utilizes ATP hydrolysis to translocate precursor proteins to the matrix (Liu *et al.*, 2003). In parallel, the TIM23^{SORT} complex in association with the respiratory chain, laterally releases membrane-spanning proteins to the inner membrane (Glick *et al.*, 1992; Chacinska *et al.*, 2009). Both TIM23 complexes are dependent on the presence of a membrane potential across the inner membrane (Chacinska *et al.*, 2009; van der Laan *et al.*, 2010). In the absence of a membrane potential, import of precursor proteins is halted at the TOM complex (Frazier *et al.*, 2003). Finally, the mitochondrial presequence protease (MPP), cleaves the N-terminal presequence after proper translocation or lateral release by the Tim23 complex (Yang *et al.*, 1988).

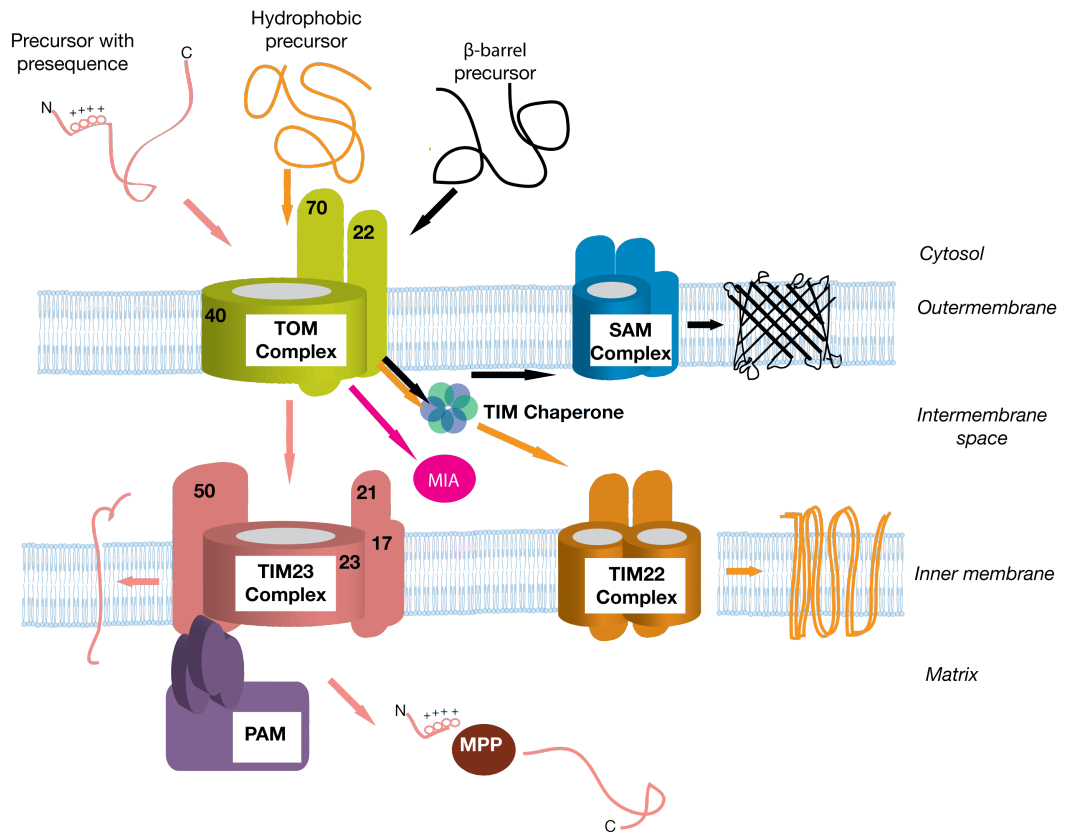


Figure 1. Overview of various mitochondrial import pathways. The TOM complex is the initial and central component in protein import pathways. Figure adapted from van der Laan *et al.* (2010)

Additionally, many IMS proteins generally lack N-terminal signals and are sorted to the IMS. Their import rather depends on internal cysteine motifs and the mitochondrial disulfide pathway, MIA pathway; this pathway has been found essential for various IMS proteins (Herrmann and Riemer, 2012). The cysteine motifs interact with the Mia40 receptor complex in the IMS (Milenkovic *et al.*, 2007; Sideris and Tokatlidis, 2007). Mia40 is an oxidoreductase, which contains a redox-active cysteine pair residues directly involved in the oxidative folding of proteins (Banci *et al.*, 2009). Furthermore, Mia40 is maintained in its oxidative state by the sulfhydryl oxidase, Erv1, which in turn is reoxidized by cytochrome *c* (Farrell *et al.*, 2005; Bihlmaier *et al.*, 2007). Oxidative protein folding by disulfide bond formation is thought to drive translocation and targeting to the mitochondrial IMS (Banci *et al.*, 2009).

2.3 Oxidative phosphorylation

Mitochondria are referred to as the powerhouse of the cell due to their central role in oxidative phosphorylation. This process, which is mediated by the respiratory chain, involves the coupled oxidation of NADH and FADH₂ by electron transport and subsequent ATP synthesis by the F₁F₀ATPase in the inner membrane (Figure 2). The respiratory chain is composed of five large multisubunit protein complexes: NADH dehydrogenase (complex I), succinate dehydrogenase (complex II), cytochrome *c* reductase/ cytochrome bc₁ complex (complex III), cytochrome *c* oxidase (complex IV), and the F₁F₀ATPase (complex V). In brief, oxidative phosphorylation follows electron transport within the respiratory chain, which causes H⁺ translocation from the matrix to the IMS by complexes I, III and IV (Boyer, 1997). This forms a proton gradient across the inner membrane. The F₁F₀ATPase then uses the proton motive force (the sum of the chemical gradient of H⁺ ions and the membrane potential) to produce ATP from ADP and inorganic phosphate (Boyer, 1997). One should note that the yeast *Saccharomyces cerevisiae* (*S.cerevisiae*), unlike most eukaryotes, does not contain a membrane embedded complex I, but rather NADH dehydrogenases associated with the inner membrane (Luttik *et al.*, 1998).

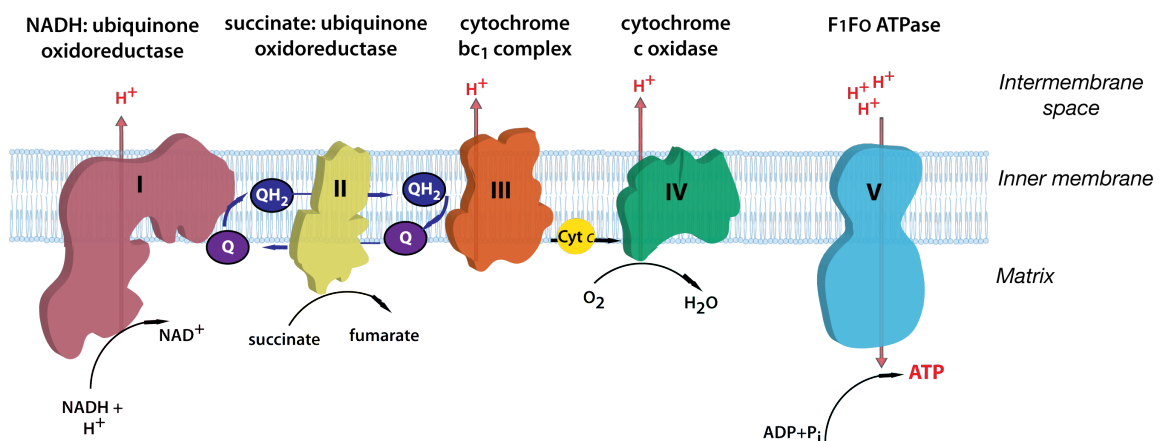


Figure 2. Overview of mitochondrial respiratory chain and oxidative phosphorylation.

2.4 Respiratory Supercomplex Formation

The molecular organization of the respiratory chain within the mitochondrial inner membrane has been addressed by two models: 1) the “liquid-state” model which postulates that respiratory chain complexes are arranged randomly and thus diffuse latterly and freely in the membrane and 2) the “solid-state” model which postulates that respiratory chain complexes associate in an ordered manner to form larger

complexes, or supercomplexes (Vonck and Schäfer, 2009). Evidence for the latter model has been firstly shown in bacteria and then in mitochondria from yeast and higher eukaryotes (Stroh *et al.*, 2004; Stuart, 2008). In *S.cerevisiae*, four large supercomplexes have been observed by BN-PAGE after solubilization of mitochondria in the mild nonionic detergent, digitonin (Figure 3). These complexes are comprised of a dimeric F_1F_0 ATPase (V_2), a dimeric complex III (III_2), and a dimeric complex III associated with one or two moieties of complex IV (III_2IV and III_2IV_2) (Stuart, 2008).

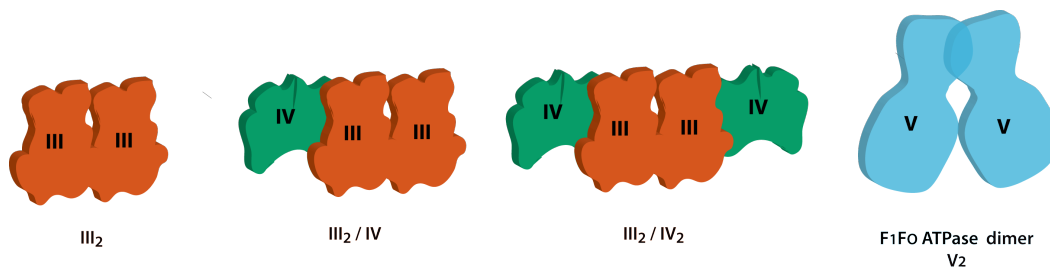


Figure 3. Structural organization of respiratory chain supercomplexes in yeast. Large supercomplexes have been observed by BN-PAGE: a dimeric F_1F_0 ATPase (V_2), a dimeric complex III (III_2), and a dimeric complex III associated with one or two moieties of complex IV (III_2IV and III_2IV_2).

In contrast, the organization of respiratory chain complexes appeared to be distinct in mammals. Supercomplexes in mammals may include complex I as well as varying copies of complex IV. Using Blue native PAGE (BN-PAGE) after digitonin solubilization, five supercomplex species were observed: a dimeric F_1F_0 ATPase (V_2), a dimeric complex III with a monomeric complex I (III_2I_1), and a dimeric complex III, with a monomeric complex I, associated with 1-3 complex IV monomers: $III_2I_1IV_1$, $III_2I_1IV_2$, or $III_2I_1IV_3$ (Schägger and Pfeiffer, 2000; Althoff *et al.*, 2011). Moreover, under different solubilization conditions such as with TritonX-100, a supercomplex containing dimeric complex III, a single complex I, and four copies of complex IV ($III_2I_1IV_4$) were observed (Vonck and Schäfer, 2009). Supercomplexes containing at least a single complex I, complex III, and a dimeric IV have been referred to as “respirasomes”, which are structural units that can autonomously carry out respiration (Schägger and Pfeiffer, 2000). Furthermore, supercomplexes have been observed in various other species, albeit different configurations, such as plants, which contain three major complexes: V_2 , III_2I_1 and III_2I_2 (Eubel *et al.*, 2003).

2.5 F₁F₀ATPase: from structure to function

The multisubunit F₁F₀ATPase is ubiquitous to all living organisms and has been found in mitochondrial, bacterial plasma membranes and thylakoid membranes in chloroplasts (Walker *et al.*, 1991; Collinson *et al.*, 1994; Boyer, 1997; Seelert and Dencher, 2011). The yeast mitochondrial F₁F₀-ATP synthase is composed of at least 17 subunits to form a soluble globular catalytic part, the F₁, and a membrane embedded part, the F₀ (Arnold *et al.*, 1998). In addition, various proteins such as Stf1p, Stf2p, and Inh1p (IF1 in humans) associate with the F₁F₀ATPase for various regulatory/inhibitory functions (Walker, 1994; Arnold *et al.*, 1998; Hong and Pederson, 2002). Figure 4 summarizes the subunit composition and nomenclature in *Escherichia coli* (*E. coli*), the yeast *S. cerevisiae*, and *Homo sapiens* (*H. sapiens*). The F₀ termed “O” due to sensitivity to the inhibitor oligomycin (Racker, 1963). The enzyme is a multimeric complex of dual genomic origin, with yeast subunits Atp6, Atp8, and Atp9 encoded on the mitochondrial genome and the remaining components being nuclear encoded (Walker *et al.*, 1991, 1995; Arnold *et al.*, 1998). A combination of structural and biochemical data has shone light on the shape of the complex and its enzymatic mechanism (Seelert and Dencher, 2011). The F₁F₀ATPase has been described as a rotary motor, in which proton translocation within the F₀ portion drives the intramolecular rotation of hydrophobic rotor subunits (subunit c oligomers) and eventually movement of a central stalk with the catalytic F₁ head; this is in concert with nucleotide binding, form the basic of ATP synthesis (Stock *et al.*, 1999).

Bacteria	Mitochondria		Domain Association
	<i>S.cerevisiae</i>	<i>H.sapiens</i>	
α	α	α	F ₁
β	β	β	
γ	γ	γ	
ϵ	δ	δ	
-	ϵ	ϵ	
δ	OSCP (Atp5)	OSCP	
<i>a</i>	6 (Atp6)	<i>a</i>	F ₀
-	8 (Atp8)	A6L	
<i>c</i>	9 (Atp9)	<i>c</i>	
<i>b</i>	4 (Atp4)	<i>b</i>	
-	<i>d</i>	<i>d</i>	
-	<i>h</i>	F6	
-	<i>f</i>	<i>f</i>	
-	<i>e</i> (Atp21)	<i>e</i>	
-	<i>g</i> (Atp20)	<i>g</i>	
-	<i>i</i> (Atp18)	-	
-	<i>k</i> (Atp19)	-	
-	Inh1	IF1	
-	Stf1	-	associated
-	Stf2	-	

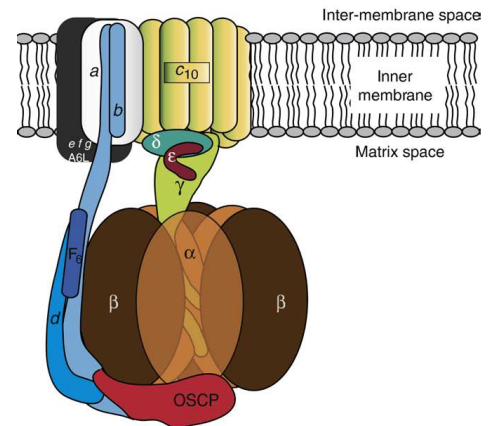


Figure 4. Nomenclature and organization of F₁F₀ATPase subunits in yeast and *H.sapiens*. (adapted from Kucharczyk *et al.*, 2009)

2.6 High ordered organization of the F₁F₀ATPase: from dimers to oligomers

Early electron micrographs revealed that the F₁F₀ATPases are found adjacent to one another (Burton, 1979). Consequently, deep-etch freeze electron microscopy of mitochondria of *Paramecium multimicronucleatum*, revealed an arrangement of F₁F₀ATPase into double rows of particles (Allen *et al.*, 1989). These initial observations, followed by biochemical isolations with mild detergents and results based on cryo-electrotomographies indicated that the F₁F₀ATPase forms ribbons composed of homodimers at the mitochondrial cristae membranes (Schägger and Pfeiffer, 2000; Strauss *et al.*, 2008; Davies *et al.*, 2011). The F₁F₀ATPase in its dimeric form, has been shown in a wide range of organisms such as mammals, plant species, *Drosophila*, and various yeast such as *P. anserina*, *N. crassa*, and *Y. lipolytica* (Straus *et al.*, 2008; Davies *et al.*, 2011). Also, higher oligomeric states of the F₁F₀ATPase homodimers have been found (Eubel *et al.*, 2003; Krause *et al.*, 2005; Thomas *et al.*, 2008; De los Rios Castillo *et al.*, 2011). Moreover, studies using atomic force microscopy revealed the F₁F₀ATPase dimers in their native environment (Buzhynskyy *et al.*, 2007). Even though there is significant evidence of the dimeric form, there is yet to be a consensus on the structural nature of homodimeric interactions. Single particle

cryoelectron microscopy studies indicate that contact sites between the two monomers are located between the two F_0 membrane portions, whereas other studies revealed an involvement of the F_1 regions (Seelert and Dencher, 2011). Furthermore, the angles between the two monomers appears to vary dependent on the organism in question: the angle varied between 45° and 70° in yeast and *Polytomella*, while it was found to 40° for bovine dimers (Seelert *et al.*, 2009).

2.7 Functional roles of the F_1F_0 ATPase dimers

In combining clear native PAGE (CN-PAGE) together with an in-gel activity F_1F_0 ATPase assay, it was shown that monomers, dimers, or oligomers of the F_1F_0 ATPase have no significant differences in ATP hydrolysis thus ruling out a role of oligomerization in activity (Krause *et al.*, 2005). This led to the proposal of other functions with respect to F_1F_0 ATPase localization at cristae membranes. First, the “quinary structure” model proposes that organizing metabolic enzymes into stoichiometric complexes increases the efficiency of substrate channeling (the direct transfer of metabolic intermediates to subsequent processing steps) (Srere, 1999). Thus together with the associations of other respiratory chain supercomplexes, a “respirasome” is formed, which allow easier electron transport between complexes. Second, a series of F_1F_0 ATPase dimers allows the formation of a strong local curvature and thus a local proton trap at the cristae apex (Strauss *et al.*, 2008). The stringent ribbon arrangement at the cristae membrane tips generates a local proton gradient in the adjacent cristae space, thus optimizing the ΔpH required for the proton motive force used for ATP synthesis (Buzhynskyy *et al.*, 2007; Strauss *et al.*, 2008; Davies *et al.*, 2011). Moreover, oligomerization of the F_1F_0 ATPase in mammals has been considered to serve a regulatory role to reduce ATP synthesis in conditions of low electron transfer activity and reduced membrane potential (Bornhövd *et al.*, 2006). In these instances, oligomerization is thought to be a first-order regulation step, which allows the inhibitor protein IF1 to consequentially bind and reduce F_1F_0 ATPase catalytic activity (Wittig and Schägger, 2009).

From a structural point of view, dimerization stabilizes the holo-enzyme structure by connecting the two-stator parts in the dimer (Wittig and Schägger, 2009). Oligomerization compensates torques generated on the stators (F_0) allowing only rotor

(F₁) movement, thus blocking energy dissipation, which may result from holo-enzyme rotation around its own axis in the absence of an adjacent monomer or holo-enzyme (Buzhynskyy *et al.*, 2007).

2.8 F₁F₀ATPase dimerization factors

In *S.cerevisiae*, various proteins have been described and characterized to be dimerization factors of the F₁F₀ATPase. The current model of F₁F₀ATPase dimerization (Figure 5) entails a step-wise assembly in which dimerization factors associate to the membrane bound F₀ (Wagner *et al.*, 2010). Assembly is mediated by sequential binding of the various subunits to form the final dimeric form. Assembly begins with the association of subunit i (Atp18), followed by subunits g (Atp20) and e (Atp21) association to form a primed monomer. Two primed monomers associate to give rise to a primed dimer (not shown). Final association of the dimerization factor k (Atp19) gives rise to the mature F₁F₀ATPase dimer.

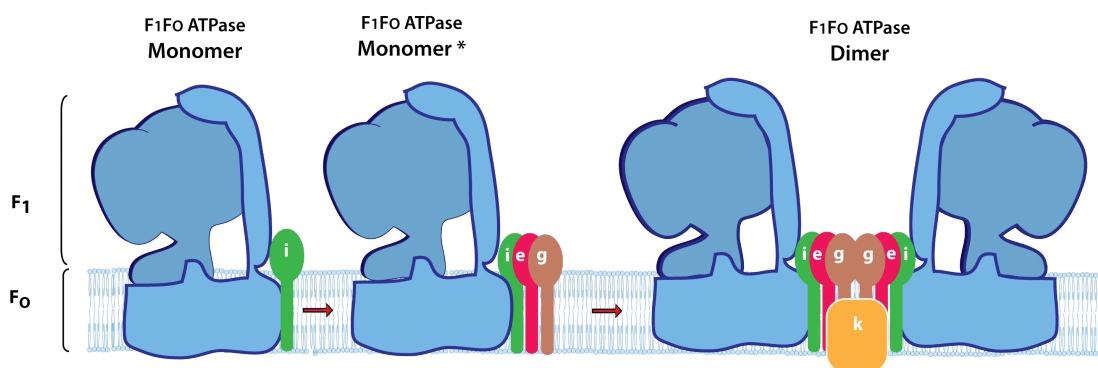


Figure 5. Stepwise assembly of the F₁F₀ATPase dimer. Sequential association of subunit g (Atp20) and subunit e (Atp21) leads to the formation of a primer monomer. Association of subunit i (Atp18) facilitates the incorporation of Atp20 and Atp21. The association of two primed monomers forms a mature dimer which stably associates with Atp19. Figure adapted from Wagner *et al.* (2010). * indicates primed monomer.

The described dimerization factors are not essential for F₁F₀ATPase activity, exemplified by unaffected growth of deletion mutants on non-fermentable media (Arnold *et al.*, 1998; Paumard *et al.*, 2002a; Soubannier *et al.*, 2002). Characteristically, these dimerization factors are of small molecular size and contain a single transmembrane domain, which allows them to exert their interaction with the membrane embedded F₀ domain (Arnold *et al.*, 1997, 1998; Soubannier *et al.*, 2002;

Paumard *et al.*, 2002a; Wagner *et al.*, 2009, 2010). Atp21 contains a C-terminal coiled-coil domain, which has been demonstrated to stabilize the F₁F₀ATPase dimeric form (Everard-Gigot *et al.*, 2005). Moreover, Atp20 and Atp21 both contain a GxxxG motif in their transmembrane domains (Arselin *et al.*, 2003; Bustos and Velours; 2005; Saddar and Stuart, 2005; Bornhövd *et al.*, 2006). This motif is characterized by two glycine residues separated by any three amino acids, and has been previously been demonstrated to stabilize homo- and heterodimers of other membrane proteins such as Glycophorin A, by supporting helix-helix interactions of neighboring membrane proteins (Russ and Engelman, 2000). To this end, a combination of crosslinking approaches and site directed mutagenesis studies has demonstrated the role of the F₁F₀ATPase dimerizations motif; any amino acids changes in the GxxxG motifs of either Atp20 or Atp21 has abolished dimerization (Arselin *et al.*, 2003).

Besides the small F₁F₀ATPase dimerization factors described above, the IF1 protein, which inhibits ATP hydrolysis and thus F₁F₀ATPase activity has been accredited with a role in promoting dimerization in mammalian mitochondria, but not in yeast (García *et al.*, 2006; Campanella *et al.*, 2009; Wittig *et al.*, 2010). Moreover, other subunits of the F₁F₀ATPase, such as subunit *a*, *b*, *h*, and γ , have been shown to play a role in dimerization (Soubannier *et al.*, 2002; Fronzes *et al.*, 2003). Subunit *a*, component of the ATPase proton channel, localizes to the monomer-monomer interface, and has been demonstrated to have an additive effect to subunits Atp20 and Atp21 in dimerization (Steed and Fillingame, 2008; Wittig *et al.*, 2008; Wittig *et al.*, 2010). The peripheral stalk, connecting the F₁ and F₀ domains, is composed of subunits *b* (subunit 4 in yeast) and *h*. Subunit *b* and *h* of two F₁F₀ATPase monomers have been shown to be in close proximity to each in the dimer and in proximity to subunits Atp18, Atp19, Atp20 and Atp21 (Spannagel *et al.*, 1998; Soubannier *et al.*, 2002; Velours and Arselin, 2000; Wittig *et al.*, 2008). Indeed, manipulation of subunit *b* first membrane segment and intermembrane space loops prevented dimerization of the F₁F₀ATPase (Soubannier *et al.*, 2002). On the other hand, the N and C termini of subunit γ , part of the catalytic rotor, have been found to be required for proper monomer assembly and dimerization (Dian *et al.*, 2008).

Whereas dimerization factors have been exclusively characterized in *S.cerevisiae*, information is still lacking on what mediates dimerization of the

F₁F₀ATPase in higher eukaryotes. Atp20 has a significant homolog (subunit g) in mammals and has been described to be part of the holo-enzyme complex, however any role in relation to F₁F₀ATPase dimerization has not been described.

2.9 F₁F₀ATPase dimerization and maintenance of cristae morphology

F₁F₀ATPase dimers and oligomers, which align across cristae membrane tips, are directly involved in the maintenance and biogenesis of cristae membranes (Giraud *et al.*, 2002; Paumard *et al.*, 2002b; Gavin *et al.*, 2004; Rak *et al.*, 2007; Velours *et al.*, 2009). F₁F₀ATPase dimers are conceived to have a role in cristae membrane morphology by inducing a strong local positive curvature of the inner membrane in the direction of the matrix (Dudkina *et al.*, 2006). This, by part, is due the characteristic angle between monomers which has the potential to form an inflexible arc and thereby protrusions of the inner membrane (Paumard *et al.*, 2002b).

Whereas dimerization does not affect ATP synthesis and overall respiratory capacity of mitochondria, the absence of F₁F₀ATPase dimers is directly linked to aberrant mitochondrial inner membrane morphologies (Paumard *et al.*, 2002b; Arselin *et al.*, 2003, 2004; De los Rios Castillo *et al.*, 2004; Minauro-Sanmiguel *et al.*, 2005). The presence of assembled dimers rather than F₁F₀ATPase activity is required for cristae biogenesis (Rak *et al.*, 2007). The absence of the small dimerization factors, Atp20 or Atp21, leads to a disorganized inner mitochondrial membrane, which lack apparent cristae (Figure 6) (Paumard *et al.*, 2002b; Arselin *et al.*, 2003; Arselin *et al.*, 2004). Absence of Atp20 or Atp21 subunits causes enlargement of CJ diameters, promotes cristae branching as well as a decrease in the number of cristae tips (Rabl *et al.*, 2009). Wildtype mitochondria contain poorly defined narrow and diminutive cristae, whereas *ATP20* and *ATP21* deletion mutants have well defined inner membrane sheets, composed of two or three concentric double leaflet membrane layers which transverse the mitochondria (Paumard *et al.*, 2002b; Arselin *et al.*, 2004). In these mutants, the inner membrane is thus described to have ‘onion-like’ structures, which are understood to be a result of uncontrolled biogenesis of the inner membrane (Arselin *et al.*, 2004).

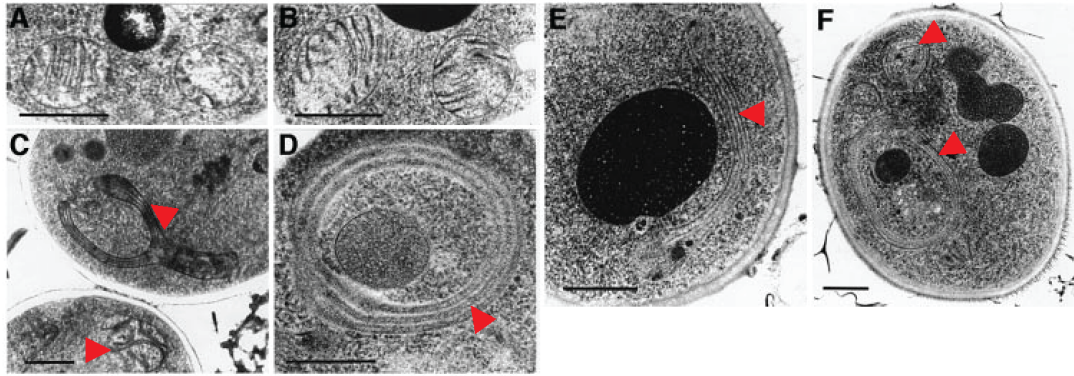


Figure 6. Aberrant mitochondrial morphology in *ATP20* and *ATP21* deletion mutants. Figure adapted from Paumard *et al.*, 2002. Electron micrographs; Scale bars indicate 0.5 μ m. Red arrows indicate abnormal mitochondria. (A) Wildtype; (B) *atp18* Δ ; (C) and (D) *atp20* Δ ; (E) and (F) *atp21* Δ .

In addition, crosslinking F_1F_0 ATPase dimers via the *b* subunits, Atp18, or γ subunits has been shown to eliminate cristae (Spannagel *et al.*, 1998; Paumard *et al.*, 2002b; Gavin *et al.*, 2004). The absence of subunit *b* (subunit 4/Atp4), involved in dimerization, also causes, albeit smaller, onion-like structures (Soubannier *et al.*, 2002). Similar small onion-like structures are also observed in ρ^- mitochondria (Paumard *et al.*, 2002b). Since *atp4* Δ mutants, which lack a fully assembled F_1F_0 ATPase and ρ^- mitochondria are respiratory deficient, smaller onion-like structures are believed to be formed due to the lack of sufficient energy for the biogenesis and extension of the inner membrane observed in *ATP20* and *ATP21* deletion mutants (Paumard *et al.*, 2002b). Nonetheless, the presence of a functional F_1F_0 ATPase is required for cristae biogenesis, exemplified by analysis of Atp1, Atp2, and Atp12 mutants, which completely lack cristae (Paumard *et al.*, 2002b). It is thus deduced that the lack of Atp20 or Atp21 in combination with an assembled functional F_1F_0 ATPase leads to the ‘onion-like’ phenotype observed in the mutants (Paumard *et al.*, 2002b; Velours *et al.*, 2009).

2.10 The inner membrane and cristae membrane architecture

Besides components of F_1F_0 ATPase, various other inner membrane proteins play a role in inner membrane and cristae organization. These proteins include Mitofilin (and its yeast homolog Fcj1) and CHCHD3 (John *et al.*, 2005; Rabl *et al.*, 2009; Darshi *et*

al., 2011). Moreover, certain proteins involved in apoptosis (OPA1/Mgm1) and mitochondrial fusion and fission play a part in determining proper cristae morphology.

The highly abundant mitochondrial protein Mitofilin is expressed as two splice variants with protein products sized 88 and 90 kDa respectively (Odgren *et al.*, 1996; Gieffers *et al.*, 1997). Mitofilin is characterized by a cleavable N-terminal targeting sequence, a membrane-anchoring domain, and central coiled coil domain (Odgren *et al.*, 1996; John *et al.*, 2005). It is anchored to the inner membrane in which the majority of its surface is exposed to the IMS and is enriched in the narrow interface located between the inner and outer membranes (Gieffers *et al.*, 1997; John *et al.*, 2005). A role for Mitofilin in cristae biogenesis has been deduced when its protein levels were down-regulated by RNA interference (RNAi) in HeLa cultured cells, in which the mitochondrial inner membrane was disorganized into a membranous labyrinth composed of tightly packed stacks of membrane sheets (John *et al.*, 2005). Moreover, the inner membranes, which had an increased inner membrane to outer membrane ratio, were devoid of cristae and cristae junctions, highlighting a role for Mitofilin in cristae junction formation (John *et al.*, 2005).

The role of Mitofilin in inner membrane biogenesis appears to be conserved in other species. Mutation of the two *C.elegans* homologs, IMMT-1 and IMMT-2, also leads to stacked inner membrane networks and to a reduced number of cristae junctions (Mun *et al.*, 2010). Interestingly, the Mitofilin *C. elegans* homologs, IMMT-1 and IMMT-2 are described to behave as large complexes associated with the F₁F₀ATPase in CN-PAGE (Mun *et al.*, 2010). The yeast homolog, Fcj1 (formation of cristae junction 1) is also involved in cristae biogenesis (Rabl *et al.*, 2009). Fcj1, like Mitofilin, is enriched at cristae junctions at the mitochondrial inner membrane and is primarily exposed to the IMS. Similarly, yeast mutants that lack Fcj1, are devoid of cristae junctions and exhibit aberrant mitochondrial morphology exemplified by parallel concentric stacks of inner membrane. A direct role for Fcj1 in cristae biogenesis has been shown by overexpression of *FCJ1*, which leads to an increase in cristae junction diameters, as well as increased cristae junction formation and branching (Rabl *et al.*, 2009).

In addition, there is an antagonism between Fcj1 and F₁F₀ATPase subunits Atp20 and Atp21 in controlling local inner membrane curvature and cristae formation. Fcj1 does not affect F₁F₀ATPase monomers or dimers but rather impairs the formation of higher oligomers (Rabl *et al.*, 2009). Whereas deletion of *FCJ1* does not affect steady state protein levels of Atp20 or Atp21, nor does the deletion of *ATP20* or *ATP21* affect Fcj1 levels, a double deletion of either *FCJ1/ATP20* or *FCJ1/ATP21* leads to the formation of concentric (vesicle-like) cristae membranes completely devoid of cristae junctions. In this antagonistic model, the presence of F₁F₀ATPase oligomers and thus dimerization factors Atp20 and Atp21 favors positive membrane curvature and ensuing formation of cristae tips (Rabl *et al.*, 2009). In contrast, Fcj1 destabilizes F₁F₀ATPase oligomerization, thus allowing cristae junction formation by favoring negative membrane curvature over positive curvature. Thus, differential localization of Fcj1 and Atp20/Atp21 at the mitochondrial inner membrane allows proper cristae junction and cristae tip formations (Rabl *et al.*, 2009).

Immunoprecipitations and a yeast two-hybrid assay indicated that Mitofilin form a homotypic interaction assembling into a large (>1 MDa) complex residing at the inner membrane/outer membrane interface (John *et al.*, 2005). Also, it was shown to interact with six other proteins: Metaxin 1, Metaxin 2, SAM50, CHCHD6, DnaJC11, and CHCHD3 (Xie *et al.*, 2007). Metaxins 1 and 2 are cytosolic proteins, which associate with the mitochondrial outer membrane and are involved in protein import to the mitochondria (Abdul *et al.*, 2000). SAM50, component of the outer membrane SAM complex is also involved in protein import and biogenesis, whereas DnaJC11 is a member of the 40 kDa heat shock protein family and may be involved in protein import and folding (Xie *et al.*, 2007). The evidence of Mitofilin interaction with the Metaxins, SAM50, and DnaJC11, thus links cristae junction formation with mitochondrial protein import. Moreover, CHCHD6 has been recently described to take part in the regulation of mitochondrial cristae morphology, cell growth, ATP production and oxygen consumption (An *et al.*, 2012).

In addition, CHCHD3 is critical for cristae structure (Darshi *et al.* 2011). The protein is highly conserved in mammals with no homologs found in fungi or plants. Knockdown of CHCHD3 resulted in fragmented cristae or even their complete loss. Moreover, the average opening diameter of cristae junctions was reduced by 50% but

number of cristae junction was not affected, indicating a possible role of CHCHD3 in cristae junction architecture and maintenance rather than formation (Darshi *et al.*, 2011).

All together, Mitofilins (Mitofilin/ Fcj1/ IMMT-1, IMMT-2) may control the formation of cristae junctions by inhibiting excessive growth and expansion of the inner membrane (John *et al.*, 2005, Rabl *et al.*, 2009, Mun *et al.*, 2010). By forming a multimeric complex via homotypic interactions, they may form a filamentous scaffold, which supports the inner membrane and prevents its expansion (John *et al.*, 2005, Xie *et al.*, 2007, Mun *et al.*, 2010). Evidence of Mitofilin interaction with the Metaxins and SAM50, not only links the cristae maintenance machinery with mitochondrial protein import, but also connects the inner membrane with the outer membrane, an interaction which may further support a rigid scaffolding model in maintenance of mitochondrial inner membrane architecture.

The overall shape of the mitochondrial reticulum is dependent on continuous mitochondrial fission and fusion processes, which regulate mitochondrial morphology and number. Mitochondrial fission in yeast is dependent on the evolutionary conserved GTPase Fzo (Mfn in mammals), Ugo1, as well as Mgm1 (OPA1 in mammals) (Okamoto and Shaw, 2005). OPA1/Mgm1, a large dynamin related GTPase, is anchored at the cristae junctions and exposed to the IMS (Olichon *et al.*, 2002). Mitochondria with mutated or depleted OPA1/Mgm1 in yeast or HeLa cultured cells have fragmented spherical mitochondria with characteristically simple inner membrane organization, an effect of disrupted mitochondrial fusion (Olichon *et al.*, 2002; Griparic *et al.*, 2004; Mannella 2008). Moreover, depletion of OPA1 leads to the formation of aberrant curved vesicle-like cristae (Olichon *et al.*, 2002). Besides its role in maintenance of the mitochondrial inner membrane, OPA1 has a role in apoptosis. Fragmentation of mitochondria during apoptosis is dependent on the proteolytic processing of OPA1 (Duvezin-Caubet *et al.*, 2006), whereas a loss of OPA1 commits cells to apoptosis in the absence of further stimuli (Olichon *et al.*, 2003). The role of OPA1 in apoptosis is proposed to involve cytochrome *c* sequestration and compartmentalization within the cristae membrane (Olichon *et al.*, 2003). This may be mediated by OPA1 localization to the inner membrane and its control of cristae junction openings, hence preventing premature release of cytochrome *c* in the absence

of apoptotic stimuli (Frezza *et al.*, 2006). Interestingly, OPA1 function links cristae biogenesis and apoptosis, which includes extensive remodeling of the cristae membrane (Scorrano *et al.*, 2002). This relationship is further exemplified by protein MICS1 that is involved in both maintenance of mitochondrial morphology and cytochrome *c* release during apoptosis (Oka *et al.*, 2008). MICS1-depleted mitochondria, like OPA1/Mgm1 mutants, had curved vesicle-like cristae (Oka *et al.*, 2008).

Mgm1 has been described to have a chaperone-like function of the F_1F_0 ATPase dimerization factor Atp21, in which the loss of Mgm1 inhibits F_1F_0 ATPase dimerization (Amutha *et al.*, 2004). This effect on dimerization might explain cristae membrane anomalies of Mgm1/OPA1 mutants (Mannella, 2008). Moreover, OPA1 has been shown to exist in a complex containing Mitofilin and SAM50, further advocating its role in the regulation of cristae morphology (Darshi *et al.*, 2011). This is further exemplified by the observation that depletion of Prohibitins (proteins involved in regulation of OPA1) leads to loss of cristae (Osman *et al.*, 2009; Zick *et al.*, 2009). Overall, OPA1/Mgm1 demonstrates a role in mitochondrial fusion in cristae morphology. In addition, loss of cristae is observed in mutants of Mdm33, a protein involved in inner membrane fission (Messerschmitt *et al.*, 2003; Okamoto and Shaw, 2005).

2.11 Models of cristae biogenesis

Evidently, various proteins integrally or peripherally associated with the mitochondrial inner membrane are involved in the biogenesis and maintenance of cristae membrane. The differences in the inner membrane morphologies of different mutants highlight the differences in the various proteins' functions exemplified by their different localizations (Figure 7). F_1F_0 ATPase dimers favor positive curvature and are vital for cristae membrane tip formation, whereas Mitofilin/Fcj1 and OPA1 are required for cristae junction maintenance. The processes governing cristae morphology yet appear to be interconnected by dependence of Atp21 on OPA1/Mgm1 (Amutha *et al.*, 2004) and modulation of Mitofilin/Fcj1 or F_1F_0 ATPase oligomerization (Rabl *et al.*, 2009).

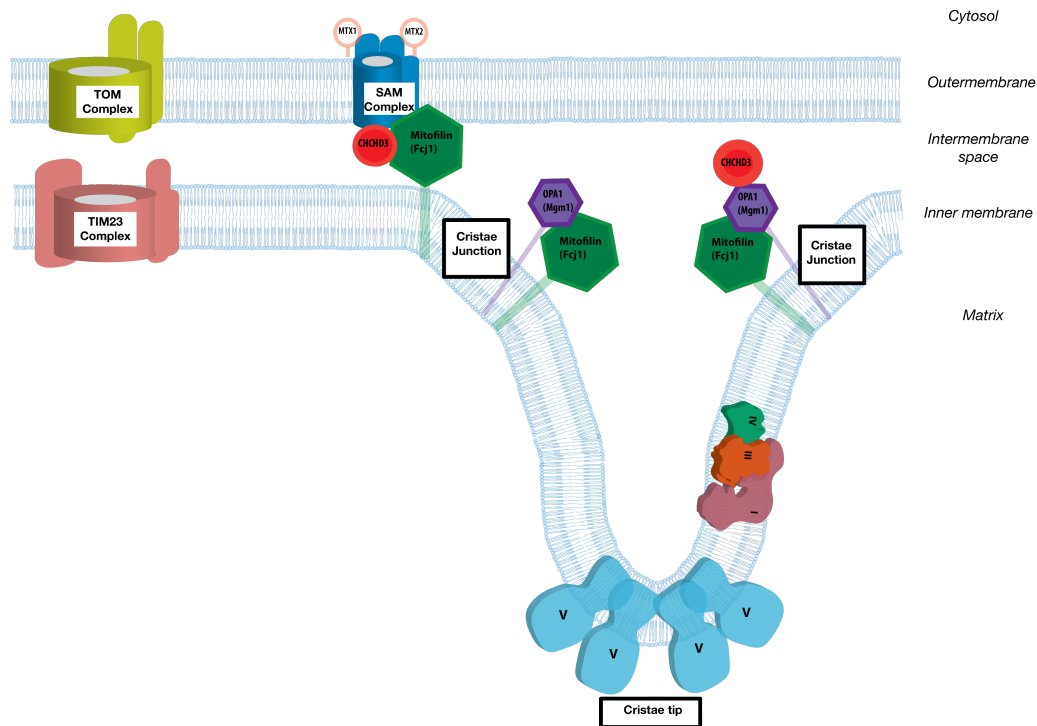


Figure 7. Overview of factors involved in cristae biogenesis and maintenance. The import translocases (TOM and TIM) are found at the IBM, whereas the respiratory chain is found at cristae membranes. The F_1F_0 ATPase is located at cristae tips/apex and contributes to cristae shape. Mitofilin and OPA1 are located at cristae openings and control cristae junction width. Mitofilin also interacts with CHCHD3, the SAM complex, and Metaxins.

With respect to cristae, various theoretical models have been proposed to explain cristae biogenesis, illustrated in Figure 8, as reviewed by Zick *et al.* (2009). Consideration of these models may provide explanations for the various aberrant phenotypes of mitochondrial morphology mutants.

A) *Invagination model / Late cristae junction model*

This model postulates that bending energy is sufficient to form spontaneous invaginations of the inner membrane giving rising to cristae membranes provided the continuous biogenesis of the inner membrane and a constant outer membrane surface (Renken *et al.*, 2002). The proposed bending energy can be derived from lipid composition and/or curvatures mediated by large protein complexes such as the F_1F_0 ATPase dimer (Paumard *et al.*, 2002a). Consequently, cristae junctions are formed once cristae membrane tips are made.

B) Balloon model / Early cristae junction model

Stable ring-like nascent cristae junction structures are formed at the IBM. Cristae are then formed by invagination, in which the nascent cristae junction structures act as an entry point for lipids and proteins (Zick *et al.*, 2009).

C) De novo vesicle germination model

Cristae membranes are formed from mitochondrial matrix vesicles that are formed 'de novo' from single phospholipids particles that later fuse to the IBM (Zick *et al.*, 2009).

D) Cristae fusion/fission model

This model proposes that cristae formation is dynamic, in which cristae membrane vesicles may continuously fuse from one side of the inner membrane to another (fission/fusion). Moreover, the observation that cristae morphology changes under different physiological conditions in a reversible manner supports dynamic rather than static nature of cristae propagation (Mannella *et al.*, 2001).

E) Fusion remnant model

This model proposes that during mitochondrial fusion, cristae junctions initially formed when the inner membrane of two mitochondria fuse together. Cristae membranes are thus remnants of the fusion event. Membrane remodeling is then required to induce curvatures leading to a tubular cristae membrane structure.

F) Hemifusion model

Similar to the 'fusion remnant' model, cristae membranes are formed in events following mitochondrial fusion. The site, at which two opposing inner membranes fuse, forms a phospholipids vesicle in the matrix, thus also combining the 'de novo vesicle germination model'. Once the vesicle is formed, it fuses to the IBM to form cristae. This model makes the assumption that inner mitochondrial fusion is mediated by hemi-fusion, a membrane fusion intermediate formed when leaflets of two opposing membranes merge while distal remain distant (Chernomordik and Kozlov, 2005). Hemi-fusion allows the formation of the cristae-vesicle.

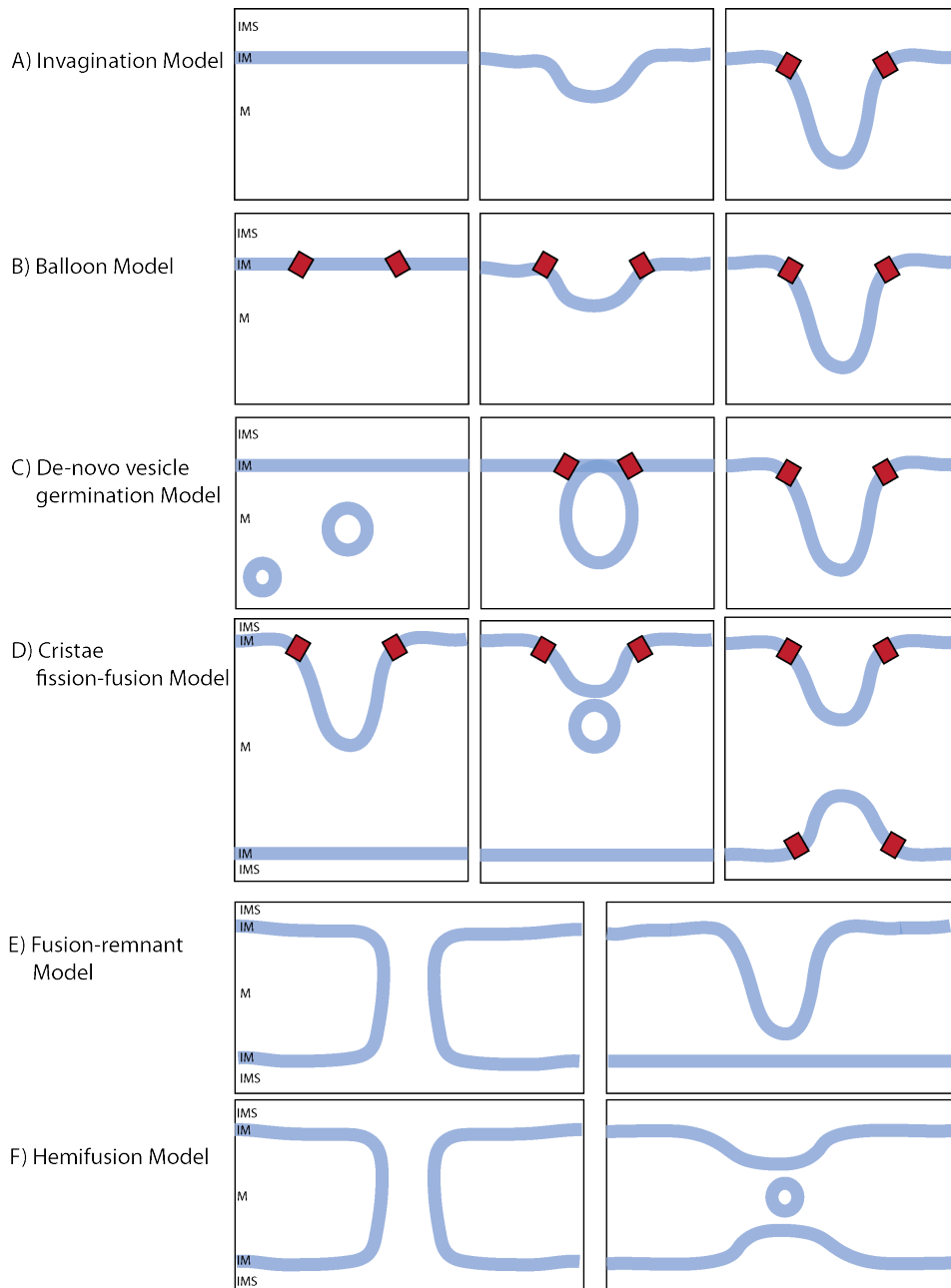


Figure 8. Hypothetical models of cristae biogenesis. Adapted from Zick *et al.* (2009). IM, inner membrane; M, matrix.

2.12 Aims of this study

Structural subunits of the F_1F_0 ATPase are involved in dimerization (Soubannier *et al.*, 2002; Fronzes *et al.*, 2003). In addition, small F_0 associated yeast proteins (Atp18, Atp19, Atp20, and Atp21) mediate dimerization in yeast (Arnold *et al.*, 1997, 1998; Soubannier *et al.*, 2002; Paumard *et al.*, 2002a; Wagner *et al.*, 2009, 2010). However, their presence does not seem to be conserved in higher eukaryotes. To this end, the aim of this study is to identify novel F_1F_0 ATPase dimerization factors in higher eukaryotes. For this purpose, an *in silico* based search will be used. The bioinformatics approach will be based on searching yeast open reading frames (ORFs) with human homologs. The search will also take into account the various characteristics of known dimerization factors. Mitochondria isolated from human cultured cells (HEK29T) cells will be used to analyze putative F_1F_0 ATPase dimerization factors. On the other hand, mitochondria isolated from *S.cerevisiae* will be used to analyze the yeast homologs. Once identified, putative factors will be characterized for possible functions in dimerization. As the F_1F_0 ATPase dimerization factors are membrane proteins (Wagner *et al.*, 2010), putative dimerization factors will be tested first for their membrane association. A role in dimerization will be assessed by investigating F_1F_0 ATPase interaction and by analyzing the various available yeast mutants. In addition, as the absence of the dimerization factors Atp20 and Atp21 lead to various aberrations in cristae morphology (Paumard *et al.*, 2002b; Arselin *et al.*, 2003; Arselin *et al.*, 2004), a role in mitochondrial architecture that putative dimerization factors might have will also be considered.

3. MATERIALS AND METHODS

3.1 Materials

3.1.1 Chemicals

Product	Supplier
Acetone	AppliChem (Steinheim, Germany)
Acetic acid	Roth (Karlsruhe, Germany)
Acrylamide/ Bisacrylamide solution	Roth (Karlsruhe, Germany)
Agar-Agar	Roth (Karlsruhe, Germany)
Adenosine triphosphate (ATP)	Sigma (Steinheim, Germany)
Agarose NEEO Ultra-Qualität Roti®garose	Roth (Karlsruhe, Germany)
Ammonium acetate	Merck (Darmstadt, Germany)
Ammoniumpersulfate (APS)	Merck (Darmstadt, Germany)
Ampicillin	AppliChem (Steinheim, Germany)
Bacto™Peptone	BD (Sparks, USA)
Bacto™ Tryptone	BD (Sparks, USA)
Bacto™ Yeast Extract	BD (Sparks, USA)
Bis-Tris	Roth (Karlsruhe, Germany)
Bovine serum albumin (BSA)	Sigma (Steinheim, Germany)
Bradford-Reagent	Bio-rad (Richmond, USA)
Bromophenolblue	Merck (Darmstadt, Germany)
6-amino Caproic acid	Sigma (Steinheim, Germany)
Coomassie Brilliant Blue G-250	Serva (Heidelberg, Germany)
Coomassie Brilliant Blue R-250	Serva (Heidelberg, Germany)
Complete Supplement Mixture – Uracil (CSM-URA)	MP Biomedicals (Eschwege, Germany)
Creatine Phosphate	Roche (Manheim, Germany)
L-Cysteine.HCl	Merck (Darmstadt, Germany)
Cytochrome <i>c</i> (bovine heart)	Sigma (Steinheim, Germany)
Desthio-Biotin	IBA GmbH (Göttingen, Germany)
3,3' Diaminobenzidine (DAB)	Sigma (Steinheim, Germany)
Digitonin	Calbiochem (La Jolla, U.S.A)
Dimethyl pimelimidate dihydrochloride (DMP)	Sigma (Steinheim, Germany)
Dimethylsulfoxide (DMSO)	Appllichem (Darmstadt, Germany)
Dipotassium hydrogen phosphate	Roth (Karlsruhe, Germany)
Dithiothreitol (DTT)	Roth (Karlsruhe, Germany)
Dulbecco's Modified Eagle Medium (DMEM)	Gibco (Karlsruhe, Germany)
Ethidium bromide	AppliChem
Ethylenediaminetetraacetic acid (EDTA)	Roth (Karlsruhe, Germany)
Glucose	Roth (Karlsruhe, Germany)
Glycerin	Roth (Karlsruhe, Germany)
Glycin	Roth (Karlsruhe, Germany)
Glycerol	Sigma (Steinheim, Germany)
Heavy isotope labeled $^{13}\text{C}_6$ $^{15}\text{N}_2$ -lysine and $^{13}\text{C}_6$ $^{15}\text{N}_4$ -arginine	Euriso-Top (Saarbrücken, Germany)
HEPES	Roth (Karlsruhe, Germany)

Herring sperm	Promega (Mannheim, Germany)
Lead(II) nitrate $Pb(NO_3)_2$	Sigma (Steinheim, Germany)
Magnesium acetate	Merck (Darmstadt, Germany)
Magnesium chloride ($MgCl_2$)	Merck (Darmstadt, Germany)
Magnesium sulfate ($MgSO_4$)	Roth (Karlsruhe, Germany)
β -Mercaptoethanol	Sigma (Steinheim, Germany)
Methanol	Roth, (Karlsruhe, Germany)
Milk	Reformhaus (Essen, Germany)
L-Methionine	Serva (Heidelberg, Germany)
3-(N-morpholino) propanesulfonic acid (MOPS)	Sigma (Steinheim, Germany)
Lithium acetate	Applichem (Darmstadt, Germany)
Nicotinamide adenine dinucleotide hydrate (NADH)	Roche (Manheim, Germany)
4-Nitrotetrazoliumchloride blue (NBT)	Sigma (Steinheim, Germany)
N,N,N',N'-Tetramethylethylene diamine (TEMED)	Roth (Karlsruhe, Germany)
Polyethylene glycol 4000 (PEG-4000)	Merck (Darmstadt, Germany)
PMSF	Roth (Karlsruhe, Germany)
Potassium acetate	Merck (Darmstadt, Germany)
Potassium chloride	Roth (Karlsruhe, Germany)
Potassium dihydrogen phosphate	Merck (Darmstadt, Germany)
Sodium borat	Sigma (Steinheim, Germany)
Sodium azide	Sigma (Steinheim, Germany)
Sodium Chloride	Roth (Karlsruhe, Germany)
Sodium deoxycholate	Sigma (Steinheim, Germany)
Sodium-dithionite (Na-dithionite)	Fluka (Steinheim, Germany)
Sorbitol	MP Biomedicals (Illkirch, France)
SDS	Roth (Karlsruhe, Germany)
Tricine	Roth (Karlsruhe, Germany)
Trifluoroacetic acid (TCA)	Merck (Darmstadt, Germany)
Tris(hydroxymethyl)-aminomethane (Tris),	Roth (Karlsruhe, Germany)
Triton X-100	Sigma (Steinheim, Germany)
Tween-20	Roth (Karlsruhe, Germany)
Yeast Nitrogen base	Difco BD (New Jersey, USA)
L-uracil	Sigma (Steinheim, Germany)

3.1.2 General buffers and solutions

Buffer	Recipe
SDS-PAGE sample buffer	2% SDS, 10% Glycerol, 60 mM Tris pH 6.8, 1% β -mercaptoethanol, 0.01% Bromophenolblue
SDS-PAGE running buffer	25 mM Tris pH 6.8, 190 mM Glycine, 1% (w/v) SDS
SDS-PAGE resolving gel buffer	1.87 M Tris pH 8.8
SDS-PAGE stacking gel buffer	0.8 M Tris pH 6.8
Transfer/Blot Buffer	20 mM Tris 150 mM Glycin 0.02% SDS

3x BN-PAGE gel Buffer	20% Methanol or Ethanol 200 mM 6-amino caproic acid 150 mM Bis-Tris /HCl pH 7.0
40x BN-PAGE Anode Buffer	2 M Bis-Tris / HCl pH 7.0
10x BN-PAGE Cathode Buffer	500 mM Tricine pH 7.0 150 mM Bis-Tris 0.2% Coomassie blue G250
10x BN Loading Dye	5% Coomassie blue G250 500 mM 6-amino caproic acid 100 mM Bis-Tris pH 7.0
10X TBS	200 mM Tris-HCl pH 7.5 1.25 M NaCl
TBS-T	1x TBS 0.1% Tween-20
TE buffer	10 mM Tris-Cl, pH 7.5. 1 mM EDTA
Standard Import Buffer	3% (w/v) fatty acid free BSA 250 mM sucrose 80 mM KCl 5 mM MgCl ₂ 2 mM KH ₂ PO ₄ 5 mM methionine 10 mM MOPS-KOH pH 7.2
SEM Buffer	250 mM sucrose 1 mM EDTA 10 mM MOPS pH 7.2
KPi Buffer	20 mM NaH ₂ PO ₄ /Na ₂ HPO ₄
10x PBS Buffer	1 M Tris 1 M Boric Acid 20 mM EDTA
Gel Staining Solution	MeOH 40% (v/v), Acetic acid 10% (v/v), H ₂ O 50% (v/v) Coomassie Serva Blue R250 0.15%
Gel Destaining Solution	MeOH 40% (v/v), Acetic acid 10% (v/v), H ₂ O 50% (v/v)
50x TAE Buffer	400 mM Tris-acetate, 10mM EDTA

3.1.3 Instruments

3.1.3.1 Centrifuges

Product	Supplier
5417R centrifuge	Eppendorf (Hamburg, Germany)
5424 centrifuge	Eppendorf (Hamburg, Germany)

5804R centrifuge	Eppendorf (Hamburg, Germany)
Sorvall RC 6 Plus	Thermo Scientific (Bad Homburg, Germany)
Sorvall RC 12BP	Thermo Scientific (Bad Homburg, Germany)
J2-MC	Beckman Coulter (Palo Alto, USA)
Optima™ MAX ultracentrifuge	Beckman Coulter (Palo Alto, USA)

3.1.3.2 Rotors

Product	Supplier
F45-30-11	Eppendorf (Hamburg, Germany)
F45-24-11	Eppendorf (Hamburg, Germany)
A-4-44	Eppendorf (Hamburg, Germany)
Sorvall F14S-6x250Y	Thermo Scientific (Bad Homburg, Germany)
Sorvall SS-34	Thermo Scientific (Bad Homburg, Germany)
Sorvall F10S-6x500Y	Thermo Scientific (Bad Homburg, Germany)
Sorvall H-12000	Thermo Scientific (Bad Homburg, Germany)
JA-20	Beckman Coulter (Palo Alto, USA)
TLA-55	Beckman Coulter (Palo Alto, USA)

3.1.3.3 Gel systems and Power supply

Product	Supplier
Mini PROTEAN® Tetra Cell	Bio-Rad (Richmond, USA)
Mini-Sub cell GT	Bio-Rad (Richmond, USA)
Hoefer SE 600 Ruby™ electrophoresis unit	GE Healthcare (Buckinghamshire, UK)
EPS-601 power supply	GE Healthcare (Buckinghamshire, UK)
GIBCO-BRL power supply 250EX	Life Technologies (Karlsruhe, Germany)
Ecoline Staredition RE107	Lauda (Lauda-Königshofen, Germany)
GD5040 gel dryer	Scie-PLas (Warwickshire, UK)
UV100 Transilluminator	Biometra (Göttingen, Germany)
T1 1 UV transilluminator	Biometra (Göttingen, Germany)

3.1.3.4 Photometers

Product	Supplier
Carry50 Bio UV/visible Spectrophotometer	Varian Inc (Palo Alto, USA)

Biophotometer	Eppendorf (Hamburg, Germany)
NanoVue	GE Healthcare (Buckinghamshire, UK)

3.1.3.5 Shakers

Product	Supplier
G25 Incubator shaker	New Brunswick Scientific Co. (Nürtingen, Germany)
innova®44 incubator shaker	New Brunswick Scientific Co. (Nürtingen, Germany)
innova®2300 platform shaker	New Brunswick Scientific Co. (Nürtingen, Germany)
Excella E10 platform shaker	New Brunswick Scientific Co. (Nürtingen, Germany)
Polymax 1040 shaker	Heidolph (Schwabach, Germany)
Shaker DRS-12	ELMI (Riga, Latvia)

3.1.3.6 Other instruments

Product	Supplier
Thermomixer Comfort	Eppendorf (Hamburg, Germany)
Savant SpeedVac concentrator	GMI (Ramsey, USA)
Vortex-GenieZ	Scientific Industries (New York, USA)
T-personal PCR machine	Biometra (Göttingen, Germany)
pH meter	inoLab (Straubing, Germany)
Potter S homogenizer	Sartorius (Göttingen, Germany)
Storm™ 820 PhosphorImager	GE Healthcare (Buckinghamshire, UK)
Fluorescence scanner FLA-9000	Fujifilm (Düsseldorf, Germany)
ÄKTApurifier system	GE Healthcare (Münich, Germany)
Superose 6 10/300 GL	GE Healthcare (Münich, Germany)
LAS 3000	Fujifilm (Düsseldorf, Germany)

3.1.4 Kits

Product	Supplier
Wizard® Plus SV Minprep DNA Purification System	Promega (Madison, USA)
Wizard® SV gel and PCR clean up System	Promega (Madison, USA)
HiSpeed® Plasmid Midi Kit	Qiagen (Hilden, Germany)

mMessage mMachine SP6	Ambion® (Austin, USA)
MEGAclear™ Purification of Transcription Reaction	Ambion® (Austin, USA)
Amersham™ Rabbit Reticulocyte Lysate System for <i>in vitro</i> translation	GE Healthcare (Buckinghamshire, UK)
Amersham™ ECL™	GE Healthcare (Buckinghamshire, UK)
Mobicol columns	MoBiTec (Göttingen, Germany)
Disposable Polypropylene Columns	Thermo Scientific (Bad Homburg, Germany)
Sulfolink Coupling Gel	Pierce (Rockford, USA)
ABI PRISM® BigDye® Terminator v1.1 Cycle Sequencing Kit	Applied Biosystems (Darmstadt, Germany)
KOD HotStart DNA polymerase	Novagen, Merck (Darmstadt, Germany)

3.1.5 Enzymes

Product	Supplier
Restriction Endonucleases	New England Biolabs (Ipswich, USA)
DNaseI	Roche (Manheim, Germany)
T4 DNA Ligase	New England Biolabs (Ipswich, USA)
Zymolyase	Seikagaku Biobusiness (Tokyo, Japan)
Proteinase K (PK)	Roche (Manheim, Germany)
Creatine Kinase (CK)	Roche (Manheim, Germany)

3.1.6 Antibodies

Table 1. Details of various antibodies used in this study

Primary Antibody	Organism	Source
α -Atp2	Yeast	AG Rehling (861)
α -ATP2	Human	Invitrogen
α -Atp5	Yeast	AG Rehling (1546)
α -Atp20	Yeast	AG Rehling (1517)
α -CHCHD3	Human	Abcam
α -Cox1	Yeast	AG Rehling (1538)
α -Cox2	Yeast	AG Rehling (1948)
α -Cox4	Yeast	AG Rehling (578)
α -COX6A1	Human	AG Rehling (3283)
α -COX	Human	Invitrogen
α -Cyt1	Yeast	AG Rehling (540)
α -F ₁ F ₀ ATPase	Human	Invitrogen
α -Fcj1	Yeast	AG Rehling (857)

α -HSPA9	Human	Abcam
α -Hsp70	Yeast	AG Rehling (657)
α -IMMT (Mitofilin)	Human	Abcam
α -MINOS1	Human	Abcam
α -Mio10	Yeast	AG Rehling (3459)
α -TACO1	Human	AG Rehling (3627)
α -Tim21	Yeast	AG Rehling (258)
α -TIM23	Human	AG Rehling (1526)
α -Tom70	Yeast	AG Rehling (657)
α -TOM70	Human	AG Rehling (3280)
α -Rip1	Yeast	AG Rehling (543)

Secondary Antibody	Organism	Source
Goat α -Rabbit	-	Dianova
Alexa Fluor	-	Invitrogen

3.1.7 Yeast strains

Table 2. Details of yeast strains used in this study including genotype and source.

Strain	Genotype	Source
BY4741	Mat a, his3- Δ 1 leu2 Δ 0 met15 Δ 0 ura3 Δ 0	Sikorski and Hieter, 1989
YPH499	Mat a, ade2-101 his3- Δ 200 leu2- Δ 1 ura3-52 trp1- Δ 63 lys2-801	Sikorski and Hieter, 1989
<i>atp20Δ</i>	Mat a, his3- Δ 1 leu2 Δ 0 met15 Δ 0 ura3 Δ 0; <i>atp20::kanMX4</i>	Open Biosystems
<i>atp2Δ</i>	Mat a, his3- Δ 1 leu2 Δ 0 met15 Δ 0 ura3 Δ 0; <i>atp2::kanMX4</i>	Open Biosystems
<i>fcj1Δ</i>	Mat a, his3- Δ 1 leu2 Δ 0 met15 Δ 0 ura3 Δ 0; <i>fcj1::kanMX4</i>	Open Biosystems
Fcj1 ^{ZZ}	Mat a, ade2-101 his3- Δ 200 leu2- Δ 1 ura3-52 trp1- Δ 63 lys2-801; <i>fcj1::FCJ1-ZZ-HIS3MX6</i>	Von der Malsburg <i>et al.</i> , 2011; Alkhaja <i>et al.</i> , 2012
<i>mio10Δ</i>	Mat a, his3- Δ 1 leu2 Δ 0 met15 Δ 0 ura3 Δ 0; <i>mio10::kanMX4</i>	Open Biosystems
Atp20 ^{ZZ}	Mat a, ade2-101 his3- Δ 200 leu2- Δ 1 ura3-52 trp1- Δ 63 lys2-801; <i>atp20::ATP20-ZZ-HIS3MX6</i>	This study; Alkhaja <i>et al.</i> , 2012
Atp5 ^{SF}	Mat a, ade2-101 his3- Δ 200 leu2- Δ 1 ura3-52 trp1- Δ 63 lys2-801; <i>atp5::ATP5-SF-HIS3MX6</i>	This study
Atp20 ^{SF}	Mat a, ade2-101 his3- Δ 200 leu2- Δ 1 ura3-52 trp1- Δ 63 lys2-801; <i>atp5::ATP20-SF-HIS3MX6</i>	This study
Mio10 ^{SF}	Mat a, ade2-101 his3- Δ 200 leu2- Δ 1 ura3-52 trp1- Δ 63 lys2-801; <i>mio10::MIO10-SF-HIS3MX6</i>	This study; Alkhaja <i>et al.</i> 2012

3.1.8 Yeast growth medium

Medium	Recipe
YPG	1% (w/v) yeast extract 2% (w/v) bactopectone 3% (w/v) glycerol
YPD	1% (w/v) yeast extract 2% (w/v) bactopectone 2% (w/v) glucose
YPS	1% (w/v) yeast extract 2% (w/v) bactopectone 2% (w/v) sucrose
SD	0.67% (w/v) yeast nitrogen base 0.7% (w/v) drop out mix of CSM-URA 20 µg/ml uracil 2% (w/v) glucose
SG	0.67% (w/v) yeast nitrogen base 0.7% (w/v) drop out mix of CSM-URA 20 µg/ml uracil 2% (w/v) glucose

3.1.9 Bacterial medium

LB medium	1% (w/v) tryptone 0.5% (w/v) yeast extract 170 mM NaCl
LB-Agar Plates	LB medium with 1.5% (w/v) agar

3.1.10 Bacterial strains

XL1-Blue	<i>SupE44 hsdR17 recA1 endA1 gyrA46 thi relA1 lac-F'[proAB+lacIq lacZΔM15 Tn10(tetr)]</i>
----------	---

3.1.11 Miscellaneous products

Product	Supplier
Polyvinylidene difluoride (PVDF) membranes	Millipore (Schwalbach, Germany)
Whatman paper	Heinemann (Schwäbisch Gmünd, Germany)
Protein Standards SDS-PAGE	Bio-Rad (Richmond, USA)
Protein Standards BN-PAGE	Amersham, GE Healthcare (Buckinghamshire, USA)
GeneLadder™ DNA Marker	Fermentas, Thermo Fisher (Bad Homburg,

Falcon tubes	Germany) BD Biosciences Cell Culture (Sparks, USA)
Eppendorf tubes	Eppendorf (Hamburg, Germany)
Strep-Tactin Sepharose	IBA GmbH (Göttingen, Germany)
Strataclean	Agilent Technologies (Santa Clara, USA)
IgG Sepharose	GE Healthcare (Buckinghamshire, UK)
FLAG Agarose	Sigma (Steinheim, Germany)
Flag peptide	Sigma (Steinheim, Germany)
Protein A Sepharose (PAS)	Pierce (Rockford, USA)

3.2 Growth of biological systems

3.2.1 Cultivation of bacteria

Bacteria were cultivated under standard conditions at 37°C with addition of appropriate antibiotics. Ampicillin was added to a final concentration of 100 mg/L.

3.2.2 Cultivation of yeast

For precultures, yeast colonies were picked and incubated in a 5-10 ml YPD preculture in a shake flask and incubated with vigorous shaking overnight at 30°C. This culture was then used to inoculate main cultures in appropriate medium in shake flasks for various applications with varying final OD₆₀₀.

3.2.3 Yeast cryo stock

Yeast strains were preserved as cryo stocks containing YPAD medium (1% yeast extract, 2 % peptone, 0.003% adenine sulfate, 2% glucose, and 15% glycerol). Yeast cells grown on plate were mixed with YPAD medium in previously autoclaved cryo tubes and stored at -80°C.

3.2.4 Growth analysis of yeast

Yeast growth tests were performed by adjusting cultured yeast to an OD₆₀₀ of 0.1 and spotting of serial dilutions onto agar plates containing 1% yeast extract, 2% peptone, with 3% glycerol (for YPG) or 2% glucose (YPD). Alternatively, plates containing synthetic medium were used: 0.67% yeast nitrogen base (Difco, BD), 0.7 g/l drop-out mix of CSM-URA (MP biomedical), 20 µg/ml of uracil, supplemented with 2%

glucose (SD) or 3% glycerol (SG).

3.2.5 Cultivation of HEK293T cells

HEK293T cells were cultured under standard condition in Dulbecco's Modified Eagle Medium containing 10% fetal bovine serum at 37°C and 5% CO₂. For SILAC analysis, cells were grown in lysine- and arginine-deficient DMEM Medium supplemented with 10 % fetal bovine serum. Light labeled medium was supplemented with normal isotope containing L-lysine and L-arginine, whereas heavy labeled medium was supplemented with heavy isotope labeled ¹³C₆¹⁵N₂-lysine and ¹³C₆¹⁵N₄-arginine (Euriso-Top, Germany).

3.3 Molecular Biology Techniques

3.3.1 PCR amplification

PCR amplification was performed using yeast genomic DNA and the KOD HiFi DNA polymerase (KOD HotStart, Novagen).

3.3.2 Determination of nucleic acid concentrations

DNA and RNA concentrations were determined photometrically using NanoVue (GE Healthcare). In brief, 1-2 µl of nucleic acid was added to the NanoVue and quantified accordingly at appropriate wavelength and settings.

3.3.3 DNA electrophoresis

PCR products and plasmids were analyzed by agarose gel electrophoresis. In brief, a gel solution composed of 0.7-1.2% (w/v) agarose (Agarose NEEO Ultra-Roti, Roth) in 1x TAE buffer gel solution with ethidium bromide was prepared and poured into UV-transparent gel trays inserted into the gel casters. Gel solutions were allowed to polymerize after the addition of well forming combs. After loading all test samples and DNA size marker (Geneladder™ DNA Marker Mix, Fermentas), gels were subjected to a voltage of 100-120 mV. Upon completion of electrophoresis, a UV100 Transilluminator or alternatively a Biometra T1 1 UV transilluminator was used to visualize DNA.

3.3.4 Sequencing DNA

Sequencing was performed by dideoxy chain termination method (Sanger *et al.*, 1977). DNA template or plasmid samples were combined with 8 pmol PCR primer, 15% v/v sequencing mix and 15% v/v sequencing buffer (ABI PRISM® BigDye® Terminator v1.1 Cycle Sequencing Kit). For sequencing templates from PCR products, the sequencing mix and sequencing buffer solutions were reduced to 10% v/v. Templates were amplified by PCR for 25-30 cycles (96°C melting for 10 seconds, 55°C annealing for 15 seconds and extension at 60°C for 4 minutes) and consequently precipitated in 48 mM EDTA, 80% ethanol followed by washing with 70% ethanol and drying DNA pellets in a SpeedVac for 2 minutes. Dried pellets were resuspended in 15 µl formadine (HiDye). Samples were analyzed by a Genetic Analyzer 3100 (Applied Biosystems) and DNA sequences analyzed by the program ApE (M. Wayne Davis).

3.3.5 Transformation of *E.coli*

Frozen heat-competent bacteria cell were thawed on ice and mixed with 30 ng DNA and incubated for 20 minutes. Cells were then heat-pulsed at 42°C for 45 seconds before a further 2 minute incubation on ice. Pre-warmed LB medium was added to each sample (9x volume) and cells were incubated for 1 hour at 37°C with gentle shaking. Approximately 100 µl of each transformation was plated on LB agar plates containing appropriate antibiotic (Ampicillin + LB agar plates with 100 mg/L Ampicillin). Plates were incubated overnight at 37°C or until appearance of colonies.

3.3.6 Transformation of yeast

Yeast cells grown overnight in YPD were pelleted and washed with distilled H₂O before treatment with 0.1 M lithium acetate to generate transformation competent cells. Transformation reactions were carried out by the addition of: 10% (v/v) carrier DNA (Herring sperm) and 5-10% (v/v) PCR product or alternatively 2% (v/v) plasmid and mixed with 5x volume of 40% PEG-4000 in lithium acetate. Samples were incubated for 30 minutes at 30°C after which, DMSO was added to a final concentration of 10% (v/v) and samples incubated for a further 20 min at 42°C with gentle shaking. After incubation, samples were centrifuged at 4000 rpm for 5 min. Pellets were resuspended in YPD and incubated with shaking for 2-4 hours at 30°C

and then washed with distilled H₂O before plating on selective medium plates and incubated at 30°C until appearance of colonies.

3.3.7 Yeast genomic DNA preparation

Yeast cells were grown to an OD₆₀₀ of 0.5-0.7, pelleted, and resuspended in Solution A (50 mM Tris/HCL pH 7.5, 10 mM EDTA, 0.3% β-mercaptoethanol, 0.5-0.25 mg/ml Zymolyase) and incubated for 1 hour at 37°C. Consequentially, SDS was added to a final concentration of 1% (v/v) together with ammonium acetate and incubation at -20°C for 15 min. Samples were pelleted, and approximately 66% of the supernatant was saved and incubated with isopropanol (40% v/v). Samples were again centrifuged and the resulting pellet was washed in 70% ethanol and dried. The dried pellet was finally resuspended in TE buffer.

3.4 Protein Biochemistry

3.4.1 TCA precipitation

Samples were treated with 0.2x of final volume with 72% TCA (w/v) stock solution and 0.01x (1/100) of sodium deoxycholate (1.25% stock solution). All samples were incubated 30 min on ice followed by centrifugation at 4°C for 30 min. The resulting pellets were washed with 500 μl ice-cold acetone followed by centrifugation at 4°C for 30 min. Pellets were dried at 37°C for 5-10 min and then resuspended in 1x SDS-PAGE sample buffer and incubated at 60°C for 15 min before SDS-PAGE analysis.

3.4.2 Whole cell extracts

Cultured yeast cells, grown to an OD₆₀₀ of 3, were pelleted, and resuspended in 1 ml H₂O with 250 mM NaOH and 1% (v/v) β-mercaptoethanol. Following a 10 min incubation on ice, proteins were TCA precipitated by the addition of 6% (v/v) TCA and incubation at 10 min on ice, followed by centrifugation at 14,000 rpm at 4°C. The protein containing pellet was further resuspended in SDS sample buffer and pH titrated with 1 M Tris-Base, followed by incubation at 60°C before subjecting samples to SDS-PAGE analysis.

3.4.3 SDS-PAGE analysis

For SDS-PAGE, components were mixed as shown in Table 3. Glass walls, spacers and combs were cleaned with 70% ethanol and assembled on a holder. A separating gel was poured between two glass plates and overlain with isopropanol until polymerized followed by pouring of the stacking gel and insertion of appropriate combs. After polymerization, combs were removed and the gel apparatus was placed into an electrophoresis chamber filled with running buffer. Large gels were run at a constant current of 30 mA and 220 mV, whereas Mini-gels were run a constant current of 25 mA and 100 mV. For the analysis of Mio10 import, a Tricine-SDS PAGE was used (Schägger and von Jagow, 1987). A 48% w/v acrylamide, 1.5% w/v bisacrylamide solution was used. A 3x gel buffer (3 M Tris, 0.3%, pH 8.45 / HCl) in used in preperation of the gel which contained a 4% stacking, 16.5% separating gel, and a 10% spacer between stacking and separating gel. In addition, a 10x cathode buffer (1 M Tris, 1 M Tricine, 1% SDS, pH 8.25) and a 10x anode buffer (2 M Tris, pH 8.9/ HCl) were used. Gels were run slowly overnight at 80 mV or 18 mA limiting.

Table 3. SDS-PAGE pipetting scheme. Constituents of SDS gel were added as indicated to make 1 SDS-PAGE gel.

	<i>Resolving Gel</i>		<i>Stacking Gel</i>
% Acrylamide	14%	12.5%	
Acrylamide/ bisacrylamide (30/0.8)	7.9 ml	6.9 ml	0.83 ml
1.87 M Tris pH 8.8	3.5 ml	3.5 ml	-
0.8 M Tris pH 6.8	-	-	0.5 ml
10% (w/v) SDS	0.17 ml	0.17 ml	50 μ l
dH ₂ O	5.3 ml	6.3 ml	3.55 ml
10% (w/v) APS	100 μ l	100 μ l	50 μ l
TEMED	10 μ l	10 μ l	10 μ l
Total Volume	17 ml	17 ml	5 ml

3.4.4 BN-PAGE Analysis

3.4.4.1 First Dimension BN-PAGE

Prior to gel pouring and preparation, all components shown in Table 4 except for APS and TEMED were mixed accordingly and stored at 4°C. Glass walls, spacers and

combs were cleaned with ethanol and assembled on a holder. A gradient separating gel was poured accordingly and overlain with isopropanol. Stacking gel was poured and combs inserted. Polymerization of BN-PAGE gel was performed overnight at 4°C or alternatively for 1 hour at RT. BN-PAGE samples were loaded at 4°C and high-molecular weight markers used, with 1x BN-PAGE loading dye used to fill in empty lanes. The gel apparatus is then transferred into the BN-PAGE electrophoresis chamber containing 4 L pre-cooled 1x Anode Buffer and 500 ml Cathode Buffer added. Gels were run at 4°C first at a constant voltage of 200 mV at the region of stacking gel and then 600 mV at the separating gel with a constant current of 30 mA. Alternatively, gels were set to 100 mV and run overnight. In the case of subsequent blotting, second dimension analysis or activity assays, the cathode buffer is exchanged, with 1x Cathode buffer containing no Coomassie Serva Blue G250, 1 hour after electrophoresis.

3.4.4.2 Second Dimension BN-PAGE

BN PAGE was performed as described above (with cathode buffer exchange). After electrophoresis gel stripes of individual lanes were excised accordingly and incubated in H₂O. Gel stripes were then placed on the upper part of an SDS-PAGE glass plate, approximately 15 mm above the expected stacking/separating gel boundary. Glass plates were assembled and separating and stacking gel solutions were poured. A 2-3 comb well was used to load markers and/or mitochondria controls. SDS-PAGE was performed as described above followed by Western blotting.

Table 4. BN-PAGE pipetting scheme. Constituents of BN gel were added as indicated to make 1 BN-PAGE gel.

% Acrylamide	Resolving Gel			Stacking Gel
	4	10	13	
3x Gel Buffer	3 ml	3 ml	3 ml	2.5 ml
Acrylamide	0.73 ml	1.82 ml	2.35	0.6 ml
Glycerol	-	1.8 ml	1.8 ml	-
10% APS (w/v)	40 µl	40 µl	40 µl	30
TEMED	4 µl	4 µl	4 µl	3
dH ₂ O	5.228 ml	2.347 ml	1.817 ml	4.367

3.4.5 Coomassie staining

After electrophoresis, gels were stained in gel staining solution for 1 hour and then destained in gel destaining solution for 1 hour.

3.4.6 Western blotting and immunodetection

Western blots were performed with PVDF membranes and detected by enhanced chemiluminescence (ECL). In brief, PVDF membranes were incubated in methanol prior to blot and blotting was performed at 250 mA and 40V for 2 hrs. After blotting, PVDF membranes were incubated in Staining solution for 30 seconds and washed with Destaining solution. Marker bands were marked and membrane washed with Destaining solution and methanol until clear. For SDS-PAGE analysis, membranes were blocked with 5% Milk-TBST for 1 hour at RT and incubated with appropriate antibody for 1 hour at RT followed by 3 x 15 min washes with TBST. Secondary antibody was applied for 1 hour at RT followed by 3x 15 min washes with TBST, and finally detection was performed by ECL. For BN-PAGE immunodetection, membranes were blocked with 10% Milk-TBST for 4 hrs or overnight and primary antibody and secondary antibody incubations were for 1 hour each at RT and detection was by ECL and a film developing machine. Alternatively, fluorescently labeled antibodies were used and detection was performed with the fluorescence scanner (FLA-9000; Fujifilm).

3.4.7 Size exclusion chromatography

Solubilized yeast and human mitochondrial protein complexes were separated by gel filtration using an ÄKTApurifier system (GE Healthcare). In brief, 200 µg of isolated mitochondria were solubilized in 200 µl GF-buffer (20 mM Tris/pH7.4, 50 mM NaCl, 0.5 mM EDTA, 10% (w/v) Glycerol, 1% (w/v) Digitonin, 1mM PMSF) for 20 min on ice. Samples were centrifuged, insoluble pellet discarded and resulting supernatants were loaded on a Superose 6 10/300 GL (GE Healthcare) equilibrated with GL-buffer (20 mM Tris/pH7.4, 50 mM NaCl, 0.5 mM EDTA, 10% (w/v) Glycerol, 0.1% (w/v) Digitonin). The resulting fractions from the ÄKTApurifier system were precipitated with TCA as described above with the exception of a further acetone wash prior to drying and resolving samples in 1x SDS sample buffer. Samples were then analyzed by SDS-PAGE and Western blotting.

3.4.8 Digital autoradiography

For detection and analysis of radioactive signals by digital autoradiography, destained gels are first placed on Whatman paper, covered with a plastic sheet and dried for 2 hours. After drying, markers on the gel are labeled with radioactive ink and covered with transparent tape. The gel is placed in an autoradiography cassette and film is exposed accordingly.

3.4.9 Isolation of mitochondria from yeast

3.4.9.1 Mitochondrial preparation YPG at 30°C

Yeast mitochondria were isolated by differential centrifugation as described by Meisinger *et al.*, 2006. For each strain, the preculture was used to inoculate 5.1-10.2 L medium to achieve an OD₆₀₀ nm of 2.0, in which yeast should be a mid-log growth phase at time of harvest. Main cultures were grown for 15-18 hrs with vigorous shaking at 30°. Yeast cells were harvested by centrifugation at 4000 rpm in a RC 12BP Sorvall centrifuge for 20 min at 18°C and supernatant was discarded. The pellets were resuspended in water and combined in a F10S centrifugation tube, and centrifuged in a Sorvall F10S-6x500Y rotor at 4000 rpm for 10 min at 18°C. Supernatant was discarded and the weight of wet cell pellet was determined. The resulting cell pellets were resuspended in DTT buffer (100 mM Tris/HCl pH 9.4, 10 mM DTT) at a concentration of 2 ml per gram yeast and incubated with shaking at 30° C for 30 min. Cell suspensions were centrifuged in a Sorvall F10S-6x500Y rotor at 4000 rpm at 18°C for 8 min. Supernatants were discarded and pellets were washed with 200 ml 1.2 M Sorbitol and cell suspension was centrifuged at 4000 rpm at 18°C for 8 min (Sorvall F10S-6x500Y rotor). Supernatants were again discarded and pellets resuspended in zymolyase buffer (20 mM KPi Buffer, 1.2 M Sorbitol), supplemented with 4 mg zymolyase per gram of yeast. Cell suspensions were incubated with shaking at 30°C for 60 min and then centrifuged at 3000 rpm at 18°C for 10 min (Sorvall F10S-6x500Y rotor). Pellets were washed with zymolyase buffer without enzyme and centrifuged at 3000 rpm at 18°C for 10 min (Sorvall F10S-6x500Y rotor). Supernatants were discarded and pellets were stored on ice and resuspended in Homogenization Buffer (0.6 M Sorbitol, 10 mM Tris/HCl pH 7.4, 1 mM EDTA, 0.2% (w/v) BSA) at a concentration of 7 ml per gram yeast. PMSF was added to a final concentration of 1 mM to each suspension. Cells were homogenized by a Potter S Homogenizer and centrifuged in a Sorvall F15S-6x250Y rotor at 3000 rpm for 5 min at 4°C. Pellets were

discarded and supernatants were transferred into fresh F15S tubes and centrifuged at 4000 rpm for 10 min at 4°C. Supernatants were discarded whereas pellets were pooled in SS-34 tubes and washed in 5 ml SEM Buffer with a final concentration of 1 mM PMSF and centrifuged in a Sorvall SS-34 rotor at 12000 rpm for 15 mins at 4°C. Supernatant was discarded and pellet was resuspended in SEM buffer and protein concentration was determined by the Bradford Assay (Bradford, 1976). Mitochondrial pellets were diluted in SEM buffer to a final concentration of 10 µg/µl, aliquoted, and stored at -80°C.

3.4.9.2 Mitochondrial Preparation from SG at 18°C

Isolation from yeast grown in SG at 18°C was performed essentially as described above with some variations. For the primary culture, yeast colonies were picked and inoculated into SD medium and grown overnight at 30°C. Final SG cultures were grown at 30°C until OD₆₀₀ of 1.0 and then transferred to 18°C until culture reached OD₆₀₀ 2.0 (generally 24 hours after temperature shift).

3.4.10 Isolation of mitochondria from HEK 293T cells

Human mitochondria were isolated from HEK293T cells as previously described (Lazarou *et al.*, 2009; Reinhold *et al.*, 2011). In brief, cells were harvested at 80-85% confluency in 1x PBS and 1 mM EDTA and homogenized in 0.1% BSA, 300 mM Trehalose, 10 mM HEPES-KOH pH 7.7, 10 mM KCl, 1 mM EDTA, 1 mM EDTA (Yamaguchi *et al.*, 2007). Homogenized cells were subjected to centrifugation at 11,000 x g at 4°C for 10 min and homogenization buffer without BSA was added to the mitochondria containing pellet.

3.4.11 Labeling of precursor proteins with [³⁵S] methionine

For *in vitro* translation, ORFs of interest were amplified by PCR as described above. Amplified PCR products containing SP6 promoter sites were transcribed using the mMessage mMachine system. Each reaction mix contained 6 µl purified PRC product, 1x SP6 reaction buffer, 1x NTP/CAP mixture and 2 µl Enzyme mix, and reactions were incubated for 2 hours at 37°C in a thermomixer. After 1 hour, 2 units of TURBO DNase were added and mixture was incubated for 15 min at 37°C. RNA sample was cleared by the Ambion Megaclear kit. Labeling of preproteins was performed using the Flexi® Rabbit Reticulocyte Lysate system (Promega). Each translation reaction

contained 20% RNA, 66% rabbit reticulocyte lysate, 70 mM potassium chloride, 1.4 mM magnesium acetate, and 1.6 mM radioactive methionine. Samples were incubated in a thermomixer at 30°C for 90 min, followed by the addition of 150 mM sucrose and non-radiolabeled methionine to a final concentration of 8 mM. Lysates were aliquoted accordingly and stored at -80°C.

3.4.12 Import and assembly of radiolabeled precursor protein

3.4.12.1 Import into yeast isolated mitochondria

Import of radiolabeled proteins into isolated yeast mitochondria were performed as described by Wiedemann *et al.*, 2006. Import reactions were performed in Standard Import Buffer and supplemented with 4 mM ATP, 4 mM NADH, 100 µg/mL creatine kinase, 5 mM creatine phosphate and 75 µg isolated mitochondria. For samples with dissipated membrane potentials, 1% (v/v) of 100 µM AVO was added whereas 1% (v/v) ethanol was added to other samples. Samples were incubated for 3 min at 25°C and import reactions were initiated with the addition of radiolabeled lysate (10-15% of total volume). Imports were stopped at appropriate time points with the addition of 1 µl 100 µM AVO and transferred to ice. Reactions were treated with 2.5 µg PK and incubated on ice for 15 min. 1 µl 0.2 M PMSF was added to halt PK activity and samples were centrifuged at 14,000 rpm for 10 min. Mitochondrial pellets were washed with 300 µl SEM buffer with 2 mM final concentration PMSF and centrifuged at 14,000 rpm for 10 min at 4°C. For SDS-PAGE analysis, pellets were resuspended in sample buffer and loaded on gels for electrophoresis. For BN-PAGE analysis, pellets were solubilized in Digitonin buffer (20 mM Tris pH 7.4, 50 mM NaCl, 0.5 mM EDTA, 10% (w/v) Glycerol, 1% (w/v) Digitonin, and 1 mM PMSF). After solubilization, samples were centrifuged at 14,000 rpm for 10 min at 4°C and the resulting supernatants were suspended in 10% (v/v) 1x BN Loading Dye, before loading on BN gels.

3.4.12.2 Import into HEK293T isolated mitochondria

Import of radiolabeled proteins into isolated human mitochondria was performed as described by Lazarou *et al.* (2009). For import of radiolabeled lysate into mitochondria from isolated mitochondria from HEK293T cells was performed essentially as described above with some notable changes. Import and assembly assays were incubated with freshly isolated mitochondria and not frozen mitochondria. Moreover,

the import buffer (20 mM HEPES /KOH pH 7.4, 250 mM sucrose, 80 mM potassium acetate, 5 mM magnesium acetate, 10 mM sodium succinate and 5 mM methionine) was used. Import reactions were performed at 37°C.

3.4.13 Protein localization analysis

To determine protein localization within isolated mitochondria, a protease protection assay was performed as previously described by Mick *et al.* (2007). Mitochondria, mitoplasts, or Triton X-100 lysed mitochondria were treated with various amounts of PK, in which then proteins were tested for localization to the mitochondrial outer membrane, mitochondrial inner membrane or matrix by SDS-PAGE and Western blot analysis. Mitochondria were resuspended in SEM buffer and treated with either 0, 20, or 100 µg PK. Swelling of isolated mitochondria was achieved by treatment in EM buffer (1 mM EDTA, 10 mM MOPS pH 7.2). The generated mitoplasts were treated with 0, 20 or 100 µg PK. Mitochondria lysed with 1% Triton X-100 were treated with 0 or 100 µg PK. In all cases, PK treatment was allowed for 10 min on ice and followed by the addition of 0.2 M PMSF and incubated on ice for 10 min. All samples were centrifuged at 14,000 rpm at 4°C. The pellets of SEM-treated mitochondria and mitoplasts and the supernatant of Triton X-100 lysed mitochondria were resuspended in SDS-PAGE loading dye and analysed in by SDS-PAGE.

3.4.14 Membrane association analysis

Analysis was performed as previously described (Mick *et al.*, 2007). To test protein membrane association, isolated mitochondria were suspended in 0.1 M carbonate buffer at pH 10.8 or 11.5, or alternatively lysed with 1% Triton X-100. All samples were incubated on ice and then subjected to ultracentrifugation at 45000 rpm for 45 min at 4°C, in a TLA-55 rotor (Beckmann). Samples were TCA precipitated and subjected to SDS-PAGE analysis.

3.4.15 In-gel activity assays

Isolated mitochondria were solubilized in digitonin buffer and subjected to BN-PAGE gels, at which, coomassie containing-cathode buffer is exchanged, with 1x clear cathode buffer after 1 hour of electrophoresis at 200 mV. In-gel activity assays were performed on sliced gel stripes or whole gels, and incubated first in appropriate equilibration buffer (as indicated in Table 5) for 15 min followed by incubation in

staining buffer at RT or 30°C until the appearance of bands. Gel stripes were incubated in 50 ml equilibration buffer and 10 ml staining buffer, whereas whole gels were incubated in 100 ml equilibration and 50 ml staining buffer. A 4-10% gradient gel was used for the assessment of cytochrome *c* oxidase, complex I, and F₁F₀ATPase monomer and dimeric forms. Alternatively, a 3-13% gradient gel was to analyze higher oligomers of F₁F₀ATPase.

Table 5. Composition of in-gel activity assay buffers. *Reduction of Cytochrome *c* (10 mg/ml) was achieved by resuspending 10 mg Cytochrome *c* in 1 ml 50 mM KPi pH 7.4 and 75 µg of Na-dithionite.

	Equilibration buffer	Staining Buffer
Complex I	5 mM Tris / HCl pH 7.4	5 mM Tris /HCl pH 7.4 2.5 mg/ml NBT (4-Nitrotetrazoliumchloride blue)
Cytochrome <i>c</i> oxidase	50 mM KPi pH 7.4	50 mM KPi pH 7.4 0.5 mg/ml DAB (3,3' Diaminobenzidine) 1 mg/ml of reduced Cytochrome <i>c</i> (bovine heart)*
F ₁ F ₀ ATPase	35 mM Tris, 220 mM Glycine pH 8.3	35 mM Tris, 220 mM Glycine pH 8.3 14 mM MgSO ₄ 0.2% Pb(NO ₃) ₂ 8 mM ATP

3.4.16 Protein complex isolation by immunoprecipitation

Isolation of yeast protein complexes was performed as previously described (Geissler *et al.*, 2002). In all cases, mitochondria isolated with tagged nuclear encoded proteins were solubilized in IP-Buffer (20 mM Tris/pH7.4, 50 mM NaCl, 0.5 mM EDTA, 10% (w/v) Glycerol, 1% (w/v) Digitonin, 1mM PMSF). After centrifugation at 14,000 rpm for 20 min, supernatants were incubated with appropriate column material in Mobicol columns for 1 hour at 4°C on an end-over-end shaker. Unbound proteins were removed by centrifugation at 100 x g for 1 min. Columns were then washed 10 times with 20x bead volume of Washing Buffer (20 mM Tris/pH7.4, 100 mM NaCl, 5 mM EDTA, 10% (w/v) Glycerol, 0.3% Digitonin, and 1 mM PMSF), and isolated proteins were eluted accordingly. For Large-scale isolation (1 mg mitochondria), solubilization of mitochondria was carried out in either Falcon tubes or 2 ml Eppendorf tubes. o indicates the appropriate experimental conditions for different isolations.

Table 6. Experimental conditions for various immunoprecipitation assays.

Described buffer were used for native elutions. Alternatively, proteins can be eluted by SDS sample buffer.

Type of tag	Binding column material	Elution Buffer
ZZ (ProteinA)	IgG Sepharose	Glycine pH 2.8
SF (Streptavidin- FLAG)	Strep-Tactin sepharose (IBA GmbH)	5 mM Desthio-Biotin, 20 mM Tris-HCl pH 7.4, 30 mM NaCl, 0.2 mM EDTA
FLAG	FLAG-agarose	Flag peptide 20 mM Tris/pH7.4, 100 mM NaCl, 5 mM EDTA, 10%(w/v) Glycerol, 0.3%(w/v) Digitonin, 1mM PMSF),

3.4.17 Crosslinking antibodies for co-immunoprecipitations

To crosslink antibodies into sepharose columns for consequent use in co-immunoprecipitations, 100 µl of Protein A Sepharose (PAS) were added to a Mobicol column and centrifuged for 1000 rpm 5 min at RT. The sepharose was then washed twice with 500 µl 0.1 M KPi buffer pH 7.4. For each column 100 µl serum premixed with 300 µl with KPi buffer were added to the column followed by incubation on an end-over-end shaker of 1 hour at RT. Flow-through from the column was saved after a 5 min centrifugation and the column was washed with 500 µl NaBorat and then incubated with NaBorat with 17.5 mg DMP for 30 min at RT. Residual crosslinker was removed, first by centrifugation for 5 min at 1000 rpm, and then washing with 700 µl 1 M Tris-HCl, pH 7.4. Mobicol columns were then incubated for 2 hours in 700 µl 1 M Tris-HCl, pH 7.4 followed by centrifugation for 5 min at 1000 rpm. The column was stored at 4°C with 600 µl PBS with a final concentration of 2 mM sodium azide.

3.4.18 Co-immunoprecipitation from isolated yeast mitochondria

Antibodies against various yeast proteins were crosslinked to columns as described above. Isolated mitochondria were solubilized in digitonin buffer and applied to columns. Biochemical isolations were carried out using as for protein complex immunoprecipitations with the exception of eluting with 100 mM glycine pH 2.8.

3.4.19 Co-immunoprecipitation from HEK293T cells

Isolation of protein complexes from human isolated mitochondria was performed either with beads coupled with antibodies raised against the F₁F₀ATPase (α -F₁F₀ATPase) or against cytochrome *c* oxidase (α -COX) (Invitrogen). Immunoprecipitation of MINOS1-containing complexes were carried out using C1orf151/MINOS1 antibodies, cross-linked to Protein A/G Agarose (Pierce, ThermoScientific). In brief, 1 mg of isolated mitochondria from HEK293T cells was solubilized in 1 ml IP-buffer (20 mM Tris/pH7.4, 50 mM NaCl, 0.5 mM EDTA, 10% (w/v) Glycerol, 1% (w/v) Digitonin, 1 mM PMSF) for 20 min on ice. Insoluble material was removed by centrifugation (14,000 rpm, 20 min, 4°C). The remaining supernatant was incubated with the individual antibody coupled beads for 1 h at 4°C on an end-over-end shaker and centrifuged at 1000 rpm for 1 min at 4°C to remove unbound protein. The pelleted beads were transferred to a Mobicol column and beads were washed 10 times with W-buffer (20 mM Tris/pH 7.4, 50 mM NaCl, 0.5 mM EDTA, 10%(w/v) Glycerol, 0.3% (w/v) Digitonin, 1mM PMSF). Samples were finally eluted by SDS-PAGE sample buffer.

3.5 Analytical Tools

3.5.1 *In silico* analysis and multiple sequence alignments

In silico analysis was performed using the Saccharomyces Genome Database (SGD). For multiple sequence alignments ClustalW 2.0.11 (Chenna *et al.*, 2003) and geneious© (Biomatters, Limited) were used. Color coding was performed by Microsoft Word 2008. Black boxes were used to indicate identical residues in at least four species whereas gray boxes indicate similar amino acids, in accordance with Erdmann *et al.*, 1991. Similarity rules used were (G=A=S, A=V, V=I=L=M, I=L=M=F=Y=W, K=R=H, D=E=Q=N, S=T=Q=N). Transmembrane predictions from primary amino acid sequences were performed by TMpred (Hofmann and Stoffel, 1993).

3.5.2 Mass spectrometry and data analysis

For the identification of MINOS1 interacting proteins, SILAC (Ong *et al.*, 2002) was used. Mitochondria from HEK29T cells grown in heavy or light isotopes (see Section)

were isolated and MINOS1 containing complexes were coimmunoprecipitated from the heavy-labeled culture, whereas a control antibody was used for light-labeled cells. The reverse (label-switch) experiment was performed by isolating MINOS1 specific complexes from light-labeled cells, whereas the control was used for heavy-labeled cells. In all cases, elutions from coimmunoprecipitations were mixed before further analysis. Eluted proteins from either Mio10^{SF} immunoprecipitations from isolated yeast mitochondria, or MINOS1 co-immunoprecipitations from HEK293T cells, were separated on 4-12% gradient SDS-PAGE gels (Invitrogen) and stained with Colloidal Coomassie Blue. SDS-PAGE gels were cut into 23 equal gel slices and proteins were in-gel digested with trypsin (Promega) as described previously (Shevchenko *et al.*, 2006). The resulting tryptic peptides from each gel slice were analyzed by nanoflow HPLC (Agilent 1100, Agilent Technologies) coupled to nanoelectrospray LTQ-Orbitrap XL mass spectrometer (Thermo Fischer Scientific). For yeast Mio10^{SF} immunoprecipitations, the raw MS files were searched and analyzed with Mascot (Mascot Daemon version 2.2.2, Matrix Science) and Scaffold 3 (Proteome Software) using the *S. cerevisiae* NCBI non-redundant protein database. The normalized fold change ratios were then calculated in Scaffold using the spectral count approach (Liu *et al.*, 2004). For SILAC analysis of MINOS1 immunoprecipitations, the raw MS files were analyzed by MaxQuant (Cox and Mann, 2008) and Mascot using IPI Human protein database (version 3.82). MaxQuant was used to analyze and visualize results with R as described (Nikolov *et al.*, 2011). Mass spectrometric analysis performed by Monika Raabe and Miroslav Nikolov (AG Urlaub, MPI-bpc, Göttingen).

3.5.3 Fluorescence microscopy

3.5.3.1 Subcellular localization by immunofluorescence

Immunofluorescence was performed with African green monkey (*Cercopithecus aethiops*) kidney epithelial cells (Vero), as previously described (Wurm *et al.*, 2010). In brief, cells were grown on cover slips under standard conditions and then fixed in 8% paraformaldehyde (PFA) and permeabilized in 0.5 % (v/v) Triton X-100. Treated cells were then incubated for 1 hour with C1orf151/MINOS1-antibody and the mitochondrial marker Cyclophilin D-antibody at a dilution of 1:400. Cells were then washed cells and incubated for 1 hour with Oregon Green 488 conjugated goat anti-mouse IgGs (1:1000; Molecular Probes) and KK114 conjugated goat anti-rabbit IgGs (1:200) (Kolmakov *et al.*, 2010). Cells were again washed and stained with DAPI

staining for 5 min before embedding in mounting medium. Fluorescence microscopy was performed with a beam scanning confocal microscope (TCS SP5, Leica Microsystems CMS GmbH, Wetzlar Germany) equipped with 1.4 NA oil immersion lenses (63 x; HCX PL APO, Leica). Microscopy was performed by Daniel Jans (AG Jakobs, MPI-bpc).

3.5.3.2 Morphology analysis by Life-cell imaging fluorescence

To visualize mitochondrial networks in yeast, cells were first transformed with a pVT100U-mitoGFP vector (Westermann and Neupert, 2000). Selected colonies were first verified for GFP expression and then cultured overnight in selective SGG-Medium (0.5g/l yeast extract, 6.7g/l yeast nitrogen base, 0.77g/l CSM-URA dropout mix, 30ml/l Glycerol, 1g/l Glucose). Cultured cells were directly used for fluorescence microscopy with no further manipulation. Images were collected by a DeltaVision microscope (Olympus IX71, Applied Precision) equipped with a 100x objective and a FITC filter and deconvolved with Softworx (Applied Precision) version 3.5.1. 10–15 Z-section images were taken for each image at 0.5 μ m intervals. Microscopy was performed by Daniel Jans (AG Jakobs, MPI-bpc).

3.5.4 Electron microscopy

For analysis of mitochondrial morphology of various mutants, electron microscopy, in which sample specific were vitrified by high pressure freezing or chemical fixed by potassium permanganate before examination.

3.5.4.1 High-pressure-freezing

Yeast cells were grown in liquid YP Lactate medium (10 g/l yeast extract, 20 g/l peptone from casein, 23 ml/l L(+)-lactic acid solution (85%), 0.02 g/l uracil, 0.02 g/l adenine sulfate) at 30°C. Cultures were allowed to reach a logarithmic growth phase (OD₆₀₀ approximately 2.0) at which point they are harvested. Cells were transferred onto 150 μ m aluminum planchette and a Leica HPM100 high pressure freezer (Leica Microsystems, Wetzlar, Germany) was used to vitrify samples followed by embedding in 0.5% glutaraldehyde, 0.1% uranylacetate and 5% H₂O (Giddings, 2003) using a freeze substitution unit (Leica EM AFS, Leica Microsystems). Samples were warmed to room temperature and the pellet was removed from the planchette

followed by embedding in expoxid resin (Agar 100, Plano) and polymerization at +80°C for 48 hours. Thin sections (60nm) were counterstained with 1% uranylacetate in methanol and lead citrate and prior to examination with a Philips CM 120 BioTwin transmission electron microscope (Philips Inc., Eindhoven, Netherlands). Microscopy and analysis were performed in collaboration with Dietmar Riedel (Mpi-bpc, Göttingen)

3.5.4.2 Chemical fixation

Chemical fixation of sample specimens with potassium permanganate was essentially performed as described by Erdmann *et al.*, 1989. Yeast cells were first cultured for 12h at 18°C in liquid SGG medium (0.5g/l yeast extract, 6.7g/l yeast nitrogen base, 0.77g/l CSM dropout mix, 30ml/l Glycerol, 1g/l Glucose). Cells were then fixed in 1.5% potassium permanganate at room temperature for 2 min, and consequentially treated with 1% uranyl acetate for 2 hours. Fixed cells were then dehydrated in a graded ethanol series and embedded in Epon 812 resin. Ultrathin sections were mounted on Formvar-coated single hole grids, and examination was performed in a Philips EM 300 (Phillips Inc., Eindhoven, Netherlands). Microscopy and analysis were performed in collaboration with Wolfgang Schliebs (Ruhr Universität Bochum, Bochum).

4. RESULTS

4.1 Identification of a putative F₁F₀ATPase dimerization factor in higher eukaryotes (*H. sapiens*)

4.1.1 *in silico* analysis: identification of Mio10 and MINOS1

Various structural subunits of the F₁F₀ATPase were described to be involved in dimerization in various species ranging from simple eukaryotes to mammals (Soubannier *et al.*, 2002; Fronzes *et al.*, 2003). In addition, subunits Atp18, Atp19, Atp20, and Atp21 have been described to play a major role in inducing dimerization in yeast by promoting F₁F₀ATPase homo-monomeric interactions (Arnold *et al.*, 1997, 1998; Soubannier *et al.*, 2002; Paumard *et al.*, 2002a; Wagner *et al.*, 2009, 2010). The presence of these small F₀ associated dimerization factors does not seem to be conserved in higher eukaryotes. Whereas homologs of subunits Atp18 and Atp19 are not found in mammals, subunits Atp20 (subunit g) and Atp21 (subunit e) are present (Kucharczyk *et al.*, 2009). However, a role of these subunits in dimerization has not been demonstrated. Thus, information is still lacking on what mediates F₁F₀ATPase dimer-interface interactions in higher eukaryotes.

An *in silico* analysis was performed in order to identify novel F₁F₀ATPase dimerization factors in higher eukaryotes (Figure 9). The bioinformatics analysis was based on searching for ORFs with protein products of similar characteristics to dimerization factors already characterized in yeast (Atp18, Atp19, Atp20, and Atp21). Most importantly, the protein should have a significant human homolog, defined by a low Expect (E) value from sequence homology searches. As illustrated in Figure 9, mitochondrial localized proteins were filtered through various parameters using the SGD database. Potential ORFs of interest would code for an uncharacterized protein with at least one transmembrane domain and a size equal to or smaller than 12 kDa. Similar to Atp20 and Atp21, the protein would contain a GxxxG motif in its transmembrane domain. Two ORFs, YJR085C and YCL057c-A complied with these conditions, both having potential human homologs based on E-values, of 3×10^{-8} and 6×10^{-6} respectively*. In this study, YCL057c-A (termed Mio10), as well as its potential human homolog C1orf151 (termed MINOS1), were analyzed.

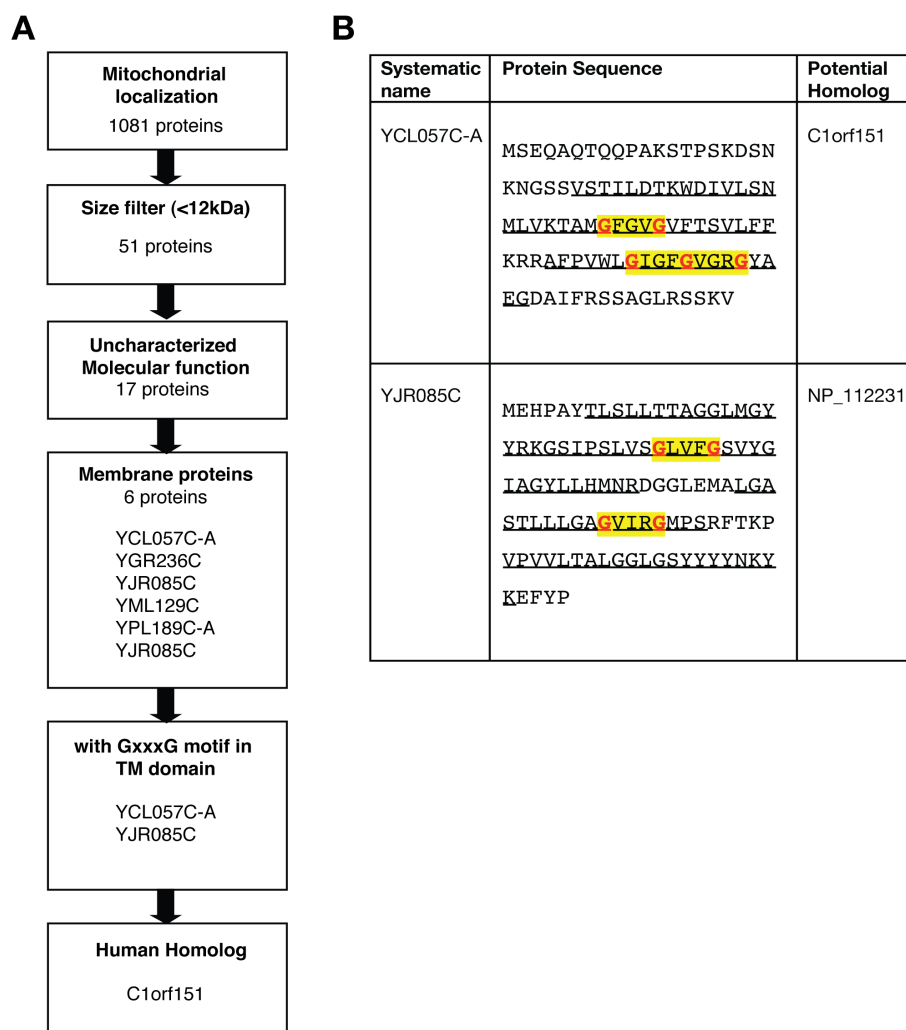


Figure 9. Identification of Mio10 and MINOS1 by *in silico* analysis. (A) The *Saccharomyces* Genome Database (SGD) was screened for all mitochondrial proteins with a size ≤ 12 kDa and uncharacterized molecular function, and consequently for membrane proteins that have significant human homology (based on E values) by BLAST search. (B) Sequences of the proteins with significant human homologs. Regions with GxxxG motifs are highlighted in yellow; glycine residues are highlighted in red. Predicted TM domains are underlined.

4.1.2 Mio10 and MINOS1 sequence analysis and alignments

Analysis of the primary amino acid sequences of Mio10 and MINOS1 indicated that both ORFs encode small proteins of 97 and 78 amino acids, of approximately 10 and 8 kDa in size, respectively (Figure 10). Sequence analysis indicated that neither has a predicted presequence. In addition, Mio10 and MINOS1 are predicted to contain two transmembrane domain each of which each contains a GxxxG motif.

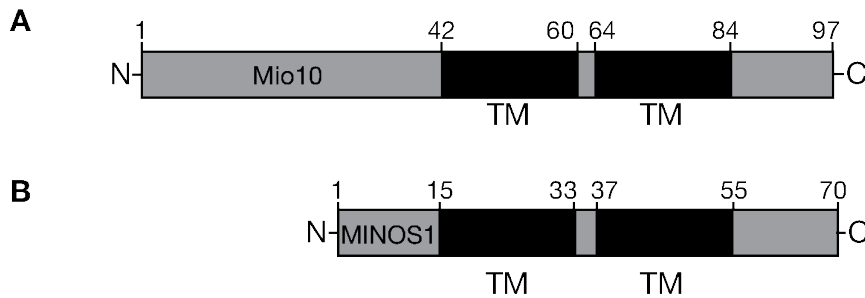


Figure 10. Molecular organization of selected proteins. (A) Mio10, and (B) MINOS1. Black boxes indicate predicted transmembrane (TM) domains. No predicted mitochondrial presequence predicted. N, amino-terminus; C, carboxyl-terminus.

Interestingly, Mio10 and MINOS1 appear to be highly conserved across all examined species. Figure 11 depicts a multiple sequence alignment of Mio10 in various yeast species. The N-termini and C-termini are weakly conserved across analyzed yeast species. Moreover, it appears that protein sequences encoding the two transmembrane domains are highly conserved with the two GxxxG motifs unaltered in all examined yeast species. The primary amino acid sequence of MINOS1 from various species representing vertebrates and invertebrates were also analyzed in a multiple sequence alignment (Figure 12). The N- and C-termini, like those of Mio10, appear to be variable across various species, whereas sequences encoding the two transmembrane domains are highly conserved, with the GxxxG motifs unaltered. This variation of N- and C-termini may indicate the importance of the transmembrane domains in Mio10 and MINOS1 function.

Sc Mio10	MSEQAQTQPAKSTPSKDSNKNKSSVSTILDTKWDIVLSNMLVKTAMGFGVGVFTSVLFF	60
Zr Mio10	MAEQQQQAQLQVTAPNK-----SILNDKWDVVLNLLVKSLGFGVGVVASVLFF	50
Vp Mio10	MSQSQELQIT-SAPTR-----SILNDKWDVVLNLFVKTSLGFGAGVLASVLLF	49
Ct Mio10	MSTETK-QELLPTPP-----ATASQNLLNDKWDVVLNLIKTGLGFGGGVLASTLFF	52
Ca Mio10	MSTEIKPQELVPS-----TASQNLLNDKWDVVLNLIKTGLGFGGGVLASTLFF	50
Dh Mio10	MVNTNKYFRMTSTEQKV----AAPSQSLNNDKWDVVLNLIKTGLGFGGGVLASTLFF	55
Pp Mio10	MSEKQLSQPVSS-----TLLNDKWDVVLANTVVKTKLGFVGGVLLSVLFF	46
Yl Mio10	MGDTVATNLQLLT-----QWDVVISNLTIVKTKLGFVGVVASVLFF	41
Cg Mio10	MSNKEETKAKTVD-----YTPVRSILNDKWDVVLNMLVKMGLGFGVGVVTSVLFF	51
Ag Mio10	MSGQLEVSAPSR-----ILNDKWDVVLNLLVVKTKLGFVGVVAVLFF	45
Lt Mio10	MSEQLKVSPTSRS-----LLNDKWDVVLNLLVVKTKLGFVGVVAVLFF	45
Kl Mio10	MSEQVQTTKAVPS-----ILDKRWDVVLNLLVAKTALGAGVGVIVAVLFF	45
Nc Mio10	MSDSTSSPVAAAPSTAM----TRPVSEALLNEKWDRCLSNLLIKSTLGLGFGVVFVSLFF	56
Mo Mio10	MSET--APPTRSP--AF----ARPVSEALLNEKWDHCLSNLLIKSTLGLGFGVVFVSLFF	52
Pa Mio10	MADTAPATTTSPTSRAV----SRPVSEALLNEKWDRCFSNLLIKSSLGLGFGVVFVSLFF	56
Tr Mio10	MSET--AAPRSPS--AI----SRPVSEALLNEKWDRCLSNLLVVKSTLGLGFGVVFVSLFF	52
Ss Mio10	MPET--SISPPAVTRP----SKPVSEALLNEKWDHCLSSLLIRSSVGLGFGVVFVSLFF	53
Tt Mio10	MADS-AESTQSVVPRA----SKPVSETLLNEKWDRAISSLLIRSSVGLGFGVVFVSLFF	55
Sp Mio10	MSTSQSSEQ-----TLNLYQWDVCLSNMNVQSGTGLGAGIVSSVLFF	41
Bd Mio10	MESQTAESKTIPS-----EELLARKWDKCLSNFVIKSGLGLTVGVSLSTLFF	47
Sc Mio10	KRRAFPVWLGIGFGVGRGYAEGDAIFR--SSAG----LRSSKV-----	97
Zr Mio10	KRRAFPVWLGIGFGLGRGYAEGDAIFR--SAAG----LRTSKA-----	87
Vp Mio10	KRRAFPVWLGIGFGIGRGYSEGDALFR--SAAG----LRKSTV-----	86
Ct Mio10	KRRAFPVWLGIGFGLGRGYSEGDALFR--SNHG----LRTVKV-----	89
Ca Mio10	KRRAFPVWLGIGFGLGRGYAEGDAIFR--SNHG----LRTVKA-----	87
Dh Mio10	KRRAFPVWLGIGFGLGRGYSEGDALFR--SNHG----LRTVKA-----	92
Pp Mio10	KRRAFPVWLGIGFGLGRGYSEGDALFR--SPAG----LRDVKA-----	83
Yl Mio10	KRRAFPVWLGIGFVAGRGVAEGDVIFRQSDAG----VRSVRA-----	79
Cg Mio10	KRRAFPVWLGIGFVAGRGYSEGDALFR--STAG----LRSVKV-----	88
Ag Mio10	KRRAFPVWLGIGFGLGRGYAEGDAIFR--SHAG----LRAVRA-----	82
Lt Mio10	KRRAFPVWLGIGFGLGRGYAEGDAIFR--SSAG----LRTVKA-----	82
Kl Mio10	KRRAFPVWVGIGFGLGRGYAEGDAIFR--TNAG----LRKVNA-----	82
Nc Mio10	KRRAFPVAVGVGFGAGRAYEFCNTSLKQAAAR----ETRAQA-----	93
Mo Mio10	KRRAFPVAVGAGFGAGRAYEFCNYNLKQATAR----ETRRQA-----	89
Pa Mio10	KRRAFPVAVGVGFGAGRAYEFCNSSLKQAAK----ETRKQA-----	93
Tr Mio10	KRRAFPAYLGAGFGAGRAYEFCNPNLKQAAAR----DLKKPSV-----	90
Ss Mio10	KRRAFPVAVGVGFGAGRAYEFCNSSFRRVVGK----DGLRVQRP-----	92
Tt Mio10	KRRAFPVAVGVGFGAGRAYEFCNSSFRRVVGK----DGLRVQRP-----	98
Sp Mio10	KRRAFPVWVGIGFGLCKSYADSNARLRTFHAI----PKQLPASSTQKKD	86
Bd Mio10	KRRGWFVGLATGFGAGMAYSQCSQSLAASTLLP---ASTPKQ-----	86

Figure 11. Alignment of Mio10 yeast homologs. Multiple sequence alignment performed by ClustalW 2.0.11. Black boxes indicate identical residues in at least four species; gray boxes indicate similar amino acids according to Erdmann *et al.*, 1991. Sc, *S. cerevisiae*; Zr, *Z. rouxii*; Vp, *V. polyspora*; Ct, *C. tropicalis*; Ca, *C. albicans*; Dh, *D. hansenii*; Pp, *P. pastoris*; Yl, *Y. lipolytica*; Cg, *C. globosum*; Ag, *A. gossypii*; Lt, *L. thermotolerans*; Kl, *K. lactis*; Nc, *N. crassa*; Mo, *M. oryzae*; Pa, *P. anserina*; Tr, *T. reesei*; Ss, *S. sclerotiorum*; Tt, *T. tonsurans*; Sp, *S. pombe*; Bd, *B. dendrobatidis*.

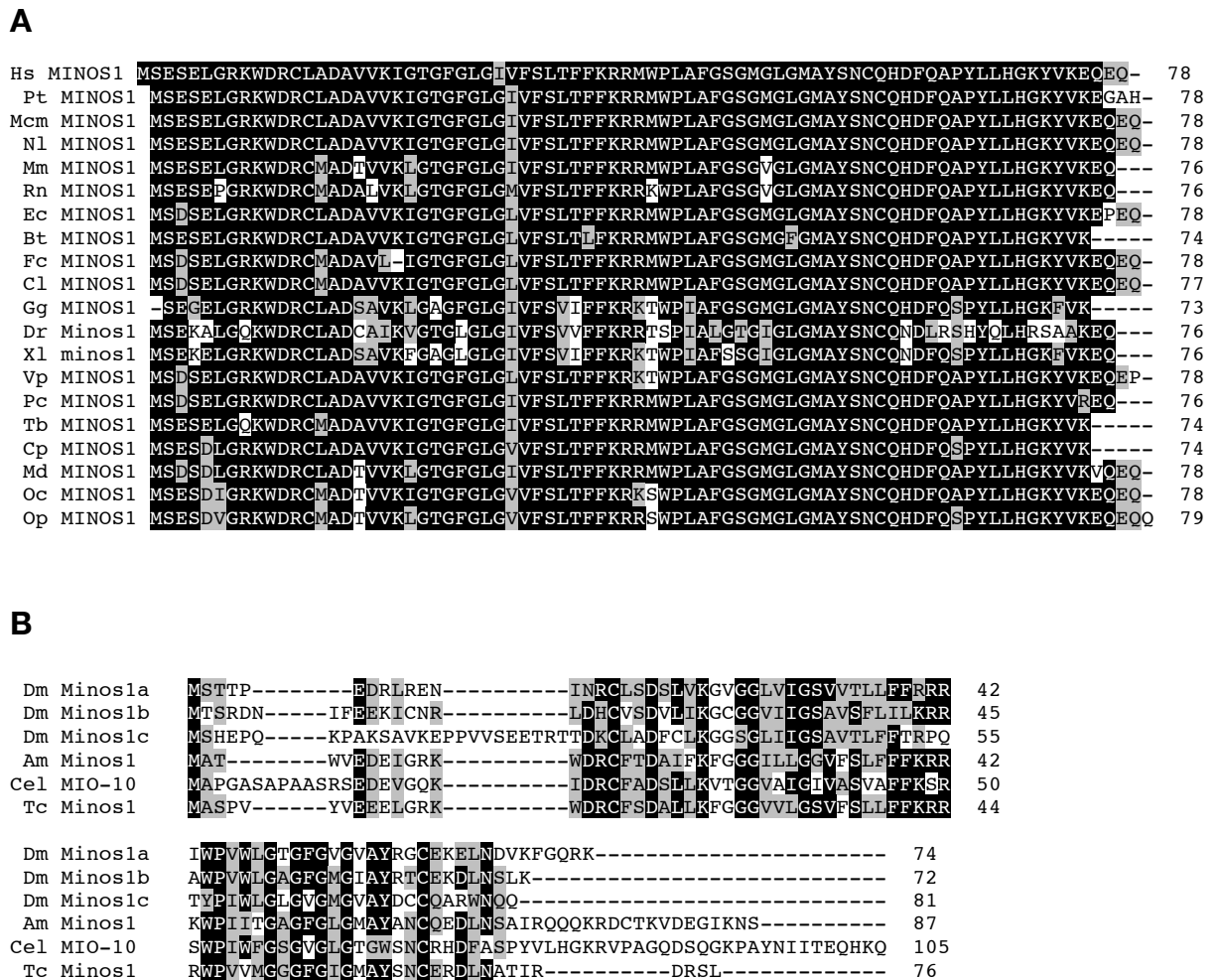


Figure 12. Alignment of MINOS1 homologs. Multiple sequences preformed by ClustalW 2.0.11. (A) Vertebrates (B) Invertebrates. Black boxes indicate identical residues in at least four species; gray boxes indicate similar amino acids according to Erdmann *et al.*, 1991. Hs, *H. sapiens*; Pt, *P. troglodytes*; Mcm, *M. mulatta*; Nl, *N. leucogenys*; Mm, *M. musculus*; Rn, *R. norvegicus*; Ec, *E. caballus*; Bt, *B. taurus*; Fc, *F. catus*; Cl, *C. lupus familiaris*; Gg, *G. gallus*; Dr, *D. rerio*; Xl, *X. laevis*; Vp, *V. pacos*; Pc, *P. capensis*; Tb, *T. belangeri*; Cp, *C. porcellus*; Md, *M. domestica*; Oc, *O. cuniculus*; Op, *O. princeps*; Dm, *D. melanogaster*; Am, *A. mellifera*; Cel, *C. elegans*; Tb, *T. castaneum*; At, *A. thaliana*; Gm, *G. max*; Os, *O. sativa*; Zm, *Z. mays*. For Dm: a, b, and c indicate different isoforms. For Cel, MINOS1 termed MIO-10 in accordance with *C. elegans* nomenclature guidelines.

4.2 Topological analysis of Mio10 and MINOS1

F₁F₀ATPase dimerization factors are membrane proteins that interact with the inner membrane embedded F₀ portion of F₁F₀ATPase (Wagner *et al.*, 2010). In order to investigate a possible role of Mio10 and MINOS1 in F₁F₀ATPase dimerization, their association with the inner membrane was investigated. To this end, antibodies that specifically recognize Mio10 and MINOS1 were required. Once these antibodies were verified, mitochondrial sublocalization and membrane association assays were performed.

4.2.1 Antibody generation and specificity

To analyze endogenous MINOS1 protein signals a commercially purchased antibody against MINOS1 was used. MINOS1 antibody specificity was tested, in which a protein extract from either whole-cell lysate or from isolated mitochondria were analyzed by Western blotting (Figure 13A). In both cases, the MINOS1 antibody recognizes a protein of approximately 10 kDa in size. The antibody non-specifically recognizes proteins of 14 and 60 kDa in size; these proteins however are not present in the mitochondrial protein extract indicating that the only the 10 kDa protein is imported and incorporated into mitochondria.

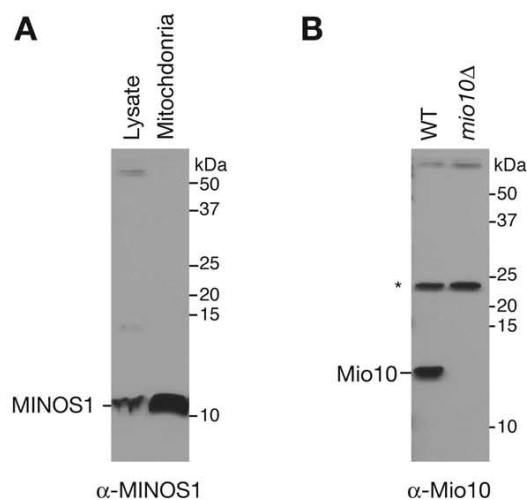


Figure 13. Antibody specificity test. (A) Western-blot analysis of HEK293T whole-cell extract (lysate) and HEK293T isolated mitochondria using MINOS1 specific antibodies. (B) Western-blot analysis of whole-cell protein extracts from wildtype and *mio10Δ* yeast culture using Mio10 specific antibodies. In (A) and (B), 10 μ g protein was loaded on each lane. * indicates non-specific antibody cross-reaction.

In contrast, an antibody was generated to analyze endogenous Mio10 protein signals by Western blot analysis (Figure 13B). This has been achieved by using a chemically synthesized peptide (EGDAIFRSSAGLRSSKV) corresponding to the C-terminal of the Mio10 protein. Antibody specificity evaluation was performed by analyzing whole-cell proteins extracts from wildtype and *mio10Δ* strains. Western blot analysis indicates that the raised antibody specifically recognizes a protein product slightly larger than 10 kDa. The antibody, however, also recognizes two nonspecific protein products of approximately 22 and 60 kDa in size. It should be noted that the antibodies against Mio10 and MINOS1 did not recognize their respective epitopes on Blue native PAGE (BN-PAGE), which can be used to characterize large complexes in their native state (Nijtmans *et al.*, 2002). For immunodetection purposes, the antibodies were primarily used with SDS-PAGE.

4.2.2 Topological analysis of Mio10

To assess whether Mio10 was a membrane protein, a carbonate extraction analysis was performed on isolated wildtype mitochondria (Figure 14A). Upon treatment with carbonate buffer, followed by high-speed centrifugation, Mio10 was carbonate resistant and remained in the membrane pellet, similar to mitochondrial integral membrane proteins Tom70 and Tim21. On the other hand, the peripherally membrane associated protein Tim44 was released into the supernatant. This result indicates that Mio10 behaves like an integral membrane protein. As a control, treatment of mitochondria with Triton X-100 (TX-100) released all proteins into the supernatant.

In addition, the sublocalization of Mio10 was assessed by a protease protection assay, in which wildtype mitochondria were treated with various concentrations of Proteinase K (Figure 14B). Tom70, which is localized at the mitochondrial outer membrane, was degraded, whereas Mio10 was protected against protease degradation. Upon osmotic disruption of the outer membrane and thus generation of mitoplasts and exposing protein contents and protein domains associated with the IMS, Mio10 was rendered accessible to protease degradation. In contrast, matrix proteins (Tim44 control) were unaffected. As the antibody is specific the C-terminus of Mio10, the partial loss of antibody signal by Western blot analysis indicates that the affected C-terminus of Mio10 is located in the IMS. This is supported by the observation that the pattern of Mio10 PK degradation pattern resembles that of Tim21, an inner membrane

protein, in which PK treatments leads to partial degradation of its IMS exposed C-terminus (Chacinska *et al.*, 2005). These results combined with membrane association results indicate that Mio10 is an integral mitochondrial inner membrane protein with its C-terminus exposed to the IMS (Figure 17).

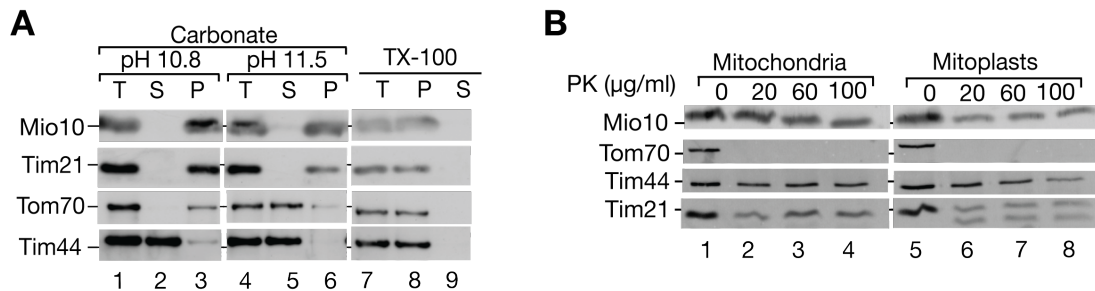


Figure 14. Mio10 is a mitochondrial IMS protein. (A) Membrane association assay. mitochondria were suspended in carbonate buffer, or alternatively lysed with 1% Triton X-100. All samples were incubated on ice and then subjected to ultracentrifugation and TCA precipitation followed by SDS-PAGE and Western blot analysis. (B) Protease protection assay; mitochondria, and mitoplasts were treated with various amounts of PK. The pellets of SEM-treated mitochondria and mitoplasts were resuspended in protein loading dye and analyzed by SDS-PAGE and Western blot analysis. T, total; P, pellet; S, supernatant; PK, Proteinase K; TX-100, TritonX-100.

4.2.3 Subcellular localization of MINOS1 by immunofluorescence

Sequence analysis of the MINOS1 ORF (C1orf151) indicated predicted a mitochondrial localization based on large-scale mitochondrial genetic screen (Baughman *et al.*, 2009). To verify this, immunofluorescence microscopy using MINOS1 specific antibodies was performed (Figure 15). Antibodies against MINOS1 and the mitochondrial marker Cyclophilin D were applied to monkey epithelial kidney cells, VERO. Image analysis revealed co-localization of MINOS1 and Cyclophilin D antibody signals, supporting the notion that MINOS1 is a mitochondrial protein. Moreover, cells were stained with the nuclear marker DAPI, indicating that both MINOS1 and Cyclophilin D localized to mitochondrial networks.

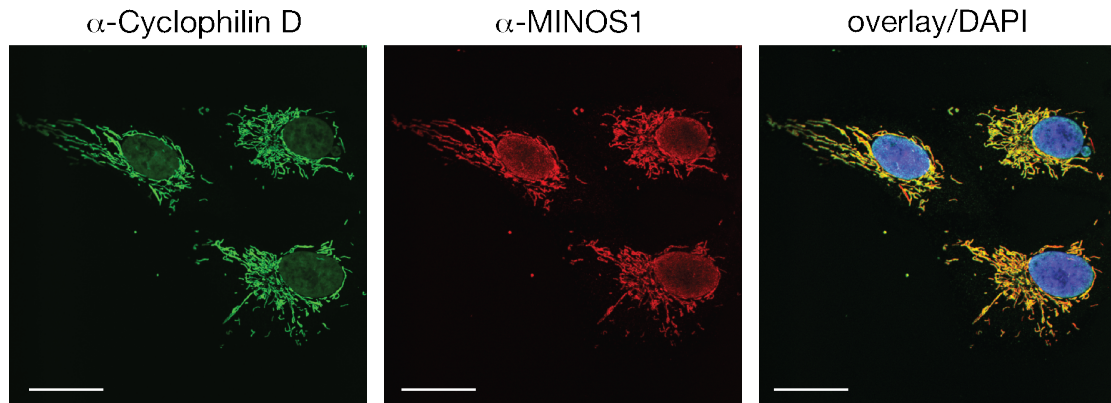


Figure 15. MINOS1 is a mitochondrial localized protein. Immunofluorescence analysis of MINOS1 localization. VERO cells were fixed in 8% paraformaldehyde (PFA) and permeabilized in 0.5 % (v/v) Triton X-100. Treated cells were then incubated for 1 hour with MINOS1-antibody and the mitochondrial marker Cyclophilin D-antibody. Cells were then washed cells and incubated with Oregon Green 488 conjugated IgGs and KK114 conjugated goat IgGs. Cells were then stained with DAPI staining before performing fluorescence microscopy. Scale bars = 10 μ m. Microscopy was performed by Daniel Jans (AG Jakobs, MPI-bpc).

4.2.4 Topological analysis of MINOS1

To test MINOS1 membrane association, a carbonate extraction analysis was performed on mitochondria isolated from HEK293T cells, in which cultured cells were treated with carbonate buffer pH 10.8 or 11.5 (Figure 16A). In all cases, MINOS1 appeared carbonate resistant and remained in the membrane pellet similar to mitochondrial integral membrane proteins TOM70 and TIM23. On the other hand, the matrix protein, TACO1, was released into the supernatant. The results thus indicate that MINOS1 is an integral membrane protein.

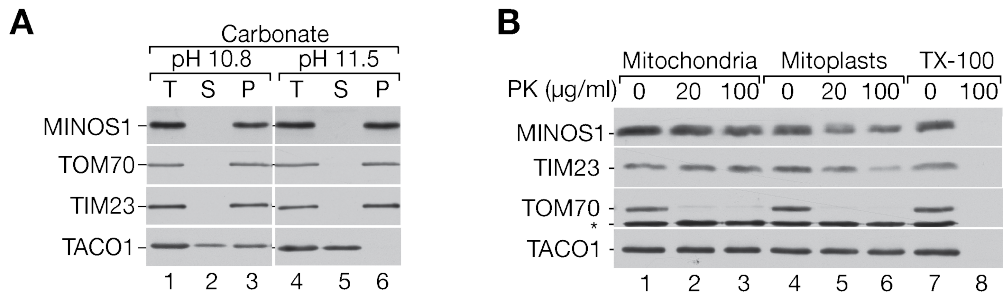


Figure 16. MINOS1 is a mitochondrial IMS protein. (A) Protease protection assay; mitochondria, mitoplasts, or Triton X-100 lysed mitochondria were treated with various amounts of PK. The pellets of SEM-treated mitochondria and mitoplasts and the supernatant of Triton X-100 lysed mitochondria were resuspended in protein loading dye and analyzed by SDS-PAGE. PK, Proteinase K; TX-100, Triton X-100. (B) Membrane association assay. Mitochondria were suspended in carbonate buffer, or alternatively lysed with 1% Triton X-100. All samples were incubated on ice and then subjected to ultracentrifugation and TCA precipitation followed by SDS-PAGE and Western blot analysis. T, total; P, pellet; S, supernatant. * indicates non-specific antibody cross-reaction.

To analyze MINOS1 sublocalization, isolated mitochondria from HEK293T cells and mitoplasts were treated with various concentrations of PK in a protease protection assay (Figure 16B). When mitochondria were treated with various concentrations of PK, MINOS1 appeared to be protected against protease degradation. TOM70, which is localized at the mitochondrial outer membrane, was degraded by PK. Moreover, when mitoplasts were treated with PK, MINOS1 was accessible to protease treatment. The matrix protein TACO1 was unaffected. MINOS1 accessibility was similar to TIM23, an inner membrane protein with its C-terminus exposed to the IMS, supporting the notion that MINOS1 has a similar topology. As a control, all proteins were degraded after treatment with T-X100. The MINOS1 pattern of PK degradation parallels that of the one observed for Mio10, and thus it was concluded that MINOS1 and Mio10 have a similar topology in the mitochondrial inner membrane. These results combined with membrane association assay results indicate that MINOS1 is an integral mitochondrial inner membrane protein with its N- and C-termini exposed to IMS. Thus based on results from the protease protection assay and membrane association assay, it is deduced that the MINOS1, together with its yeast homolog Mio10, are mitochondrial inner membrane proteins with both of their termini exposed to the IMS (Figure 17).

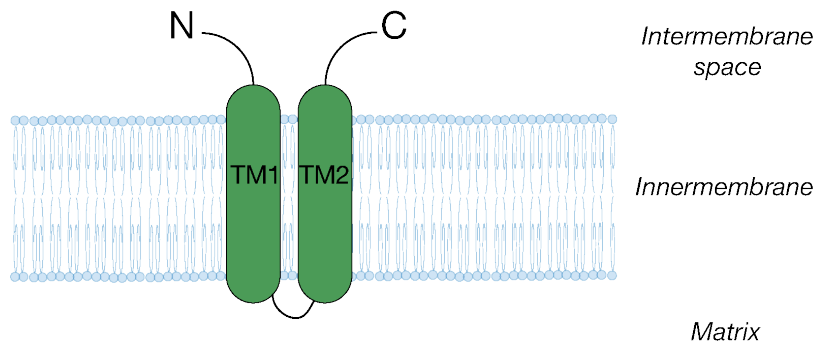


Figure 17. Topology of Mio10 and MINOS1. Subfractionation and membrane association analysis indicate that Mio10 is an integral mitochondrial inner membrane protein with its N and C termini exposed to the IMS. N, Amino-terminus; C, Carboxyl-terminus; TM, transmembrane domain.

4.3 Analysis of Mio10 and MINOS1 association with the F_1F_0 ATPase

In order to investigate the roles of Mio10 and MINOS1 with respect to F_1F_0 ATPase dimerization, Mio10 and MINOS1 containing complexes were first investigated by BN-PAGE. This technique allows the separation of large proteins complexes without their dissociation and has been useful in the analysis of various F_1F_0 ATPase dimerization factors (Arnold *et al.*, 1999; Nijtmans *et al.*, 2002; Wagner *et al.*, 2009). Because of the Mio10 and MINOS1 antibodies limitations on BN-PAGE, *in vitro* synthesized radiolabeled precursors of the proteins were used. Import and assembly were performed. In addition, interactions of Mio10 and MINOS1 with F_1F_0 ATPase were investigated by biochemical isolations from strains containing tagged F_1F_0 ATPase components.

4.3.1 *in vitro* import of Mio10 and analysis by SDS-PAGE

A ^{35}S -labeled Mio10 precursor was synthesized *in vitro* and imported into energized or membrane potential depleted wildtype mitochondria in the presence or absence of PK (Figure 18). Mio10 is imported in a non-membrane potential manner. Furthermore, Mio10 appears to be protected against PK treatment. As a control [^{35}S]Su9-DHFR was imported. This preprotein is composed of the N-terminal 69 residues of the F_1F_0 ATPase subunit 9 (Su9) precursor of *N.crassa*, fused with the mouse dihydrofolate reductase (DHFR) (Pfanner *et al.*, 1987). In contrast to Mio10 import, Su9-DHFR import indicated both membrane potential dependency and PK sensitivity.

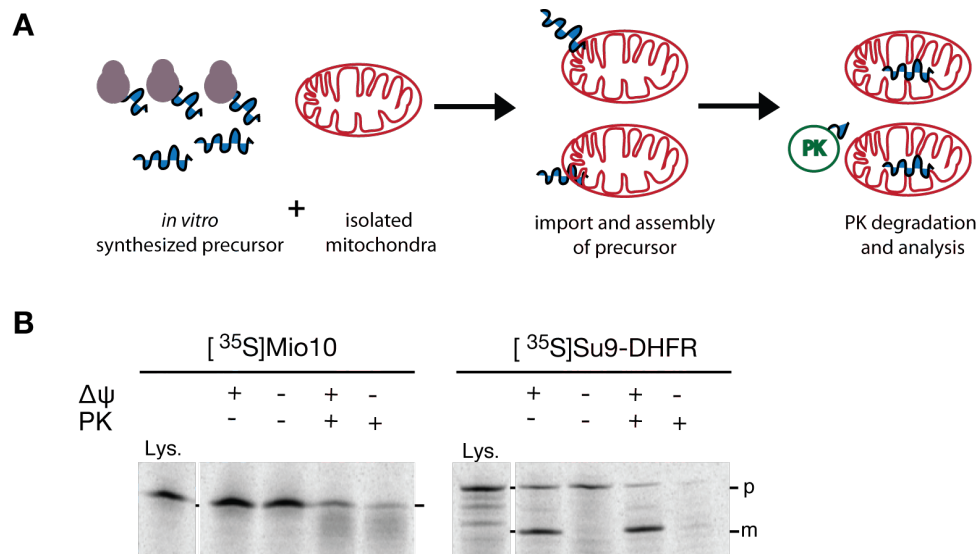


Figure 18. Import of Mio10 into mitochondria is membrane potential independent. (A) Schematic diagram representing *in vitro* import of radiolabeled lysate in mitochondria. (B) Radiolabeled Mio10 and Su9-DHFR were imported into isolated mitochondria in the presence or absence of a membrane potential for the indicated times. Samples were split and left untreated or treated with proteinase K (PK) and analyzed by Tricine-SDS-PAGE and digital autoradiography. As control, lysate containing Mio10 precursor or Su9-DHFR were applied (Lys.); p, precursor; m, mature protein.

4.3.2 Mio10 and MINOS1 assembly analysis by BN-PAGE

Radiolabeled Mio10 and MINOS1 labeled precursors were synthesized *in vitro* and imported into energized or membrane potential depleted wildtype yeast mitochondria, which were then solubilized in mild digitonin buffer and analyzed by BN-PAGE (Figure 19A). Mio10 assembles in a time and membrane potential dependent manner into complexes of various size, ranging from high molecular components (>669 kDa) to smaller complexes (approximately 160 kDa). Interestingly, MINOS1 imports and assembles in yeast mitochondria. Moreover Mio10 and MINOS1 labeled precursors were imported and assembled in HEK293T isolated mitochondria (Figure 19B). Mio10 appears to assemble in human mitochondria, at which Mio10 and also MINOS1, as in yeast mitochondria, form a range of complexes.

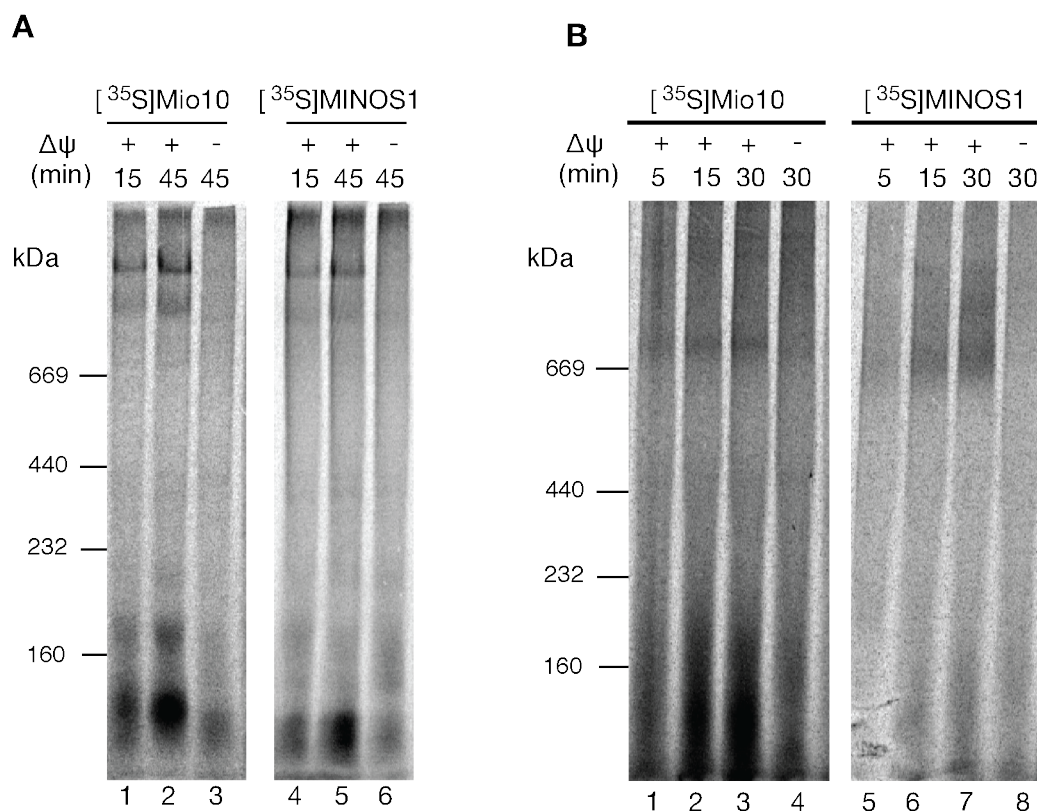


Figure 19. Mio10 and MINOS1 assemble into high molecular sized mitochondrial complexes. Radiolabeled Mio10 precursor was imported into isolated wildtype mitochondria in the presence or absence of membrane potential for the indicated times. Radiolabeled Atp21, Atp20 and Cox13 were imported in parallel. All samples were treated with proteinase K, solubilized in digitonin buffer, and subjected to BN-PAGE (4-10% gradient gel). Protein complexes signals were detected by digital autoradiography. V₂, V, III₂IV, and III₂IV₂ indicate respiratory chain complexes.

4.3.3 Comparison of Mio10 complexes assembly with the F₁F₀ATPase

In order to analyze the biogenesis of Mio10-containing complexes in mitochondria a radiolabeled precursor of Mio10 was imported into wildtype isolated mitochondria and then analyzed by BN-PAGE (Figure 20). In comparison, Cox13, a structural subunit of the cytochrome *c* oxidase, was assembled in wildtype mitochondria (Tsukihara *et al.*, 1996). Indeed, Mio10 assembles into complexes larger than respiratory chain supercomplexes, III₂IV and III₂IV₂. When Atp20 assembly was preformed in comparison, Mio10 higher complexes are observed to migrate at a similar molecular size of the F₁F₀-ATP synthase monomer and dimers. Moreover, it appears that Mio10 may associate with the F₁F₀ATPase dimer (V₂) with a lesser extent to the monomer (V) and also what appears to be an intermediate complex.

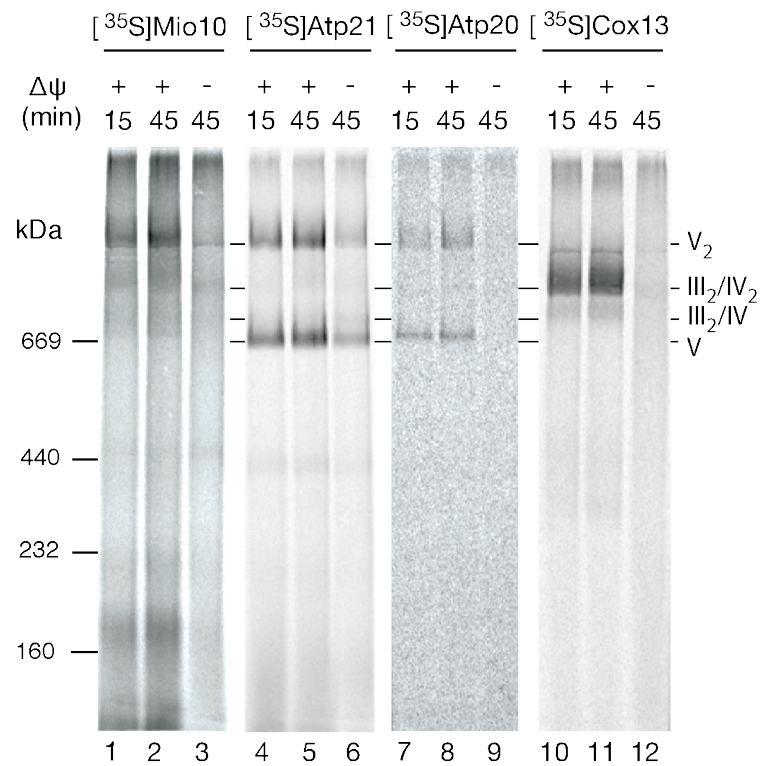


Figure 20. Mio10 comigrates with F_1F_0 ATPase complexes. Radiolabeled Mio10 precursor was imported into isolated wildtype mitochondria in the presence or absence of membrane potential for the indicated times. Radiolabeled Atp21, Atp20 and Cox13 were also imported in parallel. All Samples were treated with proteinase K, solubilized in digitonin buffer, before complex separation by BN-PAGE (4-10% gradient gel). Protein complexes signals were detected by digital autoradiography. V_2 , V, III_2IV , III_2IV_2 indicate respiratory chain complexes.

4.3.4 Analysis of Mio10 assembly in the absence of F₁F₀ATPase dimers

To verify Mio10 association with the F₁F₀ATPase, a Mio10 radiolabeled precursor protein was imported into *atp20Δ* mitochondria, which lack an assembled F₁F₀ATPase dimer due to the absence of the dimerization factor, Atp20 (Figure 21A). As a control, radiolabeled precursor of Atp21 was imported into *atp20Δ* or wildtype mitochondria. As expected, Atp21 assembles into the F₁F₀ATPase dimeric and monomeric forms in wildtype mitochondria whereas in *atp20Δ* mitochondria, it exclusively assembles to the F₁F₀ATPase monomer (Wagner *et al.*, 2009). In parallel, Mio10 does not assemble into F₁F₀ATPase dimer in *atp20Δ* mitochondria but rather shifts to the monomeric form; supporting the notion that Mio10 may be an F₁F₀ATPase associated protein. Furthermore, analysis by BN-PAGE suggests the requirement of Atp20 for proper of Mio10 assembly.

In order to rule out the possibility of post lysis association of Mio10 assembly into the F₁F₀ATPase, a ‘Mix’ assembly assay was performed (Figure 21B). Mio10 assembly was carried out as above into *atp20Δ* mitochondria and into wildtype mitochondria without addition of radiolabeled lysate (Mock); reactions were mixed before analysis by BN-PAGE (Figure 21C). If Mio10 association with the F₁F₀ATPase were non-specific, then mixing the assembly reactions would give a positive signal corresponding to the dimer. As a control, Mio10 assembly in wildtype background was performed in juxtaposition. Results however indicated that the Mio10 large complexes continue to associate with F₁F₀ATPase dimer ruling out possible non-specific association.

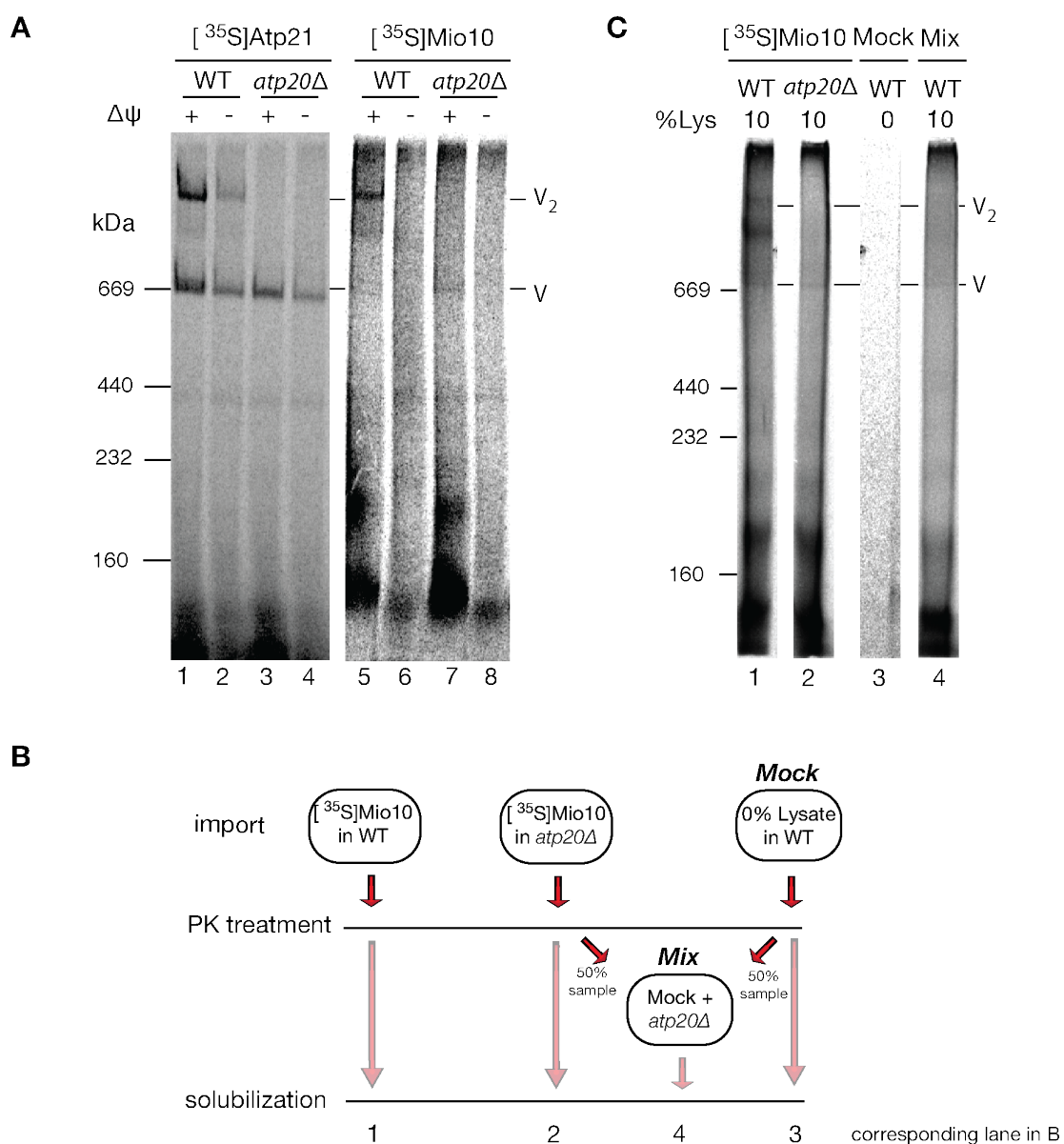


Figure 21. Mio10 assembly requires the presence of Atp20. (A) Radiolabeled Atp21 and Mio10 precursor were imported into isolated wildtype and *atp20Δ* mitochondria in the presence or absence of membrane potential for the indicated times. (B) Schematic diagram describing ‘Mix’ assembly assay. (C) Mix assembly assay. Assembly was performed in WT and in *atp20Δ*. A mock assay performed with no lysate added. After import, mitochondria were treated with PK. 50% of the *atp20Δ* assay sample was mixed with 50% of the mock. Lane 3 overexposed for clarity. (A, C) All Samples were treated with proteinase K, solubilized in digitonin buffer, before complex separation by BN-PAGE (4-10% gradient gel). Protein complexes signals were detected by digital autoradiography. V₂, V, III₂IV, III₂IV₂: respiratory chain complexes.

4.3.5 Second dimension analysis of Mio10 complexes in *atp20Δ* mitochondria

Import and assembly of radiolabeled Mio10 indicated that Mio10 associates with what appears to be the F₁F₀ATPase dimer in wildtype mitochondria, whereas this association is rendered absent in *atp20Δ* mitochondria that lack the F₁F₀ATPase dimer. To investigate this observation further, a second dimension analysis of *atp20Δ* mitochondria was performed (Figure 22). In brief, wildtype and *atp20Δ* mitochondria were solubilized in digitonin buffer followed by separation of protein complexes on BN-PAGE. Individual lanes from the BN gel were sliced and further subjected to SDS-PAGE analysis (second dimension). The aim of the approach was to examine Mio10 signals in comparison to the F₁F₀ATPase markers on second dimension as Mio10 antibodies did not recognize native Mio10 epitopes on BN-PAGE.

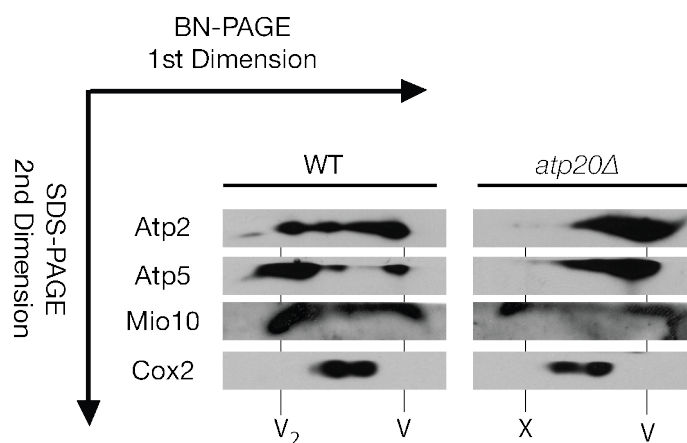


Figure 22. Mio10-containing complexes in *atp20Δ* mutants. Wildtype and *atp20Δ* mitochondria were solubilized in digitonin buffer, subjected to BN-PAGE (4-10% gradient gel). BN gel stripes were excised and subjected to SDS-PAGE. Signals were detected by Western blotting, V₂, dimer; V, monomer; X, undefined.

Immunoblotting for Atp2 or Atp5 enables detection of F₁F₀ATPase monomers and dimers and thus a tool to assess status of dimerization. In wildtype mitochondria, Atp2 or Atp5 immunoblots indicate two large distinct points corresponding to the F₁F₀ATPase monomer and dimer. In addition, Cox2 detection was used as a negative control and signals were unchanged in both wildtype and *atp20Δ* mitochondria. In *atp20Δ* mitochondria, Atp2 and Atp5 immunodetection yielded only on distinct signal corresponding to the F₁F₀ATPase monomer. Moreover, checking for Mio10 in the wildtype indicates two distinct points similar to the Atp5 and Atp2, in agreement with the import and assembly results. However, the two Mio10 specific signals remain

present in *atp20Δ* mitochondria, indicating that the Mio10 high molecular sized complex (initially argued to be the F₁F₀ATPase dimer and labeled ‘X’ in Figure 22) continues to appear even in the absence of properly assembled F₁F₀ATPase dimer. Hence, second dimension analysis argues against Mio10 assembly and/or association with the F₁F₀ATPase dimer as shown in the import and assembly assays. The Mio10-containing complex may thus have similar molecular sizes to the F₁F₀ATPase and comigrate in a similar fashion in BN-PAGE.

4.3.6 Biochemical isolation of F₁F₀ATPase components

In a further attempt to demonstrate Mio10 F₁F₀ATPase association, biochemical isolations from an Atp20^{zz} strain (in which ProteinA was C-terminally fused to Atp20) were performed (Figure 23A). Immunoprecipitation was successful in co-isolating F₁F₀ATPase subunits such as Atp5 and the Atp20^{zz} bait. However, Mio10 was not co-isolated with Atp20. Moreover, decorations for Cox2 (cytochrome *c* oxidase), Rip1 (complex III) or Tom70 (TOM) were negative. All together, immunoprecipitation indicate that in disagreement with initial assembly results, Mio10 is not stably associated with the F₁F₀ATPase.

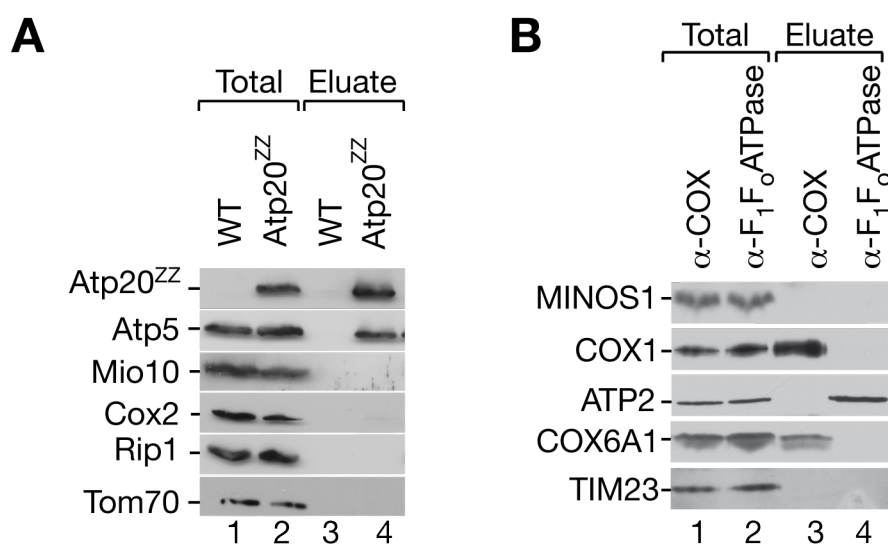


Figure 23. Mio10 and MINOS1 are not stably associated with the F₁F₀ATPase. (A) Wildtype and Atp20^{zz} mitochondria were solubilized and subjected to IgG- chromatography. Eluates were analyzed by SDS-PAGE and Western blotting. (B) Co-immunoprecipitations of cytochrome *c* oxidase (COX) and F₁F₀ATPase components from isolated HEK29T mitochondria. Eluates were analyzed by SDS-PAGE and Western blotting.

To investigate whether MINOS1 associates with the F₁F₀ATPase in higher eukaryotes, co-immunoprecipitations were performed from HEK293T mitochondria. Commercial antibodies specific to either the F₁F₀ATPase (α -F₁F₀ ATPase) or (α -COX) as a negative control were used (Figure 23B). α -COX efficiently immunoprecipitates cytochrome *c* oxidase subunits COX1 and COX6A1 but not MINOS1, ATP2, or TIM23. In contrast, (α -F₁F₀ATPase) antibodies successfully immunoprecipitated ATP2; but not MINOS1 or any of the negative controls. The results thus indicate that, as shown with Mio10 in yeast mitochondria, MINOS1 is also not stably associated with the F₁F₀ATPase.

4.4 *MIO10* deletion mutant analysis

As biochemical isolations indicated that Mio10 and MINOS1 do not associate with the F₁F₀ATPase, a possible function in mitochondrial respiration and F₁F₀ATPase activity was investigated. To this end, a *MIO10* deletion strain (*mio10* Δ), in which the YCL057c-A ORF was replaced by a kanamycin cassette (OpenBiosystems), was used. Any effect that the absence of Mio10 may have on F₁F₀ATPase dimerization and oligomerization was also investigated.

4.4.1 Growth analysis of *MIO10* deletion mutant mitochondria

To determine the effect of Mio10 on mitochondrial respiration, a growth behavior analysis was performed. Wildtype and *mio10* Δ cells were grown on fermentable (glucose) and non-fermentable (glycerol) medium plates at 30°C (Figure 24A). In addition, the non-respiring *atp2* Δ strain as well as *atp20* Δ mutants were used for comparison. A failure to grow on fermentable media may indicate respiratory chain function as shown for various respiratory chain mutants (Mick *et al.*, 2010). Indeed, all strains grow as expected on glucose, meanwhile, the *atp2* Δ mutant, which lacks a functional F₁F₀ATPase, fails to grow. The deletion of dimerization factors does not affect respiration, as the F₁F₀ATPase monomers are still functionally active (Wittig and Schägger, 2009). However, both *atp20* Δ and *atp21* Δ mutants exhibit a weak phenotype when grown on non-fermentable medium (Arnold *et al.*, 1998). Interestingly, both *mio10* Δ and *atp20* Δ appear to have similar slight growth impediments compared to wildtype and *atp2* Δ mitochondria. The results from the growth behavior analysis indicate that Mio10 may not be required for respiration.

4.4.2 Analysis of respiratory chain complexes in *mio10*Δ

The *MIO10* deletion strain was used to further assess a Mio10 role in F₁F₀ATPase assembly. Wildtype and *mio10*Δ mutant mitochondria were analyzed by BN-PAGE and Western blot analysis (Figure 24B). Immunodetection for the F₁F₀ATPase protein, Atp5, indicates F₁F₀ATPase dimerization is not affected in *mio10*Δ cells. Moreover, the absence of Mio10 does not affect complex III or cytochrome *c* oxidase assembly (indicated by immunodetection with Rip1 and Cox4 antibodies, respectively). Mio10 thus appears not to have a role in the assembly of the F₁F₀ATPase or other respiratory chain supercomplexes in yeast.

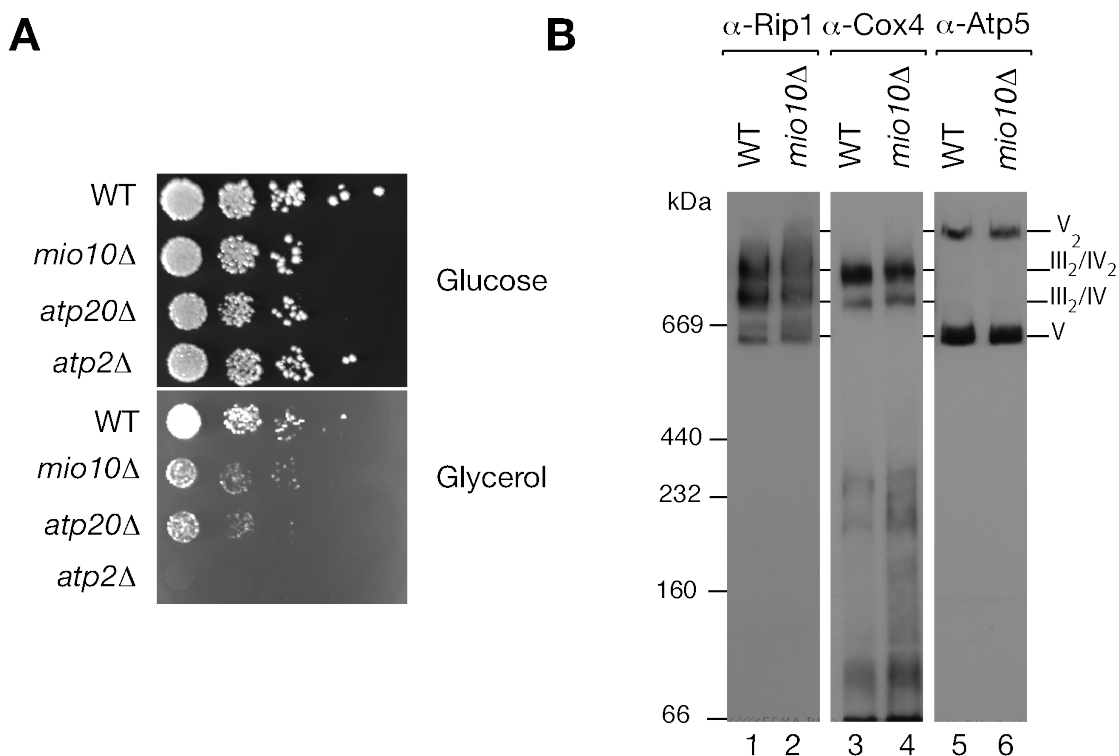


Figure 24. Mio10 is not required for mitochondrial respiration or supercomplex assembly. (A) Wildtype, *mio10*Δ, *atp20*Δ and *atp2*Δ yeast cells were spotted in serial 10-fold dilutions on fermentable (glucose) and non-fermentable (glycerol) media. (B) Wildtype and *mio10*Δ mitochondria were solubilized in digitonin buffer, subjected to BN-PAGE (4-10% gradient gel) and Western blotting.

4.4.3 Assessment of F₁F₀ATPase activity and oligomerization in *mio10*Δ mutants

Mitochondrial respiratory chain complexes retain their enzymatic activity after separation by BN-PAGE (Wittig *et al.*, 2007). To this end, an in-gel F₁F₀ATPase activity assay was performed comparing wildtype and *mio10*Δ mitochondria (Figure 25A). The in-gel activity assay (based on reverse action of the enzyme, ATP hydrolysis) indicates that F₁F₀ATPase activity is comparable in wildtype and *mio10*Δ mitochondria and is unaffected by the *MIO10* deletion. Furthermore, neither cytochrome *c* oxidase nor complex I activities were significantly affected.

Given that most of the analysis performed in this study so far focused on F₁F₀ATPase dimerization, the effect on higher F₁F₀ATPase oligomers should be not be disregarded. To this end, an in gel F₁F₀ATPase activity assay was performed on a modified BN gel to better separate higher F₁F₀ATPase oligomers (Figure 25B). As a control, *atp20*Δ were again used in parallel with *fcj1*Δ mitochondria. Deletion of *FCJ1* augments the stability of higher F₁F₀ATPase oligomers (Rabl *et al.*, 2009). A modified in-gel activity assay in which digitonin buffer conditions and the BN-PAGE gel gradient were altered. The assay revealed various bands corresponding to the F₁F₀ATPase monomer, dimer, and higher oligomers. Whereas *atp20*Δ mitochondria have an increased pool of F₁F₀ATPase monomer (at 669 kDa), there are no other apparent discrepancies between the other strains. It is thus evident, based on the in-gel activity assay, that there is no change in F₁F₀ATPase oligomerization in *mio10*Δ mitochondria compared to wildtype mitochondria. As F₁F₀ATPase activity was also not affected or did Mio10 (and MINOS1) associate with F₁F₀ATPase, results indicate that neither Mio10 nor MINOS1 are F₁F₀ATPase dimerization factors.

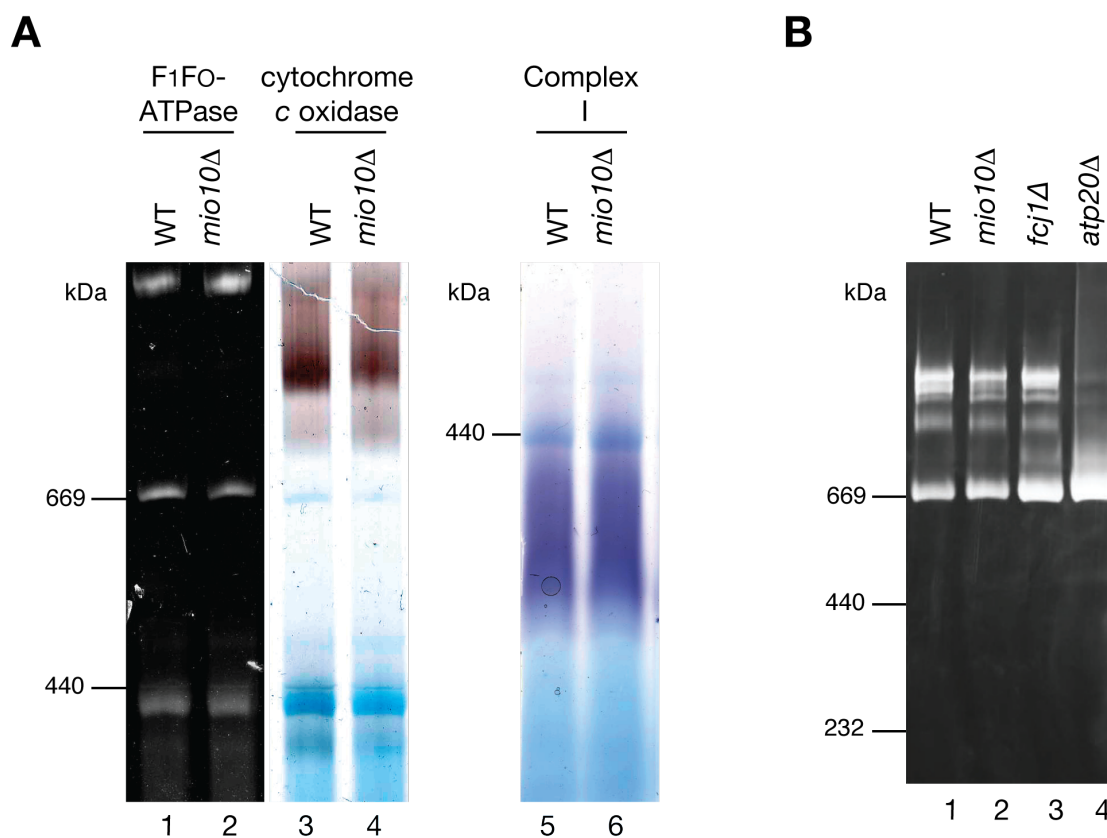


Figure 25. F₁F₀ATPase activity and oligomerization are not affected in *mio10Δ* mutants. (A) Wildtype and *mio10Δ* mitochondria were solubilized in 1% digitonin buffer and subjected to BN-PAGE (4-10% gradient gel). In-gel activity assays were carried out as described in Materials and Methods. (B) Wildtype, *mio10Δ*, *fcj1Δ*, and *atp20Δ* mitochondria were solubilized in 0.35% digitonin buffer and subjected to BN-PAGE (3-13% gradient gel). In-gel F₁F₀ATPase activity assay was performed.

4.5 Identification of Mio10 and MINOS1 interaction partners

Results so far indicate that Mio10 and MINOS1 are not involved in F₁F₀ATPase dimerization, oligomerization, or activity. A function of the proteins remains unclear. To this end, interaction partners of Mio10 and MINOS1 were isolated and analyzed by mass spectrometry with the objective of elucidating Mio10/MINOS1 functions.

4.5.1 Identification of Mio10 interaction partners

In order to identify interaction partners of Mio10, the *MIO10* ORF was C-terminally tagged with a streptavidin tag followed by a FLAG tag (SF). Yeast cells were harvested and mitochondria were isolated. Using the Mio10^{SF}, a large-scale protein isolation was performed via the streptavidin tag, and eluates were analyzed by mass spectrometry. First, eluates from the Mio10^{SF} isolation were subjected to SDS-PAGE and the gel was stained with coomassie. The SDS-PAGE was cut into 23 slices, which were then analyzed by high-resolution online liquid chromatography-tandem mass spectrometry (LC-MS/MS). Co-isolated proteins were scored based on the normalized fold change calculated using a label-free spectral count approach. Table 7 indicates specific interacting proteins with highest spectral counts, in which a normalized fold change cut-off of 0.1 was applied. The normalized fold change was calculated based on spectral counts of a specific protein and total spectral counts for all proteins in the sample. Besides the bait Mio10, Fcj1, which is involved in mitochondrial cristae formation and maintenance, had the highest sample spectral count (Rabl *et al.*, 2009). Moreover, none of the highest scoring proteins were F₁F₀ATPase associated proteins.

Indeed, the LC-MS/MS results provide a wide range of proteins, of both characterized and previously uncharacterized functions. Characterized proteins identified in the analysis range from cytochrome *c* oxidase components (Cox20), to mitochondrial import (Pam17), mitochondrial translational regulation (Mdm38), and mitochondrial ribosomal proteins (Mrpl27). These proteins, however, gave low spectral counts and their identification might be a result of nonspecific binding to the column. Interestingly, many of the highest scoring proteins (YGR235C, Aim37, Aim13, Aim46, Aim5, and Aim24), are previously uncharacterized and may be potential interacting partners of Mio10. The AIM (Altered Inheritance of Mitochondria) proteins were found by a computational screen to play a role in

mitochondrial biogenesis and inheritance (Hess *et al.*, 2009). Their interaction with Mio10 may indicate a possible role of Mio10 in mitochondrial inheritance.

Table 7. Identified proteins of the Mio10^{SF} StrepTactin-chromotography. The raw MS files were searched and analyzed with Mascot (Mascot Daemon version 2.2.2, Matrix Science) and Scaffold 3 (Proteome Software) using the *S. cerevisiae* NCBI non-redundant protein database. The normalized fold change ratios were then calculated in Scaffold using the spectral count approach (Liu *et al.*, 2004). Mass spectrometric analysis performed by Monika Raabe and Miroslav Nikolov (AG Urlaub, MPI-bpc, Göttingen).

Protein	Molecular weight	Normalized fold change (spectrum count)	Spectral counts		Unique peptides	
			Control	Sample	Control	Sample
Fcj1	61 kDa	0.09	26	614	16	59
Mio10	10 kDa	0.07	6	143	3	11
YGR235C	27 kDa	0	0	136	0	26
Aim37	27 kDa	0.05	2	126	2	25
Nde2	62 kDa	0.02	0	75	0	26
Aim13	19 kDa	0.1	4	52	3	19
Aim46	34 kDa	0.1	3	43	3	20
Aim5	12 kDa	0.1	3	40	3	11
Odc1	34 kDa	0.05	1	31	1	19
Aim38	25 kDa	0	0	29	0	12
Cox20	24 kDa	0.07	1	22	1	12
Cbp4	18 kDa	0	0	20	0	11
YBL095W	31 kDa	0	0	17	0	11
Aim31	18 kDa	0	0	16	0	11
Yhb1	45 kDa	0.1	1	13	1	8
Aim24	44 kDa	0.1	1	11	1	8
Mdm38	65 kDa	0.1	1	10	1	7
Oms1	56 kDa	0	0	9	0	7
Cir2	70 kDa	0	0	9	0	8
Pam17p	22 kDa	0	0	9	0	4
Fmp33	20 kDa	0.1	1	9	1	4
Tuf1	48 kDa	0	0	8	0	6
Mcr1	34 kDa	0	0	5	0	4
Aim45	37 kDa	0	0	5	0	4
Pet100	13 kDa	0	0	5	0	3
Sod2	24 kDa	0	0	5	0	3
Mrpl27	16 kDa	0	0	5	0	3

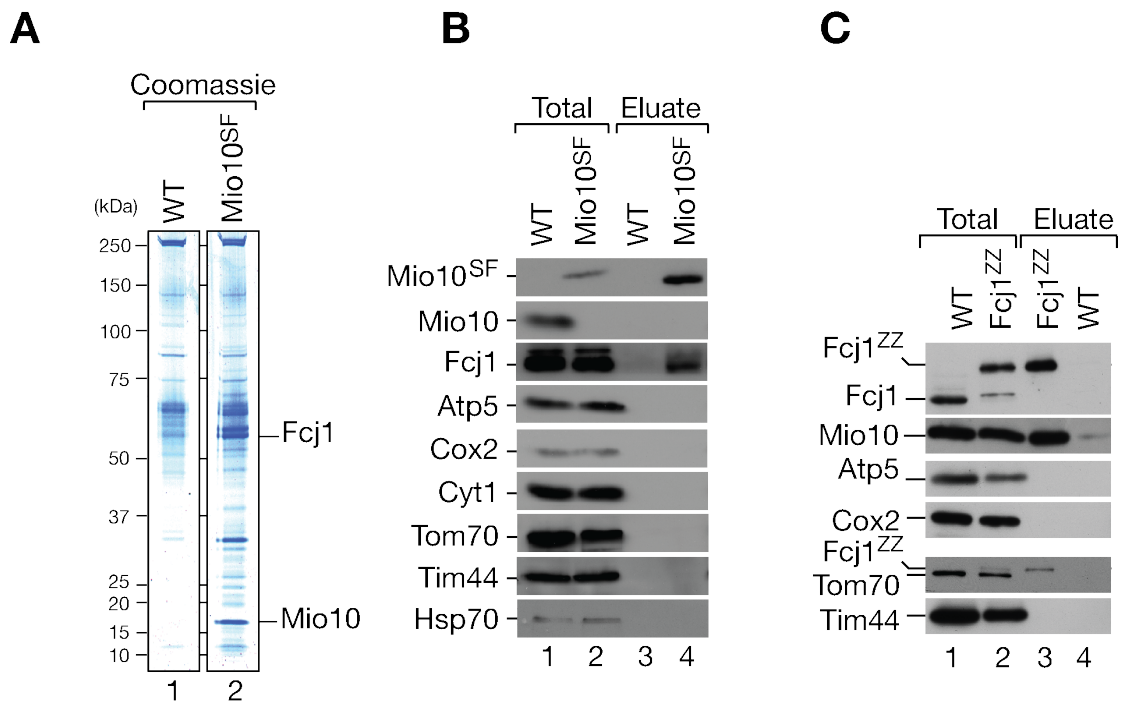


Figure 26. Mio10 interacts with Fcj1. (A) Wildtype and Mio10^{SF} mitochondria were solubilized and subjected to Strep-Tactin chromatography. Eluates were separated by SDS-PAGE and gels were coomassie stained. (B) Eluates from Strep-Tactin chromatography were analyzed by SDS-PAGE and Western blotting. (C) Wildtype and Fcj1^{ZZ} mitochondria were solubilized and subjected to IgG chromatography. Eluates were analyzed by SDS-PAGE and Western blotting.

The protein composition of coomassie stained bands was identified due to the availability of spectral counts for each slice. Figure 26A depicts the coomassie stained gel used for LC-MS/MS analysis, in which coomassie stained bands corresponding to Fcj1 and Mio10 were annotated. The results from the Mio10^{SF} complex isolation and consequent analysis indicated that Fcj1 co-isolates with Mio10. To further verify this, eluates from the Mio10^{SF} isolation were separated on an SDS-PAGE and subjected to Western blot analysis (Figure 26B). Immunoblotting for Fcj1, indicate a clear band in Mio10^{SF} eluate and a lack of signal in the wildtype control, thus verifying results from the mass spectrometry. Moreover, immunodetection for Atp5 verified that the F₁F₀ATPase is not significantly isolated with Mio10, whereas negative controls such as respiratory chain proteins; Cyt1 (complex III) and Cox2 (cytochrome *c* oxidase) and mitochondrial import machinery (Tom70 and Tim44) were all absent. Moreover, Western blot analysis indicates that the Mio10^{SF} strain does not contain any endogenous non-tagged Mio10. To further confirm Fcj1 interaction with Mio10,

mitochondrial proteins were immunoprecipitated from an Fcj1^{zz} strain (Figure 26C). Results confirm that Mio10 co-isolates with Fcj1, whereas controls such as Atp5, Cox2, Tom70, and Tim44 were negative. A Mio10 interaction with Fcj1 may indicate a role in cristae biogenesis (Rabl *et al.*, 2009).

4.5.2 Identification of MINOS1 interaction partners

Isolation of Mio10-containing complexes followed by mass spectrometric analysis revealed that Mio10 interacts with Fcj1 rather than the F₁F₀ATPase as originally hypothesized. To investigate whether the interaction is conserved across higher eukaryotes, a SILAC (stable isotope labeling of amino acids in cell culture) combined with mass spectrometry approach was carried out (Figure 27). SILAC makes use of differential isotope labeling to achieve quantitative based mass spectrometric analysis, and has been proven useful in various proteomic applications (Ong *et al.*, 2002; Ong and Mann, 2006). In brief, HEK293T cells were grown in media containing either light or heavy labeled lysine and arginine. Cultured cells were then harvested, mitochondria isolated, and consequently solubilized in a mild digitonin buffer. MINOS1-containing mitochondrial protein complexes were then immunoprecipitated by a MINOS1 specific antibody from heavy isotope containing cells, whereas a control antibody was used to immunoprecipitate proteins from light isotope containing cells. Eluates from cells with light or heavy isotope containing medium were combined and subjected to SDS-PAGE analysis; at which point the coomassie stained gel was sliced and subject to LC-MS/MS. In addition, for statistical analysis and to rule out possible false positives/negatives, the reverse (label switch) experiment was performed. In this case, MINOS1-specific antibodies were used to immunoprecipitate light isotope containing cells, whereas unspecific antibodies were used for the heavy isotope containing cells.

Spectral counts normalized ratios of heavy-over-low (H/L) for the forward and reverse experiments are presented in (Figure 28A). Enriched proteins, which satisfy the set threshold of 2.0, are labeled with a red dot whereas nonspecific/non enriched (under threshold of 2.0) are labeled with blue dots. The dot-blot clearly indicates that Mitofilin (human homolog of Fcj1) has the highest score, supporting the notion that the Mio10-Fcj1 interaction in yeast is conserved in human. Interestingly, mass spectrometric analysis also indicates that many of the known Mitofilin interacting proteins: CHCHD3, HSPA9, and DNJAC1, SAM50, MTX1, and MTX2 (green dot

with red circumference) are also immunoprecipitated with Mitofilin (Xie *et al.*, 2007; Darshi *et al.*, 2011). In addition, various other mitochondrial and non-mitochondrial proteins were enriched with MINOS1. Some of these interactions were verified by Western blot analysis of the immunoprecipitated protein samples (Figure 28B). MINOS1 specific antibodies (α -MINOS1) efficiently precipitated MINOS1, Mitofilin (IMMT), CHCHD3, and HSPA9 compared to the control antibodies. In parallel to yeast mass spectrometric analysis, MINOS1-specific antibodies do not precipitate the F_1F_0 ATPase ATP2 protein, further indicating that MINOS1 is not an F_1F_0 ATPase associated protein. Other possible interactions could not be verified due to the unavailability of antibodies. Nonetheless, mass spectrometric analysis of MINOS1 interactions indicate that MINOS1 interacts with Mitofilin, indicating that the Mio10/Fcj1 interaction is conserved across higher eukaryotes.

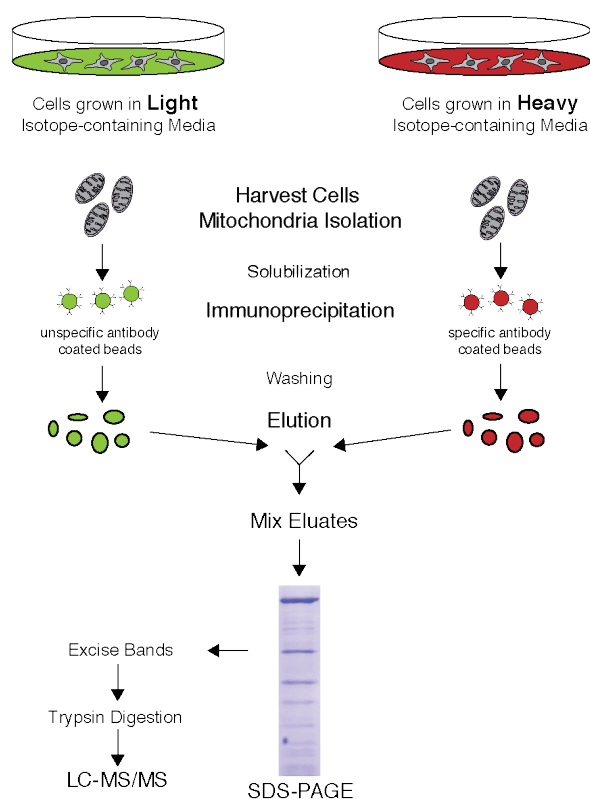


Figure 27. Schematic of the SILAC approach and mass spectrometric analysis. Figure courtesy of Markus Deckers. HEK29T cultured cells were grown in either Light or Heavy isotope containing medium. Mitochondria from each culture were isolated, solubilized and complexes were immunoprecipitated with either MINOS1 specific antibodies or control antibodies. After washing elutions were mixed and subjected to SDS-PAGE. The gel was cut into 23 equal and in-gel trypsinization was performed, followed by LC-MS/MS analysis.

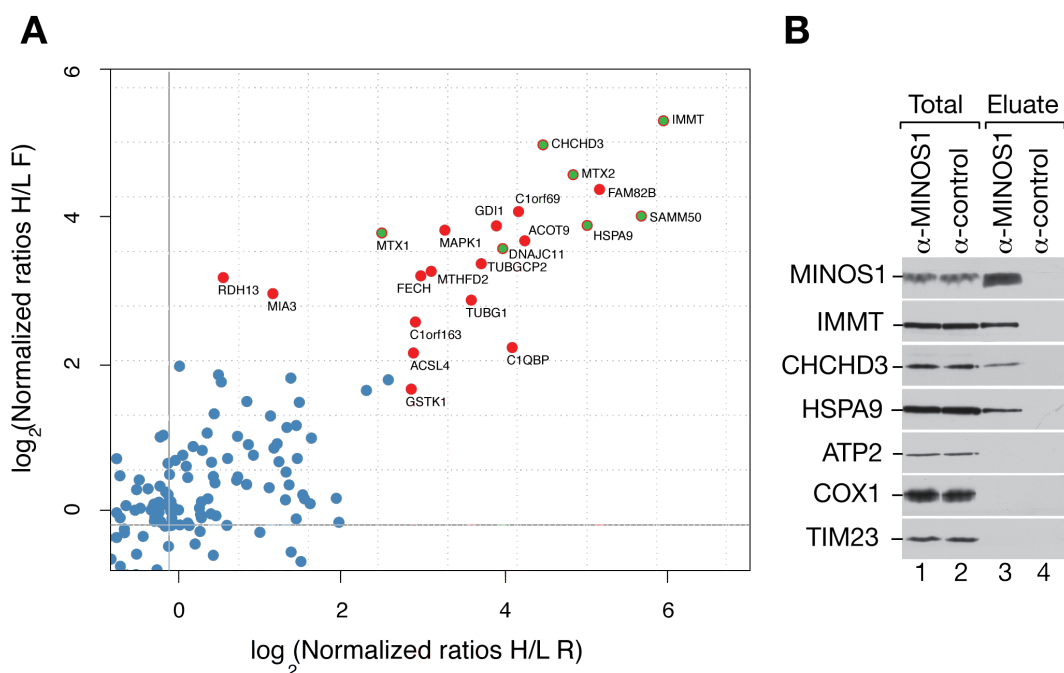


Figure 28. MINOS1 interacts with Mitofilin. Identification of MINOS1 associated proteins by co-immunoprecipitation and SILAC-MS. (A) RAW MS files from LC-MS/MS were analyzed by MaxQuant and Mascot using the IPI human protein database. Red dots indicate enriched proteins characterized by a high normalized ratio of heavy over light values (H/L). Forward F (H=MINOS1/L=Control), Reverse R (H=control/L=MINOS1, reverse ratios were inverted for plotting). Green dots with red circumference indicate known Mitofilin interacting proteins. (B) Isolated mitochondria from HEK293T cells were solubilized and subjected to Co-immunoprecipitation with MINOS1 and control antibodies. Eluates were separated by SDS-PAGE and analyzed by Western blotting. IMMT, Mitofilin. Mass spectrometric analysis performed by Miroslav Nikolov (AG Urlaub, MPI-bpc, Göttingen).

4.6 Characterization of Mio10 and MINOS1 interaction with Fcj1 and Mitofilin

To assess Mio10 and MINOS1 with respect to Fcj1 and Mitofilin complexes, solubilized wildtype mitochondria were subjected to size exclusion chromatography. Proteins were eluted in 12 fractions and subjected to SDS-PAGE and Western blot analysis (Figure 29A). Mio10 appears to form various sized complexes: a smaller complex at approximately 232 kDa (fraction 8) and a larger complex at approximately 1.2 MDa (fraction 3). The same holds true when examining Fcj1-containing complexes, which appear to elute at the same fractions as Mio10. This further supports the Fcj1 and Mio10 interaction. Moreover, it may be inferred from the size exclusion

chromatography that together, both Mio10 and Fcj1 form a large complex. It appears that the complex is larger than respiratory chain complexes formed by cytochrome *c* oxidase and F₁F₀ATPase as indicated by immunoblotting for Cox1 and Atp5 respectively. Furthermore, F₁F₀ATPase signals (Fractions 4-7) are devoid of Mio10 indicating that Mio10 does not associate with the F₁F₀ATPase.

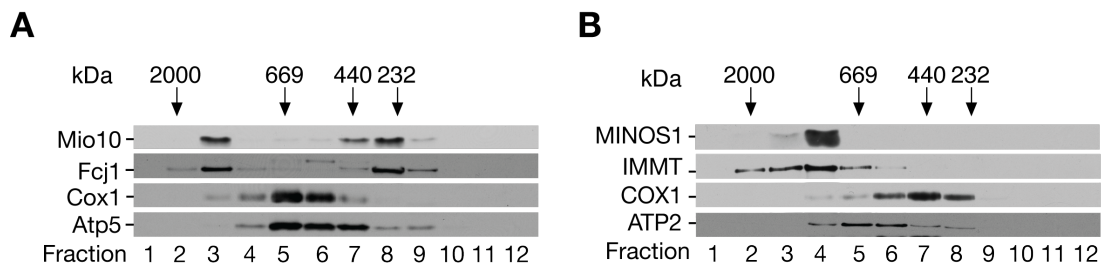


Figure 29. Mio10/Fcj1 and MINOS1/Mitofilin form large mitochondrial complexes. Wildtype yeast (A) and HEK29T (B) mitochondria were solubilized and subjected to size exclusion chromatography using a ÄKTApurifier system (GE Healthcare). The resulting fractions from the ÄKTApurifier system were TC precipitated, dried and subjected to SDS-PAGE and Western blotting. IMMT= Mitofilin.

MINOS1 containing complexes were analyzed as well by size exclusion chromatography (Figure 29B). In parallel to Mio10 in yeast, MINOS1 forms as well a large predominant protein complex of approximately 1 MDa (fractions 3-4), whereas a smaller complex is absent. Mitofilin also appears to form a large complex in the MDa range (fraction 2-5), predominantly in fraction 4 and thus appears in complex with MINOS1. The size of the MINOS1/Mitofilin complex appears to be distinctive from cytochrome *c* oxidase containing complexes (fraction 7) and F₁F₀ATPase complexes (fraction 5). The results from size exclusion chromatography thus indicate that Mio10 and MINOS1 are part of a large mitochondrial complex that contains Fcj1 in yeast and Mitofilin in higher eukaryotes.

4.7 Investigation of the role of Mio10 in mitochondrial morphology

As mass spectrometric analysis of yeast and human mitochondria in combination with size exclusion chromatography indicate that Mio10 and MINOS1 interact with Fcj1 and Mitofilin in large mitochondrial complexes. Previous reports indicate that Fcj1 and Mitofilin are involved in cristae biogenesis and inner membrane morphology (John *et al.*, 2005; Rabl *et al.*, 2009). The question, whether Mio10 or MINOS1 are also involved in mitochondrial inner membrane organization, was asked. Due to the availability of established tool and deletion strains, a role of the proteins were investigated primarily in yeast. *MIO10* deletion strains were again used to investigate whether Mio10, like Fcj1 is also involved in mitochondrial morphology. *MIO10* and *FCJI* deletions strains were further analyzed by live-cell fluorescence microscopy and electron microscopy. In all cases, an *ATP20* deletion strain was also analyzed for comparison.

4.7.1 Growth test: SG /SD medium at 18°C

MIO10 and *FCJI* deletion mutant cells were grown on minimal glucose (SD) and minimal glycerol (SG) medium plates at non-permissive temperatures of 18°C, 37°C, as well as 30°C (Figure 30). Mutant *fcj1Δ* cells have been shown to exhibit a growth defect when grown on YLac in which deletion of *FCJI* leads to altered mitochondrial inner membrane morphology, mainly by affecting numbers of cristae tips (Rabl *et al.*, 2009). Growth behavior analysis with SD and SG were used to enforce stringent growth conditions. Indeed, mutations affecting inner membrane stability are more potent at low or high non-permissive temperatures (Brandner *et al.*, 2005; Rabl *et al.*, 2009). Whereas wildtype and mutant cells all grow similarly on SD, differences are exhibited mainly when grown on SG medium. At 30°C, *mio10Δ*, *atp20Δ*, and *fcj1Δ* exhibit an impeded growth compared to wildtype cells on SG medium. Moreover, stark differences can be observed at 18°C SG, at which *mio10Δ* and *fcj1Δ* exhibit a strong growth defect, while *atp20Δ* cells exhibit a weaker phenotype. At higher temperatures, 37°C, mutant cells again exhibit a growth phenotype, although not as prominent as in 18°C. The similarity in *mio10Δ* and *fcj1Δ* highlights a possible genetic and/or functional relationship. As growth on SG, is not completely inhibited at 30°C or 37°C, a role in mitochondrial respiration is considered unlikely.

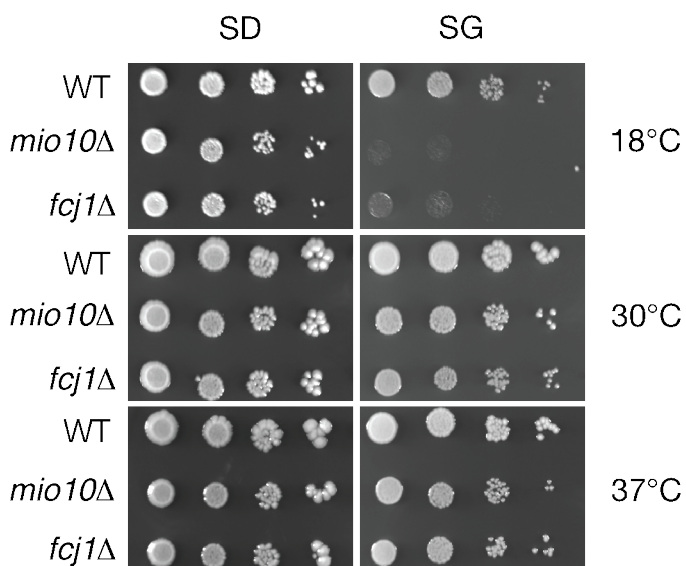


Figure 30. *MIO10* and *FCJ1* deletion mutants' growth defect at low temperatures. Wildtype, *mio10Δ*, and *fcj1Δ* yeast cells were spotted in serial 10-fold dilutions on minimal fermentable (SD) and non-fermentable (SG) minimal media. Cells were grown at 18°C, 30°C, and 37°C.

4.7.2 Protein steady state analysis of mitochondria grown at 18°C

Mitochondria were harvested from *MIO10* and *FCJ1* deletion mutant cells grown at 18°C in SG medium. The steady-state protein levels were analyzed by SDS-PAGE (Figure 31A) and BN-PAGE (Figure 31B). The deletion strains are confirmed by the absence of Mio10 and Fcj1 signals in respective strains. One should note a signal detection migrating above Fcj1 signal in *fcj1Δ* cells; this corresponds to an antibody cross reaction rather than residual Fcj1 protein. Moreover, Fcj1 protein levels appear to be slightly reduced in *mio10Δ* compared to wildtype. This effect, however, is not paralleled in *fcj1Δ* mutant cells, which have levels of Mio10 comparable to wildtype cells. Furthermore, steady-state levels of respiratory chain proteins (Rip1, Cty1, Cox2, Atp5) are not affected, whereas outer membrane proteins (Tom70, Porin) and the inner membrane protein Tim21 are also unaffected by the absence of Mio10 or Fcj1. Assembly of respiratory chain complexes in *mio10Δ* grown at 18°C in SG medium was accessed by BN-PAGE, at which assembly of the F₁F₀ATPase and complex III appear unaffected.

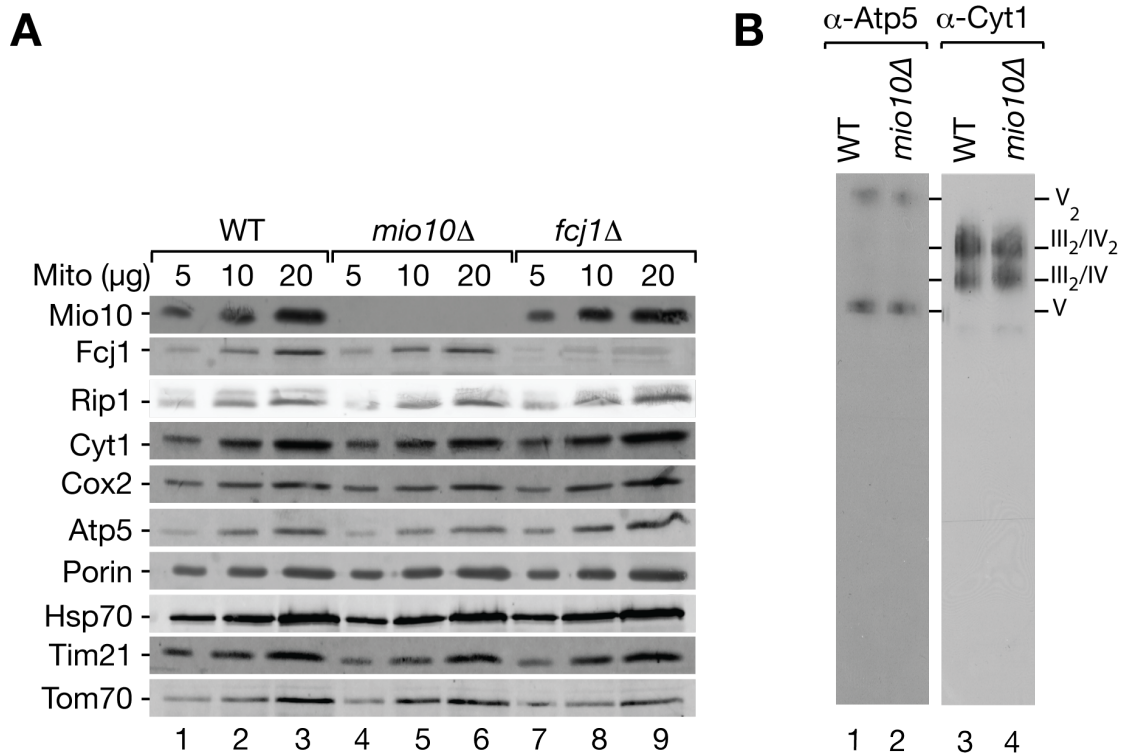


Figure 31. Protein steady-state levels are unaffected in *mio10Δ* mutants. (A) Wildtype, *mio10Δ*, and *fcj1Δ* mitochondria were subjected to SDS-PAGE and Western blotting. (B) Wildtype and *mio10Δ* mitochondria were solubilized in digitonin buffer, subjected to BN-PAGE (4-10% gradient gel) and Western blotting.

4.7.3 Live-cell fluorescence microscopy analysis of *mio10Δ* mitochondria

Mitochondria form interconnected dynamic networks of which phenotypic characteristics are dependent on the metabolic state of the cell and a balance between the processes of mitochondrial fission and fusion (Okamoto and Shaw, 2005). The organization of the mitochondrial network of *mio10Δ* mutant yeast cells was visualized by live-cell imaging (Figure 32), in which yeast cells were transformed with a mitochondrial localized GFP expressing plasmid, pVTU100U-mitoGFP (Westermann and Neupert, 2000). This allows contrasting bright fluorescent mitochondria against clear background staining, and thus proper assessment of network morphology. Wildtype mitochondria display a typical reticular mitochondrial network which transverses the majority of the cell. On the other hand, *atp20Δ* mutant cells exhibit atypical networks characterized by thickened and fragmented mitochondria. Upon analysis of both *mio10Δ* and *fcj1Δ* mutant cells, it is evident that they share a similar mitochondrial network organization. In both cases, mitochondrial networks appeared on the periphery of cell and more condensed than in the *atp20Δ* counterpart strain.

Indeed, analysis of *fcj1* Δ mitochondria is in agreement with previously published observations (Rabl *et al.*, 2009). The similarities observed in the mitochondrial networks for *mio10* Δ and *fcj1* Δ strains may support the notion of a functional relationship between the two proteins.

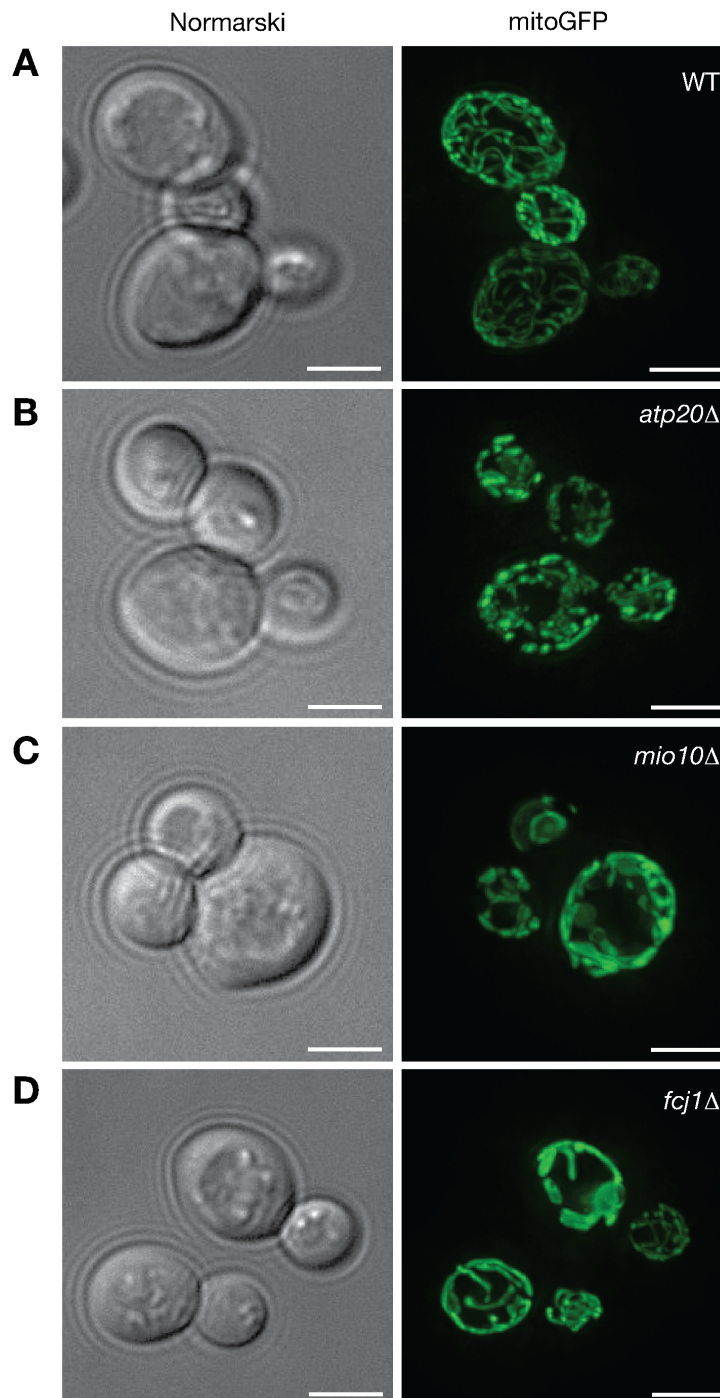


Figure 32. Mitochondrial morphology is altered in *mio10* Δ . Yeast wildtype, *atp20* Δ , *mio10* Δ and *fcj1* Δ cells transformed with plasmid pVT100U-mitoGFP and analyzed by fluorescence microscopy. Scale Bars, 2.5 μ m. Microscopy was performed by Daniel Jans (AG Jakobs, MPI-bpc, Göttingen).

4.7.4 Analysis of *mio10Δ* mitochondria by electron microscopy

The mitochondrial cristae morphology of wildtype and mutant yeast cells were further assessed with the use of electron microscopy coupled with high-pressure freezing, HPF, in order to preserve intact cellular structure (Figure 33A). Wildtype cells contain mitochondria with typical tubular cristae membranes whereas *atp20Δ* mitochondria appear to have the distinctive ‘onion-like’ inner membrane organization, previously shown for *atp20* and *atp21Δ* mutants (Paumard *et al.*, 2002; Arselin *et al.*, 2004). Mitochondria of the *ATP20* deletion mutant contain two or three lamellar cristae membranes, which span the entire organelle in a spherical manner. In contrast, analysis of *mio10Δ* and *fej1Δ* mitochondria indicated atypical yet less severe phenotype characterized by more compact transversion of the inner membrane. Moreover, in *mio10Δ* and *fej1Δ* cells, mitochondria appear to localize to the periphery of the cells, reflecting observations by live-cell fluorescent imaging.

The distinctive mitochondrial phenotypes observed from electron microscopy images were further subjected to a quantitative analysis to better define the various mutants (Figure 33B). An average of 55 images from each strain was used in the analysis, which is based on the percentage of analyzed cells that contain the various phenotypes. The tubular wildtype phenotype was termed ‘normal’, whereas onion-like phenotype as simply ‘onion-like’. The atypical phenotypes observed in *mio10Δ* and *fej1Δ* were termed ‘intermediate’. Quantification of the various mutant phenotypes indicates that a large majority (approximately 90%) of wildtype mitochondria favor ‘normal’ inner membrane arrangements with 10% having either intermediate or onion-like structures. Interestingly, unlike the wildtype cells, none of the mutants appeared to have a similar inclination to one single phenotype and appeared to contain all three phenotypes in varying amounts. For instance, whereas *atp20Δ* mitochondria tend to have ‘onion-like’ organization, approximately 50% had either normal or intermediate. The same holds true for *fej1Δ* mutants, in which approximately 50% of the cells tend to have an ‘intermediate’ phenotype, with the other 50% either ‘normal’ or ‘onion-like’. In contrast, *mio10Δ* mutants tend to favor ‘intermediate’ and ‘onion-like’ inner membrane organizations in rather similar quantities meanwhile approximately 20% were ‘normal’ in both strains.

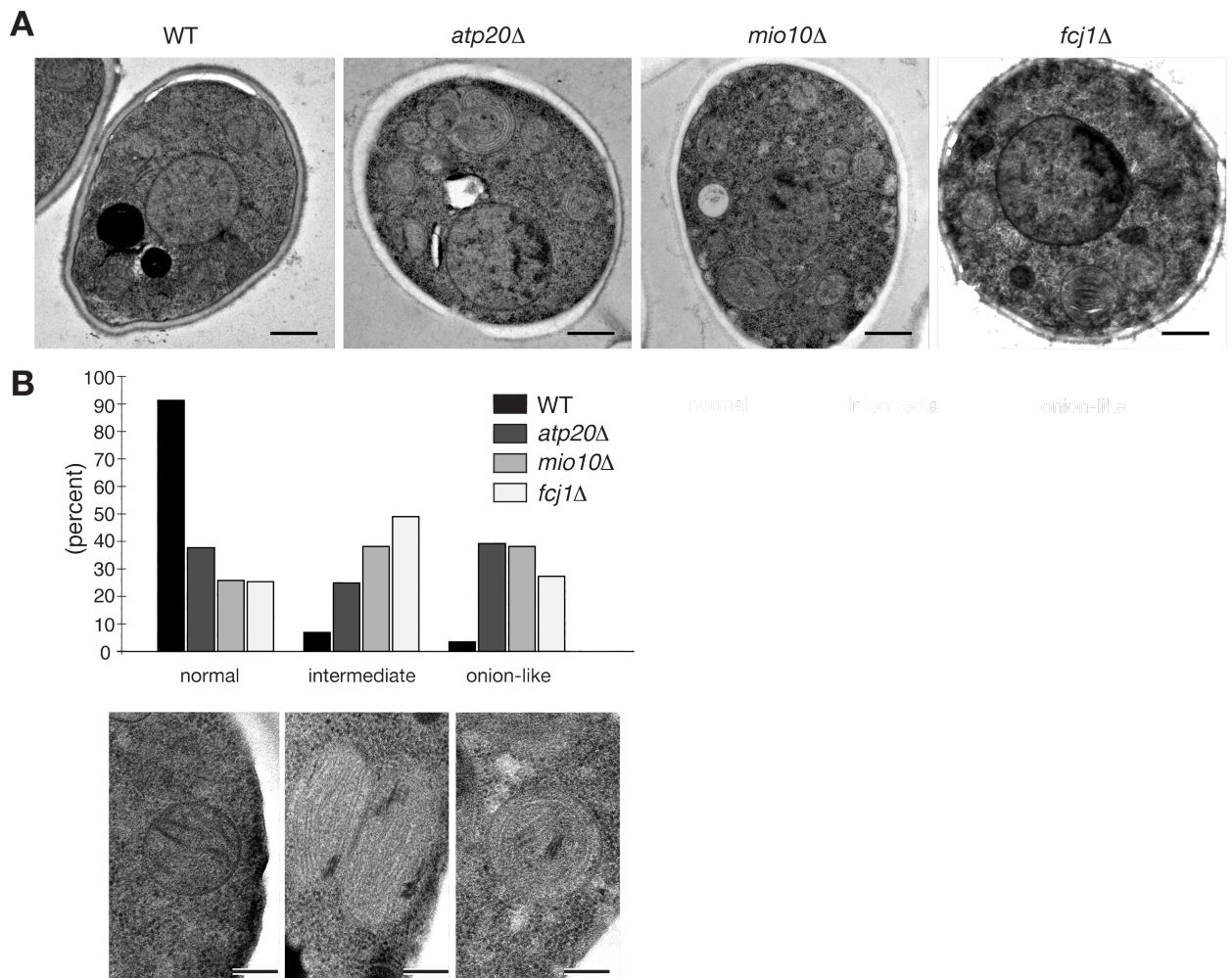


Figure 33. Aberrant cristae morphology in *mio10Δ* mitochondria. (A) Electron microscopy of yeast wildtype, *atp20Δ*, *mio10Δ* and *fcj1Δ* cells after high pressure freezing (HPF). Bars, 1 μ m. (B) Quantitative analysis of different types of mitochondria phenotypes based on electron microscopy images from HPF fixed cells; wildtype WT (n=49), *atp20Δ* (n=51), *mio10Δ* (n=61) and *fcj1Δ* (n= 57) cells. Detailed view representation of normal, intermediate and onion-like mitochondria types. Microscopy and analysis were performed in collaboration with Dietmar Riedel (Mpi-bpc, Göttingen)

In order to have an improved visualization of mutant mitochondria inner membranes, cells were chemically fixed with KMnO_4 before analysis by electron microscopy (Figure 34). Fixation by KMnO_4 allows the ‘unmasking’ of protein-phospholipids complexes generating a higher membrane contrast in electron micrographs (Bradbury 1960). Under these conditions, mitochondria from the *atp20 Δ* strain again have the onion-like organization characterized by clear various concentric layers of inner membrane. Moreover, *atp20 Δ* mitochondria appear to have poorly defined cristae, compared to the defined tubular cristae membrane in the wildtype strain. Conversely, *mio10 Δ* and *fcj1 Δ* mitochondria contain closely stacked lamellar membrane sheets which transverse horizontally the organelle (rather than spherical transversions of the *atp20 Δ* mutants). Furthermore, *mio10 Δ* and *fcj1 Δ* contain no cristae and appear to lack any recognizable cristae tips.

The results from the electron microscopy analysis of HPF and KMnO_4 fixed cells indicate that Mio10 plays a functional role in mitochondrial inner membrane organization. The ORF YCL057c-A is thus referred to Mio10 for **mitochondrial inner membrane organizer**, whereas its human homolog is referred to MINOS1, for **mitochondrial inner membrane organizing system 1**. The combination of topological analysis, mass spectrometric analysis and size exclusion chromatography, indicate that Mio10 and MINOS1 are novel interacting partners of Fcj1 and Mitofilin, and form a large inner membrane complex. This complex is termed MINOS, for **Mitochondrial Inner membrane Organizing System**. Mio10 and MINOS1 do not associate with the $\text{F}_1\text{F}_0\text{ATPase}$ or play a role in its dimerization. However by forming the MINOS complex, Mio10 and MINOS1 appears to play an essential role in cristae morphology and inner membrane architecture.

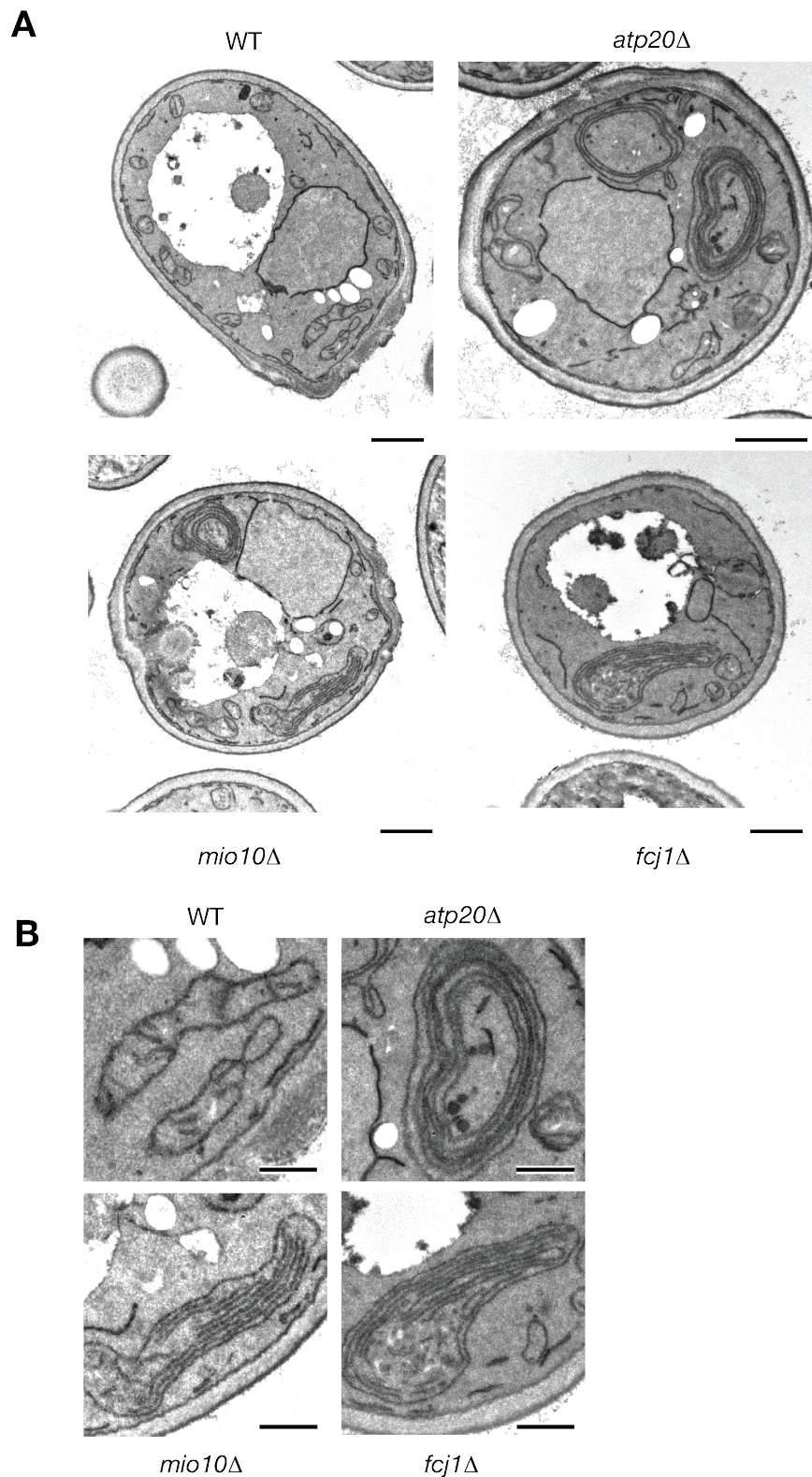


Figure 34. Absence of apparent cristae and cristae tips in *mio10Δ* mitochondria. (A) Electron microscopy analysis of wildtype, *atp20Δ*, *mio10Δ* and *fcj1Δ* cells after KMnO_4 fixation. Scale bars, 200 nm. (B) Detailed view of WT, *atp20Δ*, *mio10Δ* and *fcj1Δ* mitochondria showed in (A). Microscopy and analysis were performed in collaboration with Wolfgang Schliebs (Ruhr Universität Bochum)

5. DISCUSSION

In this study, an initial *in silico* approach to identify novel F₁F₀ATPase dimerization factors resulted in the identification of the yeast mitochondrial protein Mio10 as a potential candidate. Mio10, along with its human homolog, MINOS1, were investigated. These proteins were found to display a function unrelated to dimerization of F₁F₀ATPase, and are instead novel factors involved in the maintenance of mitochondrial cristae morphology. Whereas recent studies have in parallel identified Mio10 in yeast, this is the first study that has identified MINOS1 as a novel interaction partner of Mitofilin in higher eukaryotes. The presented findings highlight the functional and evolutionary significance of the MINOS complex as a player in mitochondrial inner membrane architecture and as multifunctional component in eukaryotic mitochondria and potentially in other cellular organelles.

5.1 Mio10 and MINOS1 are not F₁F₀ATPase dimerization factors

5.1.1 Identification of the inner membrane proteins: Mio10 and MINOS1

F₁F₀ATPase synthase dimers have been identified in various organisms ranging from yeast, mammals, and plants (Straus *et al.*, 2008; Davies *et al.*, 2011). Dimerization has various structural and functional roles. It contributes to the F₁F₀ATPase holo-enzyme structure and plays a regulatory role in conditions of low electron transfer activity and reduced membrane potential (Buzhynskyy *et al.*, 2007, Wittig and Schägger, 2009). Moreover, F₁F₀ATPase dimerization is also involved in the maintenance and biogenesis of cristae membranes (Giraud *et al.*, 2002; Paumard *et al.*, 2002b; Gavin *et al.*, 2004; Dudkina *et al.*, 2006; Rak *et al.*, 2007; Velours *et al.*, 2009). Several F₁F₀ATPase subunits, such as subunit a, b, h, and y, have been shown to contribute to dimerization in yeast and higher eukaryotes (Soubannier *et al.*, 2002; Fronzes *et al.*, 2003). In addition, several small F₀ interacting membrane proteins (Atp18, Atp19, Atp20, and Atp21) mediate dimeric interactions by binding sequentially at monomer interfaces in yeast (Arnold *et al.*, 1997, 1998; Soubannier *et al.*, 2002; Paumard *et al.*, 2002a; Wagner *et al.*, 2009, 2010). In contrast, these small dimerization factors have not been found in higher eukaryotes. Homologs of Atp20 and Atp21 are found in *H.sapiens*, however a functional role in F₁F₀ATPase dimerization has not been

identified. The exact nature of what promotes F_1F_0 ATPase monomer-monomer interactions and therefore dimerization is elusive and yet to be determined. To this end, the initial aim of this study was to identify novel F_1F_0 ATPase dimerization factors in higher eukaryotic organisms that parallel the action of small dimerization factors in yeast.

In order to identify new dimerization factors, an *in silico* based analysis was performed based on characteristics of the primary amino acid sequences of identified factors. This included a protein with a small molecular size (less than 12 kDa) and at least one transmembrane domain. Subsequently, selecting proteins with GxxxG motifs and significant potential homologs narrowed search results down. The GxxxG motifs that are found in both Atp20 and Atp21, allow helix-helix membrane interactions with neighboring proteins (Russ and Engelman, 2000). Moreover, the GxxxG motif of Atp20 and Atp21 is critical for their role in dimerization (Arselin *et al.*, 2003). The results of the *in silico* analysis yielded the ORF, YCL057c-A (Mio10). Blast search of the Mio10 primary amino acid sequence identified a potential human homolog, C1orf151 (MINOS1). The *in silico* analysis indicated a second potential dimerization factor, however Mio10/MINOS1 were selected based on the evidence that Mio10 (YCL057c-A) has been previously identified in large-scale proteomic screens and predicted to have a mitochondrial localization and that MINOS1 (C1orf151) has been found in a computational screen for regulators of oxidative phosphorylation (Sickmann *et al.*, 2003; Reinders *et al.*, 2006; Baughman *et al.*, 2009). To this end, Mio10 and MINOS1 were then characterized biochemically and functionally.

The F_1F_0 ATPase dimerization factors are membrane proteins that interact with the inner membrane embedded F_0 domain of F_1F_0 ATPase (Wagner *et al.*, 2010). In order to investigate a possible role dimerization, the association of Mio10 and MINOS1 with the inner membrane was thus investigated. Subfractionation analysis was performed in tandem with membrane association assays using isolated yeast mitochondria. The results indicated that Mio10 is indeed an integral protein of the inner membrane. It was also inferred that Mio10 localizes to the inner membrane in a manner that its N and C termini are exposed to the IMS. One should note that this topology is based on the hypothetical model that Mio10 contains two transmembrane domains. Additional analysis is thus required to verify N terminal exposure to the IMS.

This may include raising antibodies that specifically recognize the N terminus of Mio10. Furthermore, subfractionation analysis and membrane association assays of the human MINOS1 have also been performed using isolated human mitochondria from cultured HEK293T cells. The MINOS1 mitochondrial localization was also shown by confocal microscopy. These results indicated that MINOS1 is also a mitochondrial inner membrane protein that has membrane topology similar to yeast homolog.

5.1.2 Mio10 and MINOS1 complexes comigrate but not physically associate with the F₁F₀ATPase

To assess Mio10 and MINOS1 containing complexes, solubilized mitochondria were subjected to BN-PAGE after import and assembly. This approach has proven previously useful in the characterization of F₁F₀ATPase dimerization factors, as BN-PAGE can be utilized to investigate large membrane-bound protein complexes under native conditions (Schägger and von Jagow, 1991; Nijtmans *et al.*, 2002, Wagner *et al.*, 2009, 2010). Radiolabeled Mio10 and MINOS1 precursors were synthesized *in vitro* and imported in yeast and human mitochondria. Mitochondria isolated from HEK293T human cultured cells were used as a representative model of higher eukaryotes. Upon analysis by BN-PAGE, both Mio10 and MINOS1 precursors were imported into either yeast or human mitochondria as well as assemble into complexes of various sizes, ranging from small (approximately 160 kDa) to large complexes (larger than 669 kDa). The observation that both protein precursors can be interchangeably imported into both yeast and human mitochondrial systems may reflect a high level of functional conservation. Indeed, sequence analyses of Mio10 and MINOS1 across various species indicated a high level of conservation mainly clustered at predicted transmembrane domains and particularly at the GxxxG motifs. Interestingly, both the N and C termini are not conserved. This may reflect that function and perhaps mitochondrial targeting and/or import are most likely dependent on the proteins' central domains. The notion whether Mio10 and MINOS1 can functionally complement each other is yet to be determined. Preliminary complementation assays, in which the MINOS1 coding gene was expressed under various promoters in a *MIO10* deletion mutant, did not overcome growth defects observed (data not shown). Although MINOS1 does express in yeast as found by Western blot analysis, the failure to complement may be due to insufficient levels of

MINOS1 overexpression and thus further optimizations are necessary. This may also indicate that whereas sequence differences may allow import of Mio10 and MINOS1 into in different species, these differences may not allow functional complementation.

Upon further analysis by BN-PAGE in which Mio10 radiolabeled precursor was imported in parallel with respiratory chain proteins, it appeared that the large Mio10 containing complexes comigrated with the F_1F_0 ATPase dimer. In contrast, Mio10 containing complexes appeared larger than complex III or cytochrome *c* oxidase containing complexes. Moreover, Mio10 import and assembly appeared to be dependent on the presence of the F_1F_0 ATPase dimerization factors Atp20. In this case, the large Mio10 containing complexes failed to assemble in *atp20* Δ mitochondria. The effect was also shown to be specific to *atp20* Δ mitochondria and not due to nonspecific post lysis association. It should be noted that due to limitations of α -MINOS1 and α -Mio10 antibodies to recognize native epitopes on BN-PAGE, it was difficult to verify import and assembly results by Western blot analysis. As an alternative, second dimension analysis by SDS-PAGE was used. Surprisingly, second dimension analysis of Mio10 containing complexes in *atp20* Δ mitochondria revealed that the large Mio10 complex continues to be present in the absence of the F_1F_0 ATPase dimer. This indicates that the Mio10 containing complex is different from the F_1F_0 ATPase dimer. The Mio10 complex may thus have a similar size to the F_1F_0 ATPase and may thus have similar migration properties on BN-PAGE. The Mio10 assembly defect in *atp20* Δ may possibly be an artifact. The severe effects that *ATP20* deletion mutants have on the organization of the mitochondrial inner membrane may be a possible explanation for this. However, it is unclear why this specifically affects Mio10 assembly and not other F_1F_0 ATPase components, such as Atp21, which assemble to the F_1F_0 ATPase dimer as expected. In summary, analysis of Mio10 containing complexes by BN-PAGE indicates that the presence of Mio10 complexes is independent of the F_1F_0 ATPase.

5.1.3 Mio10 and MINOS1 are not stably associated with the F_1F_0 ATPase

In order to further investigate a possible Mio10 association with the F_1F_0 ATPase, a tagged Atp20 strain (Atp20^{zz}) was used to biochemically isolate the F_1F_0 ATPase and its associated components. Indeed, immunoprecipitation was successful for F_1F_0 ATPase components such as Atp5, proving the technical success of the approach.

However, Mio10 was not coisolated. These isolations were repeated using a streptavidin-flag C-terminally tagged Atp5 or Atp20 and with co-immunoprecipitations with Mio10 specific antibodies (data not shown). In all cases, Mio10 was not coisolated with the F₁F₀ATPase components. As solubilization buffer conditions and salt concentrations used in biochemical protein isolations from yeast differed from those used in BN-PAGE assembly experiments, it was taken into account that a higher salt concentration used in biochemical isolations may explain the lack of stable Mio10 association with the F₁F₀ATPase. To compensate for these changes, immunoprecipitation with the Atp20^{zz} tagged strain was repeated with BN-PAGE conditions. However, Mio10 was not coisolated with F₁F₀ATPase subunits under these conditions (data not shown). In addition, the F₁F₀ATPase and its associated components were co-immunoprecipitated from HEK29T3 isolated mitochondria using F₁F₀ATPase specific antibodies. MINOS1 was not found to associate with the F₁F₀ATPase whereas the approach was successful in isolating Atp2. Thus, the biochemical isolations from yeast and human isolated mitochondria indicate that neither Mio10 nor MINOS1 are stably associated with the F₁F₀ATPase and thus may not have a role in its dimerization.

5.1.4 Mio10 does not affect F₁F₀ATPase activity or oligomerization

Analysis of the growth behavior of the F₁F₀ATPase dimerization factors indicates that they are not essential for mitochondrial respiration or F₁F₀ATPase activity, (Arnold *et al.*, 1998; Paumard *et al.*, 2002a; Soubannier *et al.*, 2002). To assess the any effect a *MIO10* deletion may have on mitochondrial respiration, yeast *mio10Δ* cells were grown in fermentable and non-fermentable media. In fact, *mio10Δ* cells continue to grow on non-fermentable medium and have a similar growth profile as *atp20Δ* cells. Mitochondrial respiration does not seem to be compromised in *mio10Δ* mutants in comparison with *atp2Δ* cells. Atp2 is the beta subunit of the F₁F₀ATPase and together with Atp1 form the catalytic core in the F₁ component (Takeda *et al.*, 1985; Abrahams *et al.*, 1994). In addition, an in-gel activity assay was used to assess the effect of *MIO10* deletion on the activity of various respiratory chain complexes. Absence of Mio10 does not affect the enzymatic activity of F₁F₀ATPase, cytochrome *c* oxidase, or complex I. Therefore, it is concluded that Mio10 is not involved in F₁F₀ATPase activity or mitochondrial respiration.

Using the *mio10Δ* strain, a possible role for Mio10 in F₁F₀ATPase dimerization was further assessed by BN-PAGE and Western blot analysis. Immunodetection for Atp5, which allowed the detection of F₁F₀ATPase complexes, indicated the presence of intact F₁F₀ATPase dimers. Thus the absence of Mio10 does not affect dimerization. Various inner membrane proteins such as Fcj1 and its *C. elegans* homolog, IMMT-2, do not play a role in dimerization but affect the stability of the F₁F₀ATPase higher oligomers (Rabl *et al.*, 2009; Mun *et al.*, 2010). IMMT-2 was suggested to be involved in the formation of supermolecular complexes (Mun *et al.*, 2010). On the other hand, *FCJ1* overexpression reduces the stability F₁F₀ATPase due to its antagonistic effect on F₁F₀ATPase dimer mediated inner membrane organization (Rabl *et al.*, 2009). The affect of Mio10 on oligomerization of the F₁F₀ATPase was assessed using the in-gel activity assay. In contrast to previous in-gel activity assays, digitonin concentrations were reduced to 0.35% and a 3-13% BN-PAGE gel gradient was used to better solubilize and separate larger complexes. The absence of Mio10 however does not negatively or positively affect F₁F₀ATPase oligomerization. Whether *MIO10* overexpression has a similar effect on F₁F₀ATPase oligomers, as Fcj1, is yet to be determined.

5.1.5 F₁F₀ATPase dimerization in higher eukaryotes

Analysis of the *MIO10* deletion mutants indicated that Mio10 does not affect F₁F₀ATPase activity or its organization into dimers or higher oligomers. In conjunction with BN-PAGE analysis and biochemical isolations of tagged F₁F₀ATPase subunits, it is concluded that Mio10 and MINOS1 are not F₁F₀ATPase dimerization factors. This raises the question of what mediates F₁F₀ATPase dimerization in higher eukaryotes. It may be possible that different factors mediate dimerization across the species divide. The human IF1 protein promotes F₁F₀ATPase dimerization whereas its yeast homolog, Inh1, does not have a role (García *et al.*, 2006). The observation that homologs of Atp18 and Atp19 are not found whereas homologs of Atp20 and Atp21 have no proven role in F₁F₀ATPase in higher eukaryotes may indeed suggest that small dimerization factors are not required in higher eukaryotes. Nonetheless, the *in silico* approach used in this study was not successful in identifying novel dimerization factors and perhaps different approaches are needed. One possibility would be affinity purification based mass spectrometric analysis of tagged F₁F₀ATPase subunits. This may help identify novel components

that may associate with the F₁F₀ATPase in higher eukaryotes. The question of what mediates F₁F₀ATPase dimerization in higher eukaryotes remains outstanding.

5.2 The MINOS complex: Mitochondrial inner membrane organizing system complex

5.2.1 Identification of the yeast MINOS complex

As initial analysis indicated that neither Mio10 nor its human homolog MINOS1 are F₁F₀ATPase dimerization factors, the question of Mio10/MINOS1 function still remained. Biochemical isolations from a Mio10^{SF} tagged strain were performed followed by mass spectrometric analysis to identify Mio10 interaction partners. Whereas, results further verified the lack of interaction with the F₁F₀ATPase, they indicated a possible Fcj1 interaction. This was also shown when Mio10 was successfully coisolated with Fcj1 from a Fcj1^{ZZ} strain. Fcj1 and its human homolog Mitofilin, play a major role in the organization of the inner membrane as mutants that lack Fcj1 or Mitofilin exhibit aberrant cristae morphologies (John *et al.*, 2005; Rabl *et al.*, 2009). This Mio10-Fcj1 interaction suggested that Mio10 could also be involved in inner membrane organization. In addition, many of the proteins that are found in the mass spectrometric analysis either uncharacterized and/or AIM proteins (Aim5, Aim13, Aim37, Aim38, Aim45). These proteins were found in screens that affect mitochondrial inheritance and may suggest other possible roles of Mio10 (Hess *et al.*, 2009). However, due to the lack of antibodies against these proteins, it was difficult to verify some of the interactions. It should be noted that mass spectrometric analysis of Mio10^{SF} immunoprecipitation was not quantitative. The analysis was mainly based on spectral counts and normalized fold changes between elutions from tagged against wildtype untagged strains. Thus, it would be of interest to repeat the isolations with SILAC-based mass spectrometry, which might provide a more quantitative analysis that would further verify results of this study (Ong *et al.*, 2002). Nonetheless, data indicated a Mio10 interaction with Fcj1, and therefore a possible similar role in cristae biogenesis.

A function for Mio10 in mitochondrial inner membrane organization was investigated using the *mio10Δ* strain. Whereas *mio10Δ* cells were not affected at 30°C, cells lacking Mio10 showed a growth defect at 18°C and to lesser extent at 37°C when

grown on minimal non-fermentable medium. A growth defect at elevated temperatures may indicate a change in membrane biogenesis and stability as shown in various mutants involved in cardiolipin biosynthesis (Joshi *et al.*, 2009). Interestingly, *fcj1Δ* cells had a similar growth behavior to *mio10Δ* cells. Upon further investigation of mitochondria isolated from *mio10Δ* grown at 18°C, no strong changes were observed at mitochondrial protein steady state levels. Live fluorescence microscopy was used to evaluate mitochondrial network organization of *mio10Δ* cells, which appeared to be more condensed compared to the wildtype strain. In fact, *mio10Δ* and *fcj1Δ* cells displayed very similar condensed mitochondrial networks, supporting the notion of a common Mio10/Fcj1 function. In contrast, *atp20Δ* mitochondria were fragmented, highlighting their different functional role in mitochondrial membrane organization. Mitochondrial dynamics (fusion/fission) provides a mechanism for compromised mitochondria to complement their damaged components with contents from healthy mitochondria (Ziviani and Whitworth, 2010). Indeed, the aberrant mitochondrial network dynamics observed in the examined mutant strains may be due to higher mitochondrial turnover. Mitochondria are degraded by mitophagy, which is the selective autophagy of mitochondria (Kanki *et al.*, 2008). Previous studies have used an experimental system in which the mitochondrial outer membrane protein, Om45, is tagged with GFP and then used to monitor mitophagy (Kanki *et al.*, 2009). A similar system thus can be applied to investigate mitophagy in *mio10Δ* and *fcj1Δ* cells.

On the other hand, analysis by electron microscopy revealed a strong aberration in the organization of the inner membrane when Mio10 was absent. The *MIO10* and *FCJ1* deletion mutants exhibited leaflet-like stacked cristae membranes compared to the wildtype. Also, both mutant strains appear to have lost defined cristae tips. The observed phenotype is in agreement to previous reports of *fcj1Δ* mutants (Rabl *et al.*, 2009). It is also clearly distinct from the onion-like organization observed in *atp20Δ* mitochondria and thus ruling out a common function (Paumard *et al.*, 2002b). Previous work on *fcj1Δ* using tomography indicated that the observed stacked membranes have lost cristae junctions and are stacked by F₁F₀ATPase dimer interactions between one membrane and another (Rabl *et al.*, 2009). This may hold true for *mio10Δ* mitochondria, which have a remarkably similar inner membrane organization. All in all, the sum of data (biochemical isolations and *MIO10* deletion

mutants analysis) indicates that Mio10 is a novel interaction partner of Fcj1 that is also involved in mitochondrial inner membrane organization.

5.2.2 Identification of the human MINOS complex

In order to identify possible interaction partners of MINOS1 in human mitochondria, coimmunoprecipitation using MINOS1 specific antibodies were performed and isolated complexes were further analyzed. For this purpose, SILAC-based quantitative mass spectrometry analysis was performed, as well as a label-switch experiment. To this end, analysis of MINOS1 containing complexes from human isolated mitochondria indicated a significant enrichment of Mitofilin. Also, in agreement with previous studies, various Mitofilin interactors such as Metaxin 1, Metaxin 2, CHCHD3, HSPA9, DnaJC11, and SAM50 were also significantly enriched (Xie *et al.*, 2007; Darshi *et al.*, 2011; An *et al.*, 2012). This finding highlights the efficiency of the experimental approach. The evidence of MINOS1 interaction with Mitofilin and CHCHD3 links MINOS1 with a role in cristae morphology. Results also verify the model that Mitofilin, which is located at cristae junctions effectively bridges the inner the outer mitochondrial membranes (Xie *et al.*, 2007; Darshi *et al.*, 2011). The MINOS1 interactions with Mitofilin, CHCHD3, and HSPA9 were verified by Western blot analysis. However, other interacting proteins could not be verified due to the unavailability of antibodies. Nonetheless, the results from the SILAC-based approach indicate that Mio10-Fcj1 interaction is conserved in higher eukaryotes.

In contrast to the enrichment of mitochondrial proteins, various non-mitochondrial proteins were also enriched. Enrichment of GDI1 (GDP Dissociation Inhibitor), which is involved in Rab GTPase cycle, may provide a link to vesicle transport and perhaps signaling between mitochondria and the extra-mitochondrial space (Bachner *et al.*, 1995). Conversely, MIA3/TANGO1 is an endoplasmic reticulum (ER) integral membrane protein (Saito *et al.*, 2009) and may implicate ER mitochondrial interactions. Indeed, an ER-mitochondria encounter structure (ERMES), which forms a junction between the two organelles, has been previously identified in yeast (Kornmann *et al.*, 2009; Stroud *et al.*, 2011). ERMES contains an ER-anchored Mmm1, and the mitochondrial proteins Gem1, Mdm10, Mdm12, and Mdm34 (Kornmann *et al.*, 2009; Stroud *et al.*, 2011). Coincidentally, these ERMES components are also in involved mitochondrial maintenance and morphology (Okomoto and Shaw,

2005). The observation that ERMES components interact with the SAM complex further indicates a possible involvement of MINOS with ERMES (Meisinger, *et al.*, 2004, 2007). A role of ERMES in connecting mitochondria to the cytoskeleton has been also proposed (Buldogh *et al.*, 2003). This can be exemplified by Miro, the homolog of Gem1 in higher eukaryotes, which can act as an adaptor between the two organelles (Glater *et al.*, 2006; Koshiba *et al.*, 2011). This interaction between mitochondria and components of the cytoskeleton plays an essential role in proper mitochondria movement and trafficking (Okamoto and Shaw, 2005). Interestingly, FAM82B (regulator of microtubule dynamics protein 1) and TUBG1 (Tubulin), which are also components of the microtubule cytoskeleton, are enriched in the SILAC based mass spectrometric analysis (Zheng *et al.*, 1991; Oishi *et al.*, 2007). Their interaction with MINOS1/Mitofilin may thus provide a link between inner membrane organization with mitochondrial-cytoskeleton interaction. Taken together, a MIA3 and SAM interaction with the mitochondrial inner membrane MINOS complex may thus provide a novel link between the mitochondrial inner compartment and the ER. Of course, more evidence with respect to these interactions is still required to be verified before any further speculations can be made.

5.2.3 Mio10 and MINOS1 form a large complex (the MINOS complex)

Mio10 and MINOS1 containing complexes were analyzed by size exclusion chromatography. Both Mio10 and MINOS1 were found to form large complexes in the MDa range. These complexes have a similar size to complexes that contain Fcj1 and Mitofilin. This is in agreement with previous reports that described Mitofilin to form a large mitochondrial complex (John *et al.*, 2005). Taken together, in conjunction with topological and mass spectrometric analyses in yeast and human cells, results indicate that Mio10/MINOS1 form a large complex at the mitochondrial inner membrane. In human mitochondria, this complex may contain the known Mitofilin interactor CHCHD3 and bridges the mitochondrial membranes by interacting with the SAM complex. The exact composition of MINOS complex however cannot be determined from the results of this study. Moreover, this complex plays a role in cristae and inner membrane morphology, as shown by the *MIO10* deletion mutants in yeast. The absence of this complex leads to aberrant inner membrane organization. Hence, this complex was termed MINOS: **Mitochondrial Inner membrane Organizing System** (Figure 35). Evidence of MINOS components in various species from yeast,

C.elegans, and human mitochondria, as well as high sequence conservation of Mio10/MINOS1, Fcj1/Mitofilin, and CHCHD3 may reflect the functional and evolutionary importance of this complex.

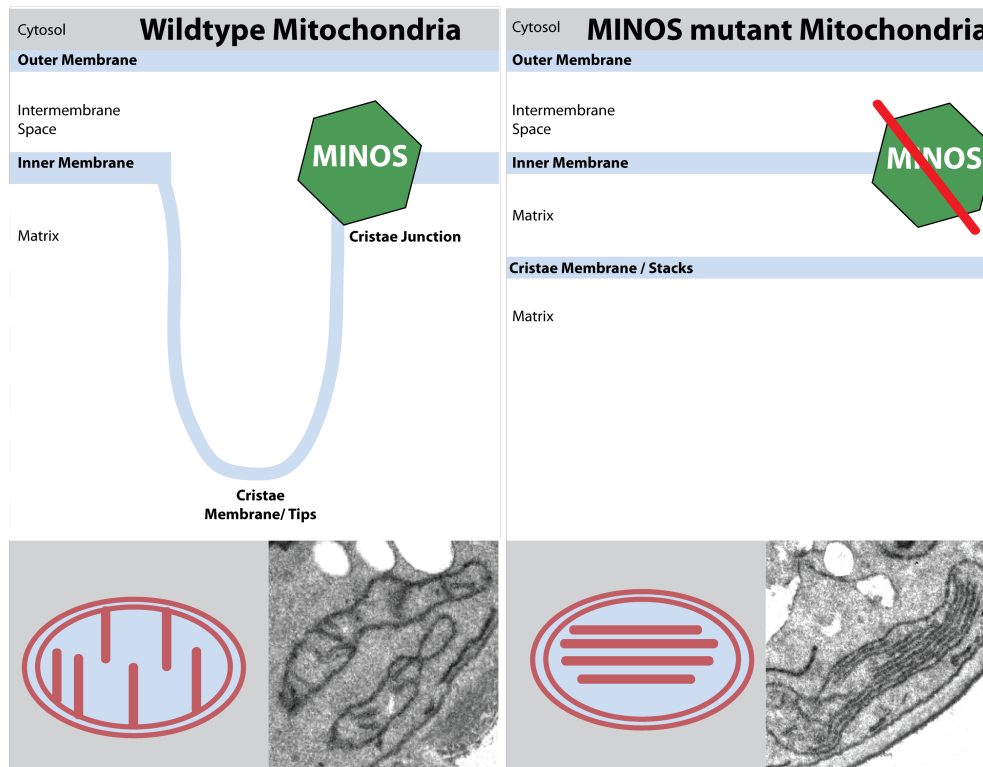


Figure 35. MINOS complex is critical for cristae biogenesis. In wildtype mitochondria, the MINOS complex sits at cristae junctions and contributes to proper cristae membrane morphology and cristae tip formation. In a MINOS mutant mitochondria (*mio10Δ* or *fcj1Δ*), the absence of the MINOS complex leads to aberrant cristae morphology exhibited by membrane stacks. Schematic representations of the phenotypes of wildtype and MINOS mutants (based on electron micrographs of *mio10Δ*) are shown the lower panel.

5.2.4 The identification of additional MINOS components

During the revision process for the Alkhaja *et al.*, 2012, three publications also reported the identification of the yeast MINOS complex (Hoppins *et al.*, 2011; Harner *et al.*, 2011; von der Malsburg *et al.*, 2011). In all three studies, Mio10 (ORF, YCL057c-A) has been identified to play a role in cristae junction formation and inner membrane organization and morphology. This role is mediated by its interaction with Fcj1. Moreover, four other components of the MINOS complex have been also identified: YGR235C, Aim5, Aim13, and Aim37. Interestingly these proteins have been identified in the mass spectrometric analysis of Mio10^{SF} biochemical isolations, performed in this study. Von der Malsburg *et al.* identified the component the MINOS in an affinity purification screen using a Fcj1^{zz} strain coupled with SILAC-based quantitative mass spectrometric analysis, whereas Harner *et al.* identified the components by analyzing the proteome of contact sites. These sites are regions at which the outer membrane and inner membrane appear to meet (Hackenbrock, 1968). In contrast, Hoppins *et al.* identified the MINOS complex using a quantitative genetic interaction map. The systematic map was based on pair-wise measurements of growth defects in double mutant cells, and focused on genes encoding mitochondrial proteins and genes that may affect mitochondrial function. The components were found in a highly correlated cluster containing Fcj1 and also to a cluster containing ERMES. Like Mio10, these identified components affect inner membrane organization and cristae morphology, however with varying degrees. Table 8 represents the components of MINOS based on the different studies in comparison to available data with respect to higher eukaryotes. The following section reviews the findings of the three independent studies, in which the nomenclature used in der Malsburg *et al.* (2011) is applied.

Table 8. The MINOS components as identified by various studies. MINOS, von der Malsburg *et al.*, 2011; MICOS, Harner *et al.*, 2011; MitOS, Hoppins *et al.*, 2011. n/a, not available homolog in respective organism(s). YGR235C = (Mio27/Msc29/Mos2)

Yeast			Higher eukaryotes
MINOS	MICOS	MitOS	MINOS
Mio10	Msc10	Mos1	MINOS1
Fcj1	Fcj1	Fcj1	Mitofilin / IMMT
Aim5	Msc12	Aim5	<i>n/a</i>
Aim13	Msc19	Aim13	<i>n/a</i>
Aim37	Msc27	Aim37	MOMA-1
Mio27	Msc29	Mos2	
<i>n/a</i>	<i>n/a</i>	<i>n/a</i>	CHCHD3

Topological analysis indicated that all identified components, besides Aim13, were integral inner membrane proteins with domains exposed to the IMS. Aim13 was shown to an IMS protein that associated peripherally to the inner membrane. Electron microscopy analysis of the different mutants indicated that *mio10Δ* and *fcj1Δ* had similar phenotypes in which mitochondria exhibited stacks of lamellar cristae. The observed phenotypes are in agreement with electron microscopy analysis performed in this doctoral study. Also, whereas *mio27Δ* mitochondrial had no considerable defects, *aim5Δ*, *aim13Δ*, *aim37Δ* exhibited intermediate phenotypes. Results indicate that Fcj1 and Mio10 are the main functional components of the MINOS complex. The conclusion that cristae membranes loose their association with the IBM is *fcj1Δ* and *mio10Δ* is also made (von der Malsburg *et al.*, 2011).

In agreement with results presented in this study, the MINOS complex was also shown to interact with the TOM and SAM complexes of the mitochondrial outer membrane (von der Malsburg *et al.*, 2011, Harner *et al.*, 2011). A MINOS interaction with Mia40 was also observed (von der Malsburg *et al.*, 2011). The Mia pathway with its components Mia40 and Erv1 mediate oxidative protein folding by disulfide bond formation, which drive translocation and proper targeting of a certain mitochondrial IMS proteins (Herrmann and Riemer, 2012). However, an interaction with Mia40 was argued to be specific to Fcj1 and not other MINOS components. Fcj1 thus may have distinct functions in either inner membrane organization or protein import. Moreover, it is shown that Fcj1 copurifies with Ugo1, which is required for mitochondrial fusion

in concert with its interaction partner Fzo1 (Sesaki and Jensen, 2004; Hoppins *et al.*, 2011). The data thus not only links the MINOS complex with mitochondrial protein import (TOM, SAM) but also to the mitochondrial network dynamics. This also parallels results of this doctoral study which indicated potential interactions with the SAM complex and also ERMES components. All in all, the results of the recent studies are in agreement with the findings of this doctoral study and support the model of the MINOS complex involvement in inner membrane organization.

5.3 Conclusions and Outlook

The mitochondrial inner membrane is morphologically dynamic. Various inner membrane proteins are known to contribute to the shape and structure of cristae membranes. F_1F_0 ATPase dimers contribute to a strong local curvature and thus the angular shape of the cristae apex (Strauss *et al.*, 2008; Seelert and Dencher, 2011). Mutants that lack the Atp20 or Atp21 dimerization factors exemplify the importance of F_1F_0 ATPase dimerization with respect to cristae morphology. These mutants clearly exhibit mutant inner mitochondrial organization that characterized by concentric ‘onion-like’ structures (Paumard *et al.*, 2002b; Arselin *et al.*, 2003; Arselin *et al.*, 2004). Moreover, Mitofilins (Fcj1 in yeast) has been previously shown to be an important determinant of cristae junction formation by acting in an antagonistic manner in inner membrane curvature with respect to F_1F_0 ATPase dimers (Rabl *et al.*, 2009). Whereas this study did not result the identification of novel F_1F_0 ATPase dimerization factors, Mio10/MINOS1 are identified as novel interaction partners of Fcj1/Mitofilin. This study also provided evidence for the MINOS complex playing a critical role in inner membrane architecture. The role of Mio10 in cristae morphology in yeast was shown by the analysis of *MIO10* deletion mutants in comparison to other strains. The results of this study is paralleled and verified by three other studies, which have in addition identified four other components of the MINOS complex (Hoppins *et al.*, 2011; Harner *et al.*, 2011; von der Malsburg *et al.*, 2011). Comparison of the phenotypes of the various MINOS mutants, indicated that the deletion of *MIO10* and *FCJI* lead to more severe cristae aberrations. The absence of either protein also leads to complete dissociation of the MINOS complex in yeast (von der Malsburg *et al.*, 2011). It thus appears that Mio10 is one the main components of the yeast MINOS complex.

Results from this study and other publications support the notion that MINOS is a multifunctional complex (Figure 36). Beside the obvious role in cristae morphology, the MINOS may play a role in mitochondrial protein import by its interaction with SAM, TOM, and MIA components (Xie *et al.*, 2007; von der Malsburg *et al.*, 2011; Harner *et al.*, 2011). By its interaction with Ugo1, the MINOS complex plays a role in fusion and mitochondrial network dynamics (Harner *et al.*, 2011). Moreover, it may have a role in mitochondrial inheritance via its components, Aim5, Aim13, and Aim37 (Hess *et al.*, 2009). MINOS interaction with cytoskeleton proteins (FAM82B and Tubulin) may indicate its role in mitochondrial trafficking. Furthermore it may play a role in ERMES and ER mitochondrial dynamics via its interaction with ER resident proteins (TANGO1). This notion is further supported by a strong genetic interaction of MINOS and ERMES genes (Hoppins *et al.*, 2011). Besides its link to apoptosis via Mitofilin interaction with OPA1 (Darshi *et al.*, 2011), the MINOS complex may also play role in cancer. Indeed, MINOS1 proteins levels are elevated in prostate cancer cells (Lin *et al.*, 2005). In addition, overexpression of CHCHD6 in human cancer cells enhances resistance to genotoxic anticancer drugs, whereas its knockdown increases its chemosensitivity (An *et al.*, 2012). Other than its proven role in inner membrane architecture, any role MINOS might have in other mitochondrial and non mitochondrial processes remains speculative and further investigations are necessary.

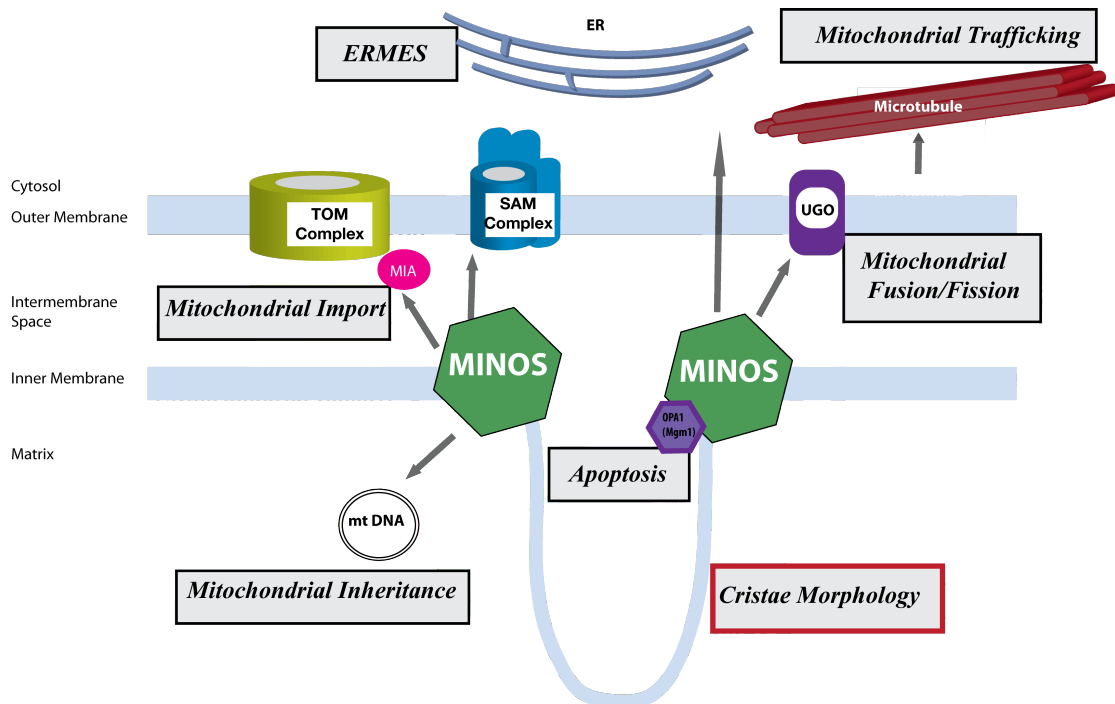


Figure 36. MINOS is a multifunctional protein. Besides the MINOS role in cristae morphology, results from various sources indicate potential MINOS interactions with ERMES (via SAM and TANGO1), mitochondrial trafficking (Tubulin), mitochondrial import (TOM, SAM, Mia40), mitochondrial fusion/fission (Ugo1), and mitochondrial inheritance (AIM proteins of the MINOS complex).

Besides the characterization of novel roles MINOS may have in mitochondria and other cellular organelles, information is still required with respect to the structure and exact function of MINOS in inner membrane organization. For instance, the exact composition of the MINOS complex in higher eukaryotes remains an open question. Still, it may be postulated from available data that MINOS in higher eukaryotes contains at least MINOS1, Mitofilin, CHCHD3 and CHCHD6. It should also be considered that the composition of the MINOS complex might vary across the species divide. A homolog of Aim5 and Aim13 is not found in higher eukaryotes whereas a homolog for CHCHD3 is not found in yeast (Herrmann, 2011). The MINOS complex may require at least Mio10/MINOS1 and Fcj1/Mitofilin, whereas other components may vary. One possible approach would be performing an affinity purification based mass spectrometric analysis of a tagged MINOS1 or Mitofilin in human cultured cells. This would be comparable to the approach in which all MINOS components were identified in yeast (von der Malsburg *et al.*, 2011). In addition, the effect of the roles of Mitofilin, CHCHD3, and CHCHD6 are well documented as their depletion leads to aberrant mitochondrial cristae (John *et al.*, 2005; Darshi *et al.*, 2011; An *et al.*, 2012). To this end, it would be valuable to investigate the effect of MINOS1 knockdown by

RNAi in human mitochondria and whether the role of MINOS1 in the MINOS complex is as essential as the yeast Mio10.

More evidence is still required to understand how the MINOS complex and its components exert their function in cristae biogenesis. It should be noted that most of the of evidence related to the roles of these inner membrane proteins have been deduced from tomographies of mutants, whether yeast or human cultured cells. These tomographies represent single-point illustrations of the mutations effects but provide limited insight onto the dynamics governing how cristae membranes are rendered 'online-like', 'stacked', or 'vesicle-like'. This further highlights the extent to which cristae propagation, maintenance, and dynamics remain to be studied.

Analysis of the MINOS mutants indicted that that MINOS complex affects cristae junction opening diameters (Rabl *et al.*, 2009; von der Malsburg *et al.*, 2011; Hoppins *et al.*, 2011). It also plays a role in maintenance of cristae tips, exemplified by the lack of cristae tips in various MINOS mutants. In the absence of MINOS components, the cristae membranes appear detached from the IBM and form stacks that are linked together with the F₁F₀ATPase (Rabl *et al.*, 2009; von der Malsburg *et al.*, 2011). MINOS might thus have a role in cristae biogenesis: cristae tip formation, cristae membrane curvature, junction maintenance; and cristae membrane propagation (Figure 37).

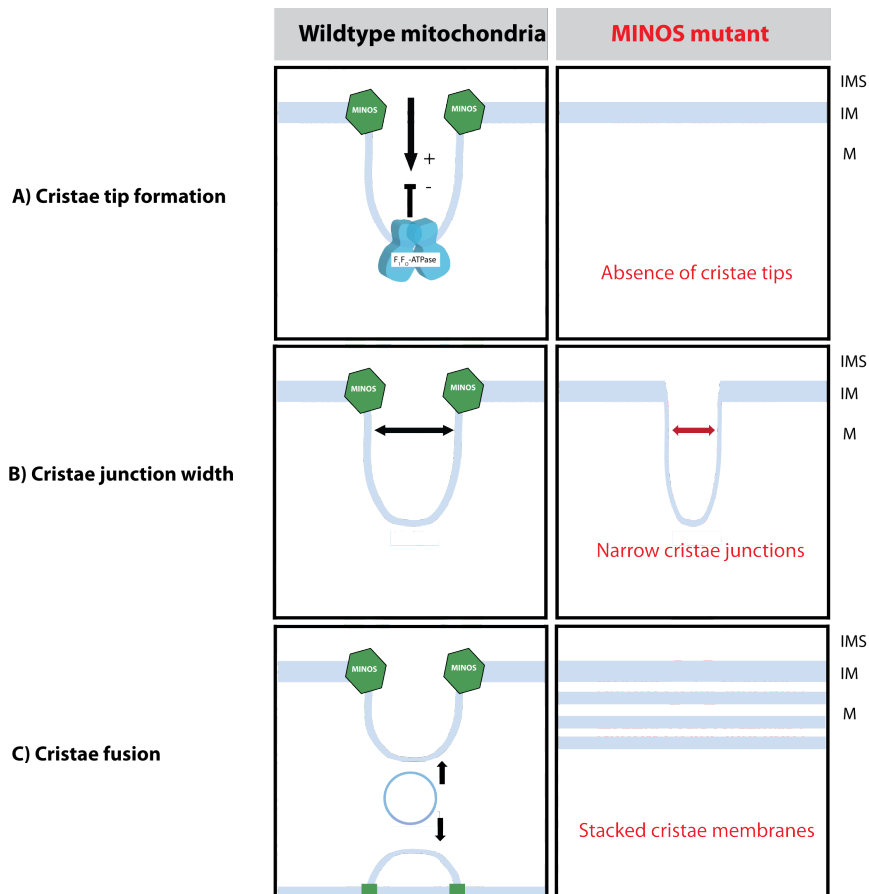


Figure 37. Overview of MINOS roles in cristae biogenesis. A) By inducing positive membrane curvature, MINOS leads to invagination of the inner membrane and eventual cristae tip formation. In the absence of MINOS, cristae tips are not found. B) The large molecular size of MINOS might regulate cristae junction width. In the absence of some MINOS components, cristae membranes appear to have narrower cristae junctions. C) MINOS might have a role in the regulation cristae fusion. In the absence of MINOS, fission of cristae membrane is active whereas fusion discontinues. This may lead to an increase in cristae vesicle, which are then stacked by F_1F_0 ATPase dimers.

MINOS may affect cristae junction due its large molecular size and by its interaction with OPA-1. OPA-1 controls cristae opening size by forming a scaffold at the opening that prevents premature release of cytochrome c under non-apoptotic conditions (Frezza *et al.*, 2006). The role of MINOS in cristae biogenesis may be explained by the invagination cristae model, which postulates that cristae tips and membranes can result from 1) continuous inner membrane biogenesis and but constant outer membrane growth and 2) large complexes that enforce membrane curvature (Renken *et al.*, 2002). The cristae membrane curvatures are mediated by the large MINOS complex (that forms a positive membrane curvature) and the F_1F_0 ATPase dimers (which form a negative curvature). Thus, in the absence of MINOS, positive membrane curvature is absent and no cristae tips are formed. However, this may be not

enough to explain the observed stacked cristae inner membranes of MINOS mutants. In this case, a cristae fusion/fission model may be applied. This model proposes that cristae formation is dynamic, in which cristae membrane vesicles may continuously fuse from one site of the inner membrane and fuse to another (Zick *et al.*, 2009). The notion that cristae propagation is dynamic is supported by the observation of certain reversible cristae morphologies (Mannella *et al.*, 2001). Stacked membranes in MINOS mutants may thus be due to continuous cristae fission but a lack of fusion. The MINOS complex may play a role in the equilibrium between cristae fusion and fission. Information is still lacking to explain a variation of phenotypes within any single MINOS mutants (wildtype, onion-like, or intermediate). Thus, it may seem that other factors may be involved with respect to MINOS and cristae morphology. Further analysis such as the analysis of multiple deletions or knockouts of MINOS components may shine light on the exact role of MINOS. Moreover, high-resolution immunoelectron microscopy analysis of mitochondrial inner membrane in the presence or absence of MINOS components may provide novel insight into the mechanism of the complex.

MINOS is not only an inner membrane organizer that forms a scaffold connecting the inner and outer mitochondrial membranes, but may feature in various other mitochondrial and extra-mitochondrial functions. Many of these functions are yet to be examined and further studies are required. Various outstanding questions remain with respect to the exact role of the MINOS complex. Nonetheless, the discovery of new MINOS components here may provide new insight and direction for future studies.

6. REFERENCES

- Abdul, K.M., Terada, K., Yano, M., Ryan, M.T., Streimann, I., Hoogenraad, N.J. and Mori, M. (2000). Functional analysis of human metaxin in mitochondrial protein import in cultured cells and its relationship with the Tom complex. *Biochem. Biophys. Res. Commun.* *276*, 1028–1034.
- Abrahams J. P., Leslie, A. G., Lutter, R., and Walker, J. E. (1994). Structure at 2.8 Å resolution of F1-ATPase from bovine heart mitochondria. *Nature.* *370*, 621–628.
- Ahting, U., Thieffry, M., Engelhardt, H., Hegerl, R., Neupert, W., and Nussberger, S. (2001). Tom40, the pore-forming component of the protein-conducting TOM channel in the outer membrane of mitochondria. *J. Cell Biol.* *153*, 1151–1160.
- Alkhaja, A. K., Jans, D. C., Nikolov, M., Vukotic, M., Lytovchenko, O., Ludewig, F., Schliebs, W., Riedel, D., Urlaub, H., Jakobs, S., and Deckers M. (2012). MINOS1 is a conserved component of mitofilin complexes and required for mitochondrial function and cristae organization. *Mol. Biol. Cell.* *23*, 247–57.
- Allen, R.D., Schroeder, C.C., and Fok, A.K. (1989). An investigation of mitochondrial inner membranes by rapid-freeze deep-etch techniques. *J. Cell Biol.* *108*, 2233–2240.
- Althoff, T., Mills, D.J., Popot, J.-L., and Kühlbrandt, W. (2011). Arrangement of electron transport chain components in bovine mitochondrial supercomplex I(1)III(2)IV(1). *EMBO J.* *30*, 4652–4664.
- Amutha, B., Gordon, D. M., Gu, Y., and Pain, D. (2004). A novel role of Mgm1p, a dynamin-related GTPase, in ATP synthase assembly and cristae formation/ maintenance. *Biochem. J.* *381*, 19–23.
- An, J., Shi, J., He, Q., Lui, K., Liu, Y., Huang, Y., and Sheikh MS. (2012). CHCM1/CHCHD6, a novel mitochondrial protein linked to regulation of mitofilin and mitochondrial cristae morphology. *J. Biol. Chem.* [Epub ahead of print]
- Andersson, S. G., Karlberg, O., Canback, B., and Kurland, C. G. (2003) On the origin of mitochondria: a genomics perspective. *Philos. Trans. R. Soc. Lond. B. Biol. Sci.* *358*, 165–177.
- Arnold, I., Pfeiffer, K., Neupert, W., Stuart, R. A., and Schägger, H. (1998). Yeast mitochondrial F1F0-ATP synthase exists as a dimer: identification of three dimer-specific subunits. *EMBO J.* *17*, 7170–7178.
- Arnold, I., Bauer, M. F., Brunner, M., Neupert, W., and Stuart, R. A. (1997). Yeast mitochondrial F1F0-ATPase: the novel subunit e is identical to Tim11. *FEBS Lett.* *411*, 195–200.
- Arnold, I., Pfeiffer, K., Neupert, W., Stuart, R. A., and Schägger, H. (1998). Yeast mitochondrial F1F0-ATP synthase exists as a dimer: identification of three dimer-specific subunits. *EMBO J.* *17*, 7170–7178.
- Arnold, I., Pfeiffer, K., Neupert, W., Stuart, R. A., and Schägger, H. (1999). ATP synthase of yeast mitochondria. Isolation of subunit j and disruption of the ATP18 gene. *J. Biol. Chem.* *274*, 36–40.
- Arselin, G., Giraud, M. F., Dautant, A., Vaillier, J., Brèthes, D., Couлары-Salin, B., Schaeffer, J., and Velours, J. (2003). The GxxxG motif of the transmembrane domain of subunit e is involved in the dimerization/oligomerization of the yeast ATP synthase complex in the mitochondrial membrane. *Eur. J. Biochem.* *270*, 1875–1884.
- Arselin, G., Vaillier, J., Salin, B., Schaeffer, J., Giraud, M. F., Dautant, A., Brèthes, D., and Velours, J. (2004). The modulation in subunits e and g amounts of yeast ATP synthase modifies mitochondrial cristae morphology. *J. Biol. Chem.* *279*, 40392–40399.

- Bachner, D., Sedlacek, Z., Korn B., Hameister H., and Poustka, A. (1995). Expression patterns of two human genes coding for different rab GDP-dissociation inhibitors (GDIs), extremely conserved proteins involved in cellular transport. *Hum. Mol. Genet.* *4*, 701–708.
- Banci, L., Bertini, I., Cefaro, C., Ciofi-Baffoni, S., Gallo, A., Martinelli, M., Sideris, D.P., Katrakili, N., and Tokatlidis, K. (2009). MIA40 is an oxidoreductase that catalyzes oxidative protein folding in mitochondria. *Nat. Struct. Mol. Biol.* *16*, 198–206.
- Becker, L., *et al.* (2005). Preprotein translocase of the outer mitochondrial membrane: reconstituted Tom40 forms a characteristic TOM pore. *J. Mol. Biol.* *353*, 1011–20.
- Bihlmaier, K., Mesecke, N., Terziyska, N., Bien, M., Hell, K., and Herrmann, J.M. (2007). The disulfide relay system of mitochondria is connected to the respiratory chain. *J. Cell Biol.* *179*, 389–395.
- Bradford, M. M. (1976). A rapid and sensitive method for the quantitation of microgram quantities of protein utilizing the principle of protein-dye binding. *Anal Biochem.* *72*, 248–54.
- Brandner, K., Mick, D. U., Frazier, A. E., Taylor, R. D., Meisinger, C., and Rehling, P. (2005). Taz1, an outer mitochondrial membrane protein, affects stability and assembly of inner membrane protein complexes: implications for Barth Syndrome. *Mol Biol Cell.* *2005*, *11*, 5202–5214.
- Baughman, J. M., Nilsson, R., Gohil, V. M., Arlow, D. H., Gauhar, Z., and Mootha, V. K. (2009). A computational screen for regulators of oxidative phosphorylation implicates SLIRP in mitochondrial RNA homeostasis. *J. Biol. Chem.* *284*, e1000590.
- Bornhövd, C., Vogel, F., Neupert, W., and Reichert, A. (2006). Mitochondrial membrane potential is dependent on oligomeric state of F1F0-ATP synthase supracomplexes. *J. Biol. Chem.* *281*, 13990–13998.
- Boyer, P. D. (1997). The ATP synthase--a splendid molecular machine. *Annu. Rev. Biochem.* *66*, 717–749.
- Boldogh, I. R., Nowakowski, D. W., Yang, H. C., Chung, H., Karmon, S., Royes, P., and Pon, L. A. (2003). A protein complex containing Mdm10p, Mdm12p, and Mmm1p links mitochondrial membranes and DNA to the cytoskeleton-based segregation machinery. *Mol. Biol. Cell.* *14*, 4618–4627.
- Burton, P.R. (1979). Fine structure of mitochondria of *Spirostomum ambiguum* as seen in sectioned and negatively-stained preparations. *J. Protozool.* *17*, 295–299.
- Bustos, D. M., and Velours, J. (2005). The modification of the conserved GXXXG motif of the membrane-spanning segment of subunit g destabilizes the supramolecular species of yeast ATP synthase. *J. Biol. Chem.* *280*, 29004–29010.
- Buzhynskyy, N., Sens, P., Prima, V., Sturgis, J. N., and Scheuring, S. (2007). Rows of ATP synthase dimers in native mitochondrial inner membranes. *J. Biol. Chem.* *282*, 2870–2876.
- Campanella, M., Parker, N., Tan, C.H., Hall, A.M., and Duchon, M.R. (2009). IF1: setting the pace of the F1F0-ATP synthase. *Trends Biochem. Sci.* *34*, 343–350.
- Chacinska, A., Lind, M., Frazier, A. E., Dudek, J., Meisinger, C., Geissler, A., Sickmann, A., Meyer, H. E., Truscott, K. N., Guiard, B., Pfanner, N., and Rehling, P. (2005). Mitochondrial presequence translocase: switching between TOM tethering and motor recruitment involves Tim21 and Tim17. *Cell.* *120*, 817–29.
- Chacinska, A., Koehler, C.M., Milenkovic, D., Lithgow, T., and Pfanner, N. (2009). Importing Mitochondrial Proteins: Machineries and Mechanisms. *Cell.* *137*, 628–644.
- Chenna, R., Sugawara, H., Koike, T., Lopez, R., Gibson, T. J., Higgins, D. G., and Thompson, J. D. (2003). Multiple sequence alignment with the Clustal series of programs. *Nucleic Acids Res.* *31*, 3497–

3500.

Chernomordik, L. V., and Kozlov, M. M. (2005). Membrane hemifusion: crossing a chasm in two leaps. *Cell*. *123*, 375–82.

Collinson, I. R., Runswick, M. J., Buchanan, S. K., Fearnley, I. M., Skehel, J. M., van Raaij, M. J., Griffiths, D. E., and Walker, J. E. (1994). Fo membrane domain of ATP synthase from bovine heart mitochondria: purification, subunit composition, and reconstitution with F1-ATPase. *Biochemistry*. *33*, 7971–7978.

Cox, J., and Mann, M. (2008). MaxQuant enables high peptide identification rates, individualized p.p.b.-range mass accuracies and proteome-wide protein quantification. *Nat. Biotechnol.* *26*, 1367–1372.

Curran, S. P., Leuenberger, D., Oppliger, W., and Koehler, C. M. (2002). The Tim9p-Tim10p complex binds to the transmembrane domains of the ADP/ATP carrier. *EMBO J.* *21*, 942–53.

Darshi, M., Mendiola, V. L., Mackey, M. R., Murphy, A. N., Koller, A., Perkins, G. A., Ellisman, M. H., and Taylor, S. S. (2011). ChChd3, an inner mitochondrial membrane protein, is essential for maintaining crista integrity and mitochondrial function. *J. Biol. Chem.* *286*, 2918–2932.

De los Rios Castillo, D., Zarco-Zavala, M., Olvera-Sanchez, S., Pardo, J. P., Juarez, O., Martinez, F., Mendoza-Hernandez, G., García-Trejo, J. J., and Flores-Herrera, O. (2011). Atypical cristae morphology of human syncytiotrophoblast mitochondria: role for complex V. *J. Biol. Chem.* *286*, 23911–23919.

Dian, E.A., Papatheodorou, P., Emmrich, K., Randel, O., Geissler, A., Kolling, R., Rassow, J., and Motz, C. (2008). Role of gamma-subunit N- and C-termini in assembly of the mitochondrial ATP synthase in yeast. *J. Mol. Biol.* *377*, 1314–1323.

Dolezal, P., Likic, V., Tachezy, J., and Lithgow, T. (2006). Evolution of the molecular machines for protein import into mitochondria. *Science*. *313*, 314–318.

Duvezin-Caubet, S., Jagasia, R., Wagener, J., Hofmann, S., Trifunovic, A., Hansson, A., Chomyn, A., Bauer, M. F., Attardi, G., Larsson, N. G., Neupert, W., and Reichert, A.S. (2006). Proteolytic processing of OPA1 links mitochondrial dysfunction to alterations in mitochondrial morphology. *J. Biol. Chem.* *281*, 37972–37979.

Dudkina, N. V., Sunderhaus, S., Braun, H. P., and Boekema, E. J. (2006). Characterization of dimeric ATP synthase and cristae membrane ultrastructure from *Saccharomyces* and *Polytomella* mitochondria. *FEBS Lett.* *580*, 3427–3432

Egner, A., Jakobs, S., and Hell, S. W. (2002) Fast 100-nm resolution three-dimensional microscope reveals structural plasticity of mitochondria in live yeast. *Proc Natl. Acad. Sci. U S A.* *99*, 3370–3375.

Erdmann, R., Veenhuis, M., Mertens, D., and Kunau, W. H. (1989). Isolation of peroxisome-deficient mutants of *Saccharomyces cerevisiae*. *Proc. Natl. Acad. Sci. USA.* *86*, 5419–5423.

Eubel, H., Jansch, L., and Braun, H. P. (2003). New insights into the respiratory chain of plant mitochondria. Supercomplexes and a unique composition of complex II. *Plant Physiol.* *133*, 274–286.

Everard-Gigot, V., Dunn, C. D., Dolan, B. M., Brunner, S., Jensen, R. E., and Stuart, R.A. (2005). Functional analysis of subunit e of the F1FO-ATP synthase of the yeast *Saccharomyces cerevisiae*: importance of the N-terminal membrane anchor region. *Eukaryot. Cell.* *4*, 346–355.

Farrell, S.R., and Thorpe, C. (2005). Augmenter of liver regeneration: a flavin- dependent sulfhydryl oxidase with cytochrome c reductase activity. *Biochemistry.* *44*, 1532–1541.

Frazier, A. E., Chacinska, A., Truscott, K. N., Guiard, B., Pfanner, N., and Rehling, P. (2003). Mitochondria use different mechanisms for transport of multispinning membrane proteins through the intermembrane space. *Mol. Cell. Biol.* *23*, 7818–28.

- Frey, T.G., and Mannella, C.A. (2000). The internal structure of mitochondria. *Trends Biochem. Sci.* *25*, 319–324.
- Frezza, C. *et al.* (2006). OPA1 controls apoptotic cristae remodeling independently from mitochondrial fusion. *Cell.* *126*, 177–189.
- Fronzes, R., Chaignepain, S., Bathany, K., Giraud, M. F., Arselin, G., Schmitter, J. M., Dautant, A., Velours, J., and Brèthes D. (2003). Topological and functional study of subunit h of the F1Fo ATP synthase complex in yeast *Saccharomyces cerevisiae*. *Biochemistry.* *42*, 12038–12049.
- Fontanesi, F., Soto, I. C., Horn, D., and Barrientos, A. (2006) Assembly of mitochondrial cytochrome c-oxidase, a complicated and highly regulated cellular process. *Am J Physiol Cell Physiol*, *291*, 1129–1147.
- García, J. J., Morales-Ríos, E., Cortés-Hernandez, P., and Rodríguez-Zavala, J. S. (2006). The inhibitor protein (IF1) promotes dimerization of the mitochondrial F1Fo-ATP synthase. *Biochemistry.* *42*, 12695–12703.
- Gavin, P. D., Prescott, M., Luff, S. E., and Devenish, R. J. (2004). Cross-linking ATP synthase complexes in vivo eliminates mitochondrial cristae. *J. Cell. Sci.* *117*, 2333–2343.
- Geissler, A., Chacinska, A., Truscott, K. N., Wiedemann, N., Brandner, K., Sickmann, A., Meyer, H. E., Meisinger, C., Pfanner, N., and Rehling P. (2002). The mitochondrial presequence translocase: an essential role of Tim50 in directing preproteins to the import channel. *Cell.* *111*, 507–518.
- Giddings, T. H. (2003). Freeze-substitution protocols for improved visualization of membranes in high-pressure frozen samples. *J. Microsc.* *212*, 53–61.
- Giraud, M. F., Paumard, P., Soubannier, V., Vaillier, J., Arselin, G., Salin, B., Schaeffer, J., Brèthes, D., di Rago, J. P., and Velours, J. (2002). Is there a relationship between the supramolecular organization of the mitochondrial ATP synthase and the formation of cristae? *Biochim. Biophys. Acta.* *1555*, 174–180.
- Gieffers, C., Koriath, F., Heimann, P., Ungermann, C., and Frey, J. (1997). Mitofilin is a transmembrane protein of the inner mitochondrial membrane expressed as two isoforms. *Exp. Cell. Res.* *232*, 395–9.
- Glater, E. E., Megeath, L. J., Stowers, R. S., and Schwarz, T.L. (2006). Axonal transport of mitochondria requires Milton to recruit kinesin heavy chain and is light chain independent. *J. Cell. Biol.* *173*, 545–557.
- Glick, B. S., Brandt, A., Cunningham, K., Müller, S., Hallberg, R. L., and Schatz, G. (1992). Cytochromes c1 and b2 are sorted to the intermembrane space of yeast mitochondria by a stop-transfer mechanism. *Cell.* *69*, 809–822.
- Gray, M.W., Burger, G., and Lang, B. F. (1999) Mitochondrial evolution. *Nature.* *283*, 1476–1481.
- Gray, M.W. (2011). The incredible shrinking organelle. *EMBO Rep.* *9*, 873.
- Griparic, L., van der Wel, N. N., Orozco, I.J., Peters, P.J., and van der Blik, A.M. (2004). Loss of the intermembrane space protein Mgm1/OPA1 induces swelling and localized constrictions along the lengths of mitochondria. *J Biol Chem.* *279*, 18792–18798.
- Hackenbrock, C. R. (1968) Chemical and physical fixation of isolated mitochondria in low-energy and high-energy states. *Proc. Natl. Acad. Sci. USA.* *61*, 598–605.
- Harner, M., Körner, C., Walther, D., Mokranjac, D., Kaesmacher, J., Welsch, U., Griffith, J., Mann, M., Reggiori, F., and Neupert, W. (2011). The mitochondrial contact site complex, a determinant of mitochondrial architecture. *EMBO J.* *30*, 4356–4370.

- Hess, D.C., et al. (2009). Computationally driven, quantitative experiments discover genes required for mitochondrial biogenesis. *PLoS Genet.* 5, e1000407.
- Herrmann, J. M. (2011). MINOS is plus: a Mitofilin complex for mitochondrial membrane contacts. *Dev Cell.* 21, 599–600.
- Herrmann, J. M., and Riemer, J. (2012). Mitochondria disulfide relay: a redox regulated protein import into the intermembrane space. *J. Biol. Chem.* 287, 4426–4433.
- Hofmann, K. and Stoffel, W. (1993). TMBASE—a database of membrane spanning proteins segments. *Biol. Chem. Hoppe-Seyler*, 374, 166.
- Holland, H. D. (1994) Early proterozoic atmospheric change. In *Early life on earth* (ed. S. Bengtson), pp. 237–244. New York: Columbia University Press.
- Hong, S., and Pedersen, P. L. (2002). ATP synthase of yeast: structural insight into the different inhibitory potencies of two regulatory peptides and identification of a new potential regulator. *Arch. Biochem. Biophys.* 405, 38–43.
- Hoppins, S., Lackner, L., and Nunnari, J. (2007). The machines that divide and fuse mitochondria. *Annu. Rev. Biochem.* 76, 751–780.
- Hoppins, S., Collins, S. R., Cassidy-Stone, A., Hummel, E., Devay, R. M., Lackner, L. L., Westermann, B., Schuldiner, M., Weissman, J. S., and Nunnari, J. (2011). A mitochondrial-focused genetic interaction map reveals a scaffold-like complex required for inner membrane organization in mitochondria. *J. Cell. Biol.* 195, 323–40.
- John, G. B., Shang, Y., Li, L., Renken, C., Mannella, C. A., Selker, J. M., Rangell, L., Bennett, M. J., and Zha, J. (2005). The mitochondrial inner membrane protein mitofilin controls cristae morphology. *Mol. Biol. Cell.* 16, 1543–1554.
- Kanki, T., and Klionsky, D. J. (2008). Mitophagy in yeast occurs through a selective mechanism. *J. Biol. Chem.* 283, 32386–32393.
- Kanki, T., Kang, D., and Klionsky, D. J. (2009). Monitoring mitophagy in yeast: the Om45-GFP processing assay. *Autophagy.* 5, 1186–1189.
- Karlberg, O., Canbäck, B., Kurland, C.G, and Andersson, S.G. (2000). The dual origin of the yeast mitochondrial proteome. *3*, 170–187.
- Krause, F., Reifschneider, N. H., Goto, S., and Dencher, N. A. (2005). Active oligomeric ATP synthases in mammalian mitochondria. *Biochem. Biophys. Res. Commun.* 329, 583–590.
- Kolmakov, K., Belov, V. N., Bierwagen, J., Ringemann, C., Müller, V., Eggeling, C., and Hell, S. W. (2010). Red-emitting rhodamine dyes for fluorescence microscopy and nanoscopy. *Chemistry.* 16, 158–166.
- Koshiba, T., Holman, H. A., Kubara, K., Yasukawa, K., Kawabata, S., Okamoto, K., MacFarlane, J., and Shaw, J. M. (2011). Structure-function analysis of the yeast mitochondrial Rho GTPase, Gem1p: implications for mitochondrial inheritance. *J. Biol. Chem.* 286, 354–362.
- Kucharczyk, R., Zick, M., Bietenhader, M., Rak, M., Couplan, E., Blondel, M., Caubet, S.D., and di Rago, J.P. (2009). Mitochondrial ATP synthase disorders: molecular mechanisms and the quest for curative therapeutic approaches. *Biochim. Biophys. Acta.* 1, 186–99.
- Lazarou, M., Smith, S. M., Thorburn, D. R., Ryan, M. T., and McKenzie. M. (2009). Assembly of nuclear DNA-encoded subunits into mitochondrial complex IV, and their preferential integration into supercomplex forms in patient mitochondria. *FEBS J.* 276, 6701–6713.

- Lin, B., *et al.* (2005). Evidence for the presence of disease-perturbed networks in prostate cancer cells by genomic and proteomic analyses: a systems approach to disease. *Cancer. Res.* *65*, 3081–3091.
- Liu, Q., D'Silva, P., Walter, W., Marszalek, J., and Craig, E. A. (2003). Regulated cycling of mitochondrial Hsp70 at the protein import channel. *300*, 139–41.
- Liu, H., Sadygov, R. G., and Yates, J. R. 3rd. (2004). A model for random sampling and estimation of relative protein abundance in shotgun proteomics. *Anal. Chem.* *76*, 4193–4201.
- Luttik, M.A., Overkamp, K.M., Kötter, P., de Vries, S., van Dijken, J.P., and Pronk, J.T. (1998). The *Saccharomyces cerevisiae* NDE1 and NDE2 genes encode separate mitochondrial NADH dehydrogenases catalyzing the oxidation of cytosolic NADH. *J. Biol. Chem.* *38*, 24529–24534.
- Maçasev, D., Whelan, J., Newbigin, E., Silva-Filho, M. C., Mulhern, T. D., and Lithgow, T. (2004). Tom22', an 8-kDa trans-site receptor in plants and protozoans, is a conserved feature of the TOM complex that appeared early in the evolution of eukaryotes. *Mol. Biol. Evol.* *21*, 1557–1564.
- Mannella, C. A., Pfeiffer, D. R., Bradshaw, P. C., Moraru, I. I., Slepchenko, B., Loew, L. M., Hsieh, C. E., Buttle, K., and Marko, M. (2001). Topology of the mitochondrial inner membrane: dynamics and bioenergetic implications. *IUBMB Life.* *52*, 93–100.
- Mannella, C.A. (2008). Structural diversity of mitochondria: functional implications. *Ann. N. Y. Acad. Sci.* *1147*, 171–179.
- Meisinger, C., *et al.* (2004). The mitochondrial morphology protein Mdm10 functions in assembly of the preprotein translocase of the outer membrane. *Dev. Cell.* *7*, 61–71.
- Meisinger, C., Pfanner, N., and Truscott, K. N. (2006). Isolation of yeast mitochondria. *Methods. Mol. Biol.* *313*, 33–39.
- Meisinger, C., *et al.* (2007). The morphology proteins Mdm12/Mmm1 function in the major beta-barrel assembly pathway of mitochondria. *EMBO. J.* *26*, 2229–2239.
- Messerschmitt, M., Jakobs, S., Vogel, F., Fritz, S., Dimmer, K. S., Neupert, W., and Westermann, B. (2003). The inner membrane protein Mdm33 controls mitochondrial morphology in yeast. *J. Cell. Biol.* *160*, 553–564.
- Minauro-Sanmiguel, F., Wilkens, S., and García, J.J. (2005). Structure of dimeric mitochondrial ATP synthase: novel F0 bridging features and the structural basis of mitochondrial cristae biogenesis. *Proc. Natl. Acad. Sci. U S A.* *35*, 12356–12358.
- Mick, D. U., Wagner, K., van der Laan, M., Frazier, A. E., Perschil, I., Pawlas, M., Meyer, H. E., Warscheid, B., and Rehling, P. (2007). Shy1 couples Cox1 translational regulation to cytochrome c oxidase assembly. *EMBO J.* *26*, 4347–4358.
- Mick, D. U., Vukotic, M., Piechura, H., Meyer, H. E., Warscheid, B., Deckers, M., and Rehling, P. (2010). Coa3 and Cox14 are essential for negative feedback regulation of COX1 translation in mitochondria. *J. Cell. Biol.* *191*, 141–54.
- Mick, D.U., Fox, T.D., and Rehling, P. (2011). Inventory control: cytochrome c oxidase assembly regulates mitochondrial translation. *Nat. Rev. Mol. Cell. Biol.* *2011*, *1*, 14–20.
- Milenkovic, D., Gabriel, K., Guiard, B., Schulze-Specking, A., Pfanner, N., and Chacinska, A. (2007). Biogenesis of the essential Tim9-Tim10 chaperone complex of mitochondria: site-specific recognition of cysteine residues by the inter-membrane space receptor Mia40. *J. Biol. Chem.* *282*, 22472–22480.
- Mun, J. Y., Lee, T. H., Kim, J. H., Yoo, B. H., Bahk, Y. Y., Koo, H. S., and Han, S. S. (2010). *Caenorhabditis elegans* mitofilin homologs control the morphology of mitochondrial cristae and influence reproduction and physiology. *J. Cell. Physiol.* *224*, 784–756.

- Muto, T., Obita, T., Abe, Y., Shodai, T., Endo, T., and Kohda, D. (2001) NMR identification of the Tom20 binding segment in mitochondrial presequences. *J. Mol. Biol.* *306*, 137–43.
- Neupert, W., and Herrmann, J. M. (2007). Translocation of proteins into mitochondria. *Annu. Rev. Biochem.* *76*, 723–49.
- Nijtmans, L. G., Henderson, N. S., and Holt, I. J. (2002). Blue Native electrophoresis to study mitochondrial and other protein complexes. *Methods.* *26*, 327–34.
- Nikolov, M., Stuetzer, A., Mosch, K., Krasauskas, A., Soeroes, S., Stark, H., Urlaub, H., and Fischle, W. (2011). Chromatin affinity purification and quantitative mass spectrometry defining the interactome of histone modification patterns. *Mol. Cell. Proteomics.* *10*, M110.005371.
- Odgren, P. R., Toukatly, G., Bangs, P. L., Gilmore, R., and Fey, E. G. (1996). Molecular characterization of mitofilin (HMP), a mitochondria-associated protein with predicted coiled coil and intermembrane space targeting domains. *J. Cell. Sci.* *109*, 2253–2264.
- Oka, T., Sayano, T., Tamai, S., Yokota, S., Kato, H., Fujii, G., and Mihara, K. (2008). Identification of a novel protein MICS1 that is involved in maintenance of mitochondrial morphology and apoptotic release of cytochrome c. *Mol. Biol. Cell.* *19*, 2597–2608.
- Olichon, A., Emorine, L. J., Descoins, E., Pelloquin, L., Bricchese, L., Gas, N., Guillou, E., Delettre, C., Valette, A., Hamel, C. P., Ducommun, B., Lenaers, G., and Belenguer, P. (2002). The human dynamin-related protein OPA1 is anchored to the mitochondrial inner membrane facing the inter-membrane space. *FEBS Lett.* *523*, 171–176.
- Olichon, A., Baricault, L., Gas, N., Guillou, E., Valette, A., Belenguer, P., and Lenaers, G. (2003). Loss of OPA1 perturbs the mitochondrial inner membrane structure and integrity, leading to cytochrome c release and apoptosis. *J. Biol. Chem.* *278*, 7743–7746.
- Ong, S. E., Blagoev, B., Kratchmarova, I., Kristensen, D. B., Steen, H., Pandey, A., and Mann, M. (2002). Stable isotope labeling by amino acids in cell culture, SILAC, as a simple and accurate approach to expression proteomics. *Mol. Cell Proteomics.* *1*, 376–386.
- Ong S. E., and Mann M. (2006) A practical recipe for stable isotope labeling by amino acids in cell culture (SILAC). *Nat. Protoc.* *1*, 2650–2660.
- Okamoto, K., and Shaw, J.M. (2005). Mitochondrial morphology and dynamics in yeast and multicellular eukaryotes. *Annu. Rev. Genet.* *39*, 503–536.
- Osman, C., Merkwirth, C., Langer, T. (2009). Prohibitins and the functional compartmentalization of mitochondrial membranes. *J. Cell. Sci.* *122*, 3823–3830.
- Pan, Y. (2011). Mitochondria, reactive oxygen species, and chronological aging: a message from yeast. *Exp. Gerontol.* *46*, 847–852.
- Paschen, S. A., Waizenegger, T., Stan, T., Preuss, M., Cyrklaff, M., Hell, K., Rapaport, D., and Neupert, W. (2003). Evolutionary conservation of biogenesis of beta-barrel membrane proteins. *Nature.* *426*, 862–866.
- Pfanner, N., and Geissler, A. (2001). Versatility of the mitochondrial protein import machinery. *Nat. Rev. Mol. Cell. Biol.* *2*, 339–349.
- Paumard, P., Arselin, G., Vaillier, J., Chaignepain, S., Bathany, K., Schmitter, J. M., Brèthes, D., and Velours, J. (2002a). Two ATP synthases can be linked through subunits i in the inner mitochondrial membrane of *Saccharomyces cerevisiae*. *Biochemistry.* *41*, 10390–10396.
- Paumard, P., Vaillier, J., Couлары, B., Schaeffer, J., Soubannier, V., Mueller, D. M., Brèthes, D., di Rago, J. P., and Velours, J. (2002b). The ATP synthase is involved in generating mitochondrial cristae morphology. *EMBO J.* *21*, 221–230.

- Pfanner, N., Tropschug, M., and Neupert, W. (1987). Mitochondrial protein import: nucleoside triphosphates are involved in conferring import-competence to precursors. *Cell*. *49*, 815–823.
- Peixoto, P. M., Grana, F., Roy, T. J., Dunn, C. D., Flores, M., Jensen, R. E., and Campo, M. L. (2007). Awakening TIM22, a dynamic ligand-gated channel for protein insertion in the mitochondrial inner membrane. *J. Biol. Chem.* *282*, 18694–18701.
- Rabl, R., Soubannier, V., Scholz, R., Vogel, F., Mendl, N., Vasiljev-Neumeyer, A., Körner, C., Jagasia, R., Keil, T., Baumeister, W., Cyrklaff, M., Neupert, W., and Reichert, A. S. (2009). Formation of cristae and crista junctions in mitochondria depends on antagonism between Fcjl and Sufe/g. *J. Cell Biol.* *185*, 1047–1063.
- Racker, E. A mitochondrial factor conferring oligomycin sensitivity on soluble mitochondrial ATPase. (1963). *Biochem. Biophys. Res. Commun.* *10*, 435–439.
- Rak, M., Tetaud, E., Godard, F., Sagot, I., Salin, B., Duvezin-Caubet, S., Slonimski, P. P., Rytka, J., and di Rago, J.P. (2007). Yeast cells lacking the mitochondrial gene encoding the ATP synthase subunit 6 exhibit a selective loss of complex IV and unusual mitochondrial morphology. *J Biol Chem.* *15*, 10853–10864.
- Rehling, P., Model, K., Brandner, K., Kovermann, P., Sickmann, A., Meyer, H. E., Kühlbrandt, W., Wagner, R., Truscott, K.N., and Pfanner, N. (2003). Protein insertion into the mitochondrial inner membrane by a twin-pore translocase. *Science*. *299*, 1747–1751.
- Reinders, J., Zahedi, R. P., Pfanner, N., Meisinger, C., and Sickmann, A. (2006). Toward the complete yeast mitochondrial proteome: multidimensional separation techniques for mitochondrial proteomics. *J. Proteome. Res.* *5*, 1543–1554.
- Reinhold, R., Bareth, B., Balleininger, M., Wissel, M., Rehling, P., and Mick, D. U. (2011). Mimicking a SURF1 allele reveals uncoupling of cytochrome c oxidase assembly from translational regulation in yeast. *Hum. Mol. Genet.* *20*, 2379–2393.
- Renken, C., Siragusa, G., Perkins, G., Washington, L., Nulton, J., Salamon, P., Frey, T. G. (2002). A thermodynamic model describing the nature of the crista junction: a structural motif in the mitochondrion. *J. Struct. Biol.* *138*, 137–44.
- Russ, W. P., and Engelman, D. M. (2000). The GxxxG motif: a framework for transmembrane helix-helix association. *J. Mol. Biol.* *296*, 911–919.
- Saddar, S., and Stuart, R. A. (2005). The yeast F(1)F(0)-ATP synthase: analysis of the molecular organization of subunit g and the importance of a conserved GXXXG motif. *J. Biol. Chem.* *280*, 24435–24442.
- Saito, K., Chen, M., Bard, F., Chen, S., Zhou, H., Woodley, D., Polischuk, R., Schekman, R., and Malhotra V. TANGO1 facilitates cargo loading at endoplasmic reticulum exit sites. *Cell*. *136*, 891–902.
- Sanger, F., Nicklen, S., and Coulson, A. R. (1977). DNA sequencing with chain-terminating inhibitors. *Proc. Natl. Acad. Sci U S A.* *74*, 5463–7.
- Schägger, H., and von Jagow, G. (1987). Tricine-sodium dodecyl sulfate polyacrylamide gel electrophoresis for the separation of proteins from 1 to 100 kDa. *Anal. Biochem.* *166*, 368–379.
- Schägger, H., and von Jagow, G. (1991). Blue native electrophoresis for isolation of membrane protein complexes in enzymatically active form. *Anal Biochem.* *199*, 223–31.
- Schägger, H., and Pfeiffer, K. (2000). Supercomplexes in the respiratory chains of yeast and mammalian mitochondria. *EMBO J* *19*, 1777–1783.
- Scorrano, L., Ashiya, M., Buttle, K., Weiler, S., Oakes, S. A., Mannella, C. A., and Korsmeyer, S. J.

- (2002). A distinct pathway remodels mitochondrial cristae and mobilizes cytochrome c during apoptosis. *Dev. Cell.* *2*, 55–67.
- Seelert, H., Dani, D.N., Dante, S., Hauss, T., Krause, F., Schäfer, E., Frenzel, M., Poetsch, A., Rexroth, S., Schwassmann, H.J., Suhai, T., Vonck, J., and Dencher, N.A. (2009). From protons to OXPHOS supercomplexes and Alzheimer's disease: structure-dynamics-function relationships of energy-transducing membranes. *6*, 657–671.
- Seelert, H., and Dencher, N.A. (2011). ATP synthase superassemblies in animals and plants: two or more are better. *Biochim. Biophys. Acta.* *9*, 1185–1197.
- Shevchenko, A., Tomas, H., Havlis, J., Olsen, J. V., and Mann, M. (2006). In-gel digestion for mass spectrometric characterization of proteins and proteomes. *Nat. Protoc.* *1*, 2856–2860.
- Sicheritz-Ponten T, Kurland CG, and Andersson SGE. (1998). A phylogenetic analysis of the cytochrome b and cytochrome c oxidase I genes support an origin of mitochondria from within the Rickettsiaceae. *Biochem. Biophys. Acta.* *1365*, 545–551.
- Sickmann, A., Reinders, J., Wagner, Y., Joppich, C., Zahedi, R., Meyer, H. E., Schönfisch, B., Perschil, I., Chacinska, A., Guiard, B., Rehling, P., Pfanner, N., and Meisinger C. (2003). The proteome of *Saccharomyces cerevisiae* mitochondria. *Proc. Natl. Acad. Sci. USA.* *100*, 13207–13212.
- Sideris, D.P., and Tokatlidis, K. (2007). Oxidative folding of small Tims is mediated by site-specific docking onto Mia40 in the mitochondrial intermembrane space. *Mol. Microbiol.* *65*, 1360–1373.
- Spannagel, C., Vaillier, J., Arselin, G., Graves, P.V., Grandier-Vazeille, X., and Velours, J. (1998). Evidence of a subunit 4 (subunit b) dimer in favor of the proximity of ATP synthase complexes in yeast inner mitochondrial membrane, *Biochim. Biophys. Acta.* *1414*, 260–264.
- Steed, P.R., and Fillingame, R.H. (2008). Subunit a facilitates aqueous access to a membrane embedded region of subunit c in *Escherichia coli* F1FO ATP synthase, *J. Biol. Chem.* *283*, 12365–12372.
- Stock, D., Leslie, A.G., Walker, J.E. (1999). Molecular architecture of the rotary motor in ATP synthase. *Science.* *5445*, 1700–1705.
- Stroh, A., Anderka, O., Pfeiffer, K., Yagi, T., Finel, M., Ludwig, B., and Schägger, H. (2004). Assembly of respiratory complexes I, III, and IV into NADH oxidase supercomplex stabilizes complex I in *Paracoccus denitrificans*. *J. Biol. Chem.* *6*, 5000–5007.
- Strauss, M., Hofhaus, G., Schröder, R. R., and Kühlbrandt, W. (2008). Dimer ribbons of ATP synthase shape the inner mitochondrial membrane. *EMBO J.* *27*, 1154–1160.
- Stuart, R.A. (2008). Supercomplex organization of the oxidative phosphorylation enzymes in yeast mitochondria. *J. Bioenerg. Biomembr.* *5*, 411–417.
- Stuart, R.A., and Rehling, P. (2008). Mitochondrial biogenesis: is an old dog still teaching us new tricks? Meeting on the Assembly of the Mitochondrial Respiratory Chain. *EMBO. Rep.* *1*, 33-38.
- Srere P. A. (1999). Heterologous protein–protein interactions—quinary structures. *Methods* *19*, 193.
- Soubannier, V., Vaillier, J., Paumard, P., Coulary, B., Schaeffer, J., and Velours, J. (2002). In the absence of the first membrane-spanning segment of subunit 4(b), the yeast ATP synthase is functional but does not dimerize or oligomerize. *J. Biol. Chem.* *277*, 10739–10745.
- Szklarczyk, R., and Huynen, M.A. (2010). Mosaic origin of the mitochondrial proteome. *Proteomics.* *22*, 4012-4024.
- Takeda M., Vassarotti, A., and Douglas, M. G. (1985). Nuclear genes coding the yeast mitochondrial adenosine triphosphatase complex. Primary sequence analysis of ATP2 encoding the F1-ATPase beta-

- subunit precursor. *J. Biol. Chem.* *260*, 15458-15465.
- Thomas, D., Bron, P., Weimann, T., Dautant, A., Giraud, M. F., Paumard, P., Salin, B., Cavalier, A., Velours, J., and Brèthes, D. (2008). Supramolecular organization of the yeast F1Fo-ATP synthase. *Biol. Cell.* *100*, 591–601.
- Tsukihara, T., Aoyama, H., Yamashita, E., Tomizaki, T., Yamaguchi, H., Shinzawa-Itoh, K., Nakashima, R., Yaono, R., and Yoshikawa, S. (1996). The whole structure of the 13-subunit oxidized cytochrome c oxidase at 2.8 Å. *Science* *272*, 1136-44.
- van der Laan, M., Hutu, D.P., and Rehling, P. (2010). On the mechanism of preprotein import by the mitochondrial presequence translocase. *Biochim. Biophys. Acta.* *6*, 732-732.
- Velours, J. and Arselin, G. (2000). The *Saccharomyces cerevisiae* ATP synthase. *J Bioenerg Biomembr.* *32*, 383-90.
- Velours, J., Dautant, A., Salin, B., Sagot, I., and Brèthes, D. (2009). Mitochondrial F1F0-ATP synthase and organellar internal architecture. *Int. J. Biochem. Cell. Biol.* *41*, 1783–1789.
- Visser, W., Van Spronsen, E. A., Nanninga, N., Pronk, J. T., Gijs Kuenen, J., and van Dijken, J. P. (1995) Effects of growth conditions on mitochondrial morphology in *Saccharomyces cerevisiae*. *Antonie Van Leeuwenhoek.* *67*, 243-253.
- von der Malsburg, K., et al. (2011). Dual role of mitofilin in mitochondrial membrane organization and protein biogenesis. *Dev Cell.* *21*, 694-707.
- Vonck, J., and Schäfer, E. (2009). Supramolecular organization of protein complexes in the mitochondrial inner membrane. *Biochim. Biophys. Acta.* *1*, 117-24.
- Vogel, F., Bornhövd, C., Neupert, W., and Reichert, A. S. (2006). Dynamic subcompartmentalization of the mitochondrial inner membrane. *J. Cell. Biol.* *175*, 237–247.
- Vogel, F., Bornhövd, C., Neupert, W., and Reichert, A.S. (2006). Dynamic subcompartmentalization of the mitochondrial inner membrane. *J Cell Biol* *175*, 237-47.
- Wagner, K., Rehling, P., Sanjuán Szklarz, L. K., Taylor, R. D., Pfanner, N., and van der Laan, M. (2009). Mitochondrial F1Fo-ATP synthase: the small subunits e and g associate with monomeric complexes to trigger dimerization. *J. Mol. Biol.* *392*, 855–861.
- Walker, J. E., Lutter, R., Depuis, A. and Runswick, M. J. (1991). Identification of the subunits of F1F0-ATPase from bovine heart mitochondria. *Biochemistry.* *30*, 5369–5378.
- Walker, E. (1994). The regulation of catalysis in ATP synthase. *Curr. Opin. Struct. Biol.* *4*, 912–918.
- Walker, J. E., Colinson, I. R., van Raaij, M. J. and Runswick, M. J. (1995). Structural analysis of ATP synthase from bovine heart mitochondria. *Methods. Enzymol.* *260*, 163–190.
- Wagner, K., Perschil, I., Fichter, C. D., and van der Laan, M. (2010). Stepwise assembly of dimeric F(1)F(o)-ATP synthase in mitochondria involves the small F(o)-subunits k and i. *Mol. Biol. Cell.* *21*, 1494–1504.
- Westermann, B. and Neupert, W. (2000). Mitochondria-targeted green fluorescent proteins: convenient tools for the study of organelle biogenesis in *Saccharomyces cerevisiae*. *Yeast.* *16*, 1421–1427.
- Wiedemann, N., Kozjak, V., Chacinska, A., Schönfisch, B., Rospert, S., Ryan, M. T., Pfanner, N., and Meisinger, C. (2003). Machinery for protein sorting and assembly in the mitochondrial outer membrane. *EMBO J.* *22*, 565–71.
- Wiedemann, N., Pfanner, N., and Rehling, P. (2006). Import of precursor proteins into isolated yeast mitochondria. *Methods. Mol. Biol.* *313*, 373–83.

- Wittig, I., Karas, M., and Schägger, H. (2007). High resolution clear native electrophoresis for in-gel functional assays and fluorescence studies of membrane protein complexes. *Mol Cell Proteomics*. *6*, 1215–1225.
- Wittig, I., and Schägger, H. (2009). Supramolecular organization of ATP synthase and respiratory chain in mitochondrial membranes. *Biochim. Biophys. Acta*. *6*, 672-680.
- Wittig, I., Meyer B., Heide, H., Steger, M., Bleier, L., Wumaier, Z., Karas, M., and Schägger, H. (2010). Assembly and oligomerization of human ATP synthase lacking mitochondrial subunits a and A6L. *Biochim. Biophys. Acta*. *1797*, 1004–1011.
- Wu, Y., and Sha, B. (2006) Crystal structure of yeast mitochondrial outer membrane translocon member Tom70p. *Nat. Struct. Mol. Biol.* *13*, 589-93.
- Wurm, C. A., Suppanz, I. E., Stoldt, S., and Jakobs, S. (2010). Rapid FLAsH labelling in the budding yeast *Saccharomyces cerevisiae*. *J. Microsc.* *240*, 6–13.
- Xie, J., Marusich, M. F., Souda, P., Whitelegge, J., and Capaldi, R. A. (2007). The mitochondrial inner membrane protein mitofilin exists as a complex with SAM50, metaxins 1 and 2, coiled-coil-helix coiled-coil-helix domain-containing protein 3 and 6 and DnaJC11. *FEBS Lett.* *581*, 3545–3549.
- Yamaguchi, R., Andreyev, A., Murphy, A. N., Perkins, G. A., Ellisman, M. H., and Newmeyer, D. D. (2007). Mitochondria frozen with trehalose retain a number of biological functions and preserve outer membrane integrity. *Cell Death Differ.* *14*, 616–624.
- Yang, M., Jensen, R. E., Yaffe, M. P., Oppliger, W., and Schatz, G. (1988). Import of proteins into yeast mitochondria: the purified matrix processing protease contains two subunits which are encoded by the nuclear MAS1 and MAS2 genes. *EMBO J.* *7*, 3857-3862.
- Zheng, Y., Jung, M. K., and Oakley, B. R. (1991). Gamma-tubulin is present in *Drosophila melanogaster* and *Homo sapiens* and is associated with the centrosome. *Cell*. *65*, 817–823.
- Zick, M., Rabl, R., and Reichert AS. (2009). Cristae formation-linking ultrastructure and function of mitochondria. *Biochim. Biophys. Acta*. *1*, 5–19.

ACKNOWLEDGMENTS

First of all, I would like to thank Peter Rehling for the PhD opportunity in his lab, for his patience and continuous support. I would like to thank Markus Deckers for his supervision throughout the process. Special thanks goes to Melina Vucotic, Sasha Lytovchenko, and especially Fabian Ludewig for technical support and assistance. I would like to thank also all current and former members of the Rehling group for creating an amiable working environment (Christian Schulz, David Mick, Robert Reinhold, Bettina Bareth, Jan Dudek, Sven Dennerlein, Maria Levchenko, Jan Moritz Wuttke, Jonathan Melin, Isotta Lorenzi, Martina Balleininger, Mirjam Wissel, Cristine Vollmer, and Dana Hutu). I would also like to thank all other members of the Department of Biochemistry II especially Frau Engelmann (who makes me practice German) and Sarah Zafar (for her continuous health advice).

I would like to Reinhard Jahn and Markus Zweckstetter for their continuous support and insight in thesis committee meetings.

To all authors on the Alkhaja *et al.*, 2012 publication: thank you for the fruitful collaboration! Thanks goes to Daniel Jans, Stefan Jakobs, Miroslav Nikolov, Henning Urlaub, Wolfgang Schliebs, and Dietmar Riedel. I would also like to Monika Raabe for her technical assistance.

Of course all of this would not be possible without the IMPRS Molecular Biology coordination office current and past members. Thank you Steffen Burkhardt, Kerstin Grüniger, and Ivana Jurik. I would also like to thank other members of the GGNB coordination office for all their hard work.

Studying and living in Göttingen has been interesting. It is "the best of times" and on some occasions "the worst of times". Yet, what makes it memorable is the Göttingen family of friends I have acquired over the last couple of years. I tried to look for a smart quote that I can write here, but words cannot simply express my gratitude. Thank you Derya, Natalia, Andrew, Alonso, Suenke, Jonas, Stephanie, Andrea, Matthieu, Sanaz, Ahmed, and Chris. You have always been there, through the bittersweet times. And of course: Sadeem, thank you for making me smile again, for inspiring me, for making Göttingen a happier place!

I would also like to thank my family back home (in Bahrain and Jeddah) who has supported me in all means possible. To my parents, I dedicate this to you.

CURRICULUM VITAE

Personal

Born 02/03/1985, Manama, Bahrain

Education

Doctor of Philosophy, Molecular Biology

Georg-August University, Göttingen, Germany (2008-2012)

Thesis title: **The identification and characterization of Mio10 and MINOS1 as novel regulators of mitochondrial inner membrane organization**

Supervisor: Prof. Dr. Peter Rehling Dept. Biochemistry II
Georg August University Göttingen
University Medicine

Masters of Science; Molecular Biology, International Max Planck Research School,
Georg-August University, Göttingen, Germany (2007-2009)

Thesis title: **Investigating the role of Mss51 in cytochrome c oxidase biogenesis and assembly**

Supervisor: Prof. Dr. Peter Rehling Dept. Biochemistry II
Georg August University
Göttingen University Medicine

Bachelor of Science, Biochemistry w/ Molecular Biology (Industrial)

University of Leeds, Leeds, United Kingdom (2003-2007)

Primary and Secondary Education

Bahrain Bayan School, Isa Town, Bahrain (1991-2003)